A STUDY OF NEGATIVE DAMPING PHENOMENON IN FLOATING OFFSHORE WIND TURBINES AND THE ROLE OF NON-LINEAR WAVE FORCES

A Thesis

by

ALWIN JOSE

Submitted to the Office of Graduate and Professional Studies of
Texas A&M University
in partial fulfillment of the requirements for the degree of

MASTER OF SCIENCE

Chair of Committee,	Jeffrey Falzarano
Committee Members,	Moo-Hyun Kim
	Richard S. Mercier
Head of Department,	Sharath Girimaji

August 2018

Major Subject: Ocean Engineering

ABSTRACT

Floating Offshore Wind Turbine (FOWT) is a fairly new concept. There are limited number of full-scale prototypes to provide real data. Therefore, most of the research today is reliant on numerical models. This is required, so that adequate amount of confidence can be gained before venturing into large scale production. The major challenge ahead is proving their reliability and robustness. There need to be supporting studies that consider most factors that can go wrong. The computer program FAST was a groundbreaking contribution from National Renewable Energy Laboratory in this regard. FAST is capable of doing an integrated loading analysis of FOWTs. However, the numerical model used for the hydrodynamics can be improved further.

Non-linear hydrostatic and wave forces on floating structures become very important during large amplitude waves and motions. SIMDYN, a blended time domain computer program developed by Marine Dynamics Laboratory, Texas A&M University, is capable of capturing the role of such forces. SIMDYN has previously been used to demonstrate that nonlinear hydrostatics become very important in the problem of parametric excitation. In the current work, SIMDYN is coupled with FAST. FAST-SIMDYN is now a tool that is capable of studying large amplitude motions of FOWTs in extreme seas.

FAST-SIMDYN was then used to study the classic instability of negative damping. This phenomenon occurs in FOWTs that use conventional land based control. The development of platform pitch and surge instability are studied in relation to different wave and wind scenarios. The objective of this project was to do an analysis to see if non-linear hydrodynamic forces do play a significant role in large amplitude motions induced by negative damping. Such a study would give an idea on whether the development of more

sophisticated hydrodynamic modules is justified. This study indicated that non-linear hydrostatic and non-linear Froude Krylov forces resulted in higher platform pitch and heave motions compared to that obtained using a corresponding linear analysis. A bifurcation was also identified, which was induced by the controller algorithm. The system motion response depended on the wind speed history more than what was expected as a result of the bifurcation. This was used to explain the large motions obtained near the controller algorithm transition region.

DEDICATION

To my beloved parents

Jose and Mercy

ACKNOWLEDGMENTS

I would like to thank my advisor Dr. Jeffrey Falzarano who was there to constantly guide, encourage and inspire me throughout the course of Project and my graduate school. Next I would like to thank Dr. M.H. Kim and Dr. Richard Mercier for the courses they taught me and for their valuable role in my committee.

I would like to show my sincere appreciation for Abhilash Somayujula, Amitava Guha, Marco Masciola, Yujie Liu, Naveen Thomas, Jobin K Joy, Richards Sunny and Emil Thomas who were instrumental in giving the right guidance and support through the different stages of the project.

I thank my loving parents and sister who were always there for me, standing by me in all the decisions I took. Their Love and affection was the main driving factor behind this project.

Above all, I thank the God for making this endeavor possible!

CONTRIBUTORS AND FUNDING SOURCES

Contributors

This work was supported by a thesis committee consisting of Professors Jeffrey Falzarano and Moo-Hyun Kim of the Ocean Engineering Department and Professor Richard S. Mercier of the Civil Engineering Department.

The source code for FAST was provided by National Renewable Energy Laboratory (NREL). The source code for SIMDYN was provided by Abhilash Somayajula. The frequency domain analysis in Chapter 5 was done with help of Amitava Guha and Yujie Liu, who provided me with their programs MDL HydroD and MDL MULTIDYN respectively and support for the same.

All other work conducted for the thesis was completed by the student independently.

Funding Sources

This work was supported in part by the American Bureau of Shipping Scholarship and Dr. Jeffrey Falzarano. All the remaining expenses were borne by the author's personal funds.

NOMENCLATURE

OGAPS	Office of Graduate and Professional Studies at Texas A&M University
B/CS	Bryan and College Station
TAMU	Texas A&M University
MDL	Marine Dynamics Laboratory
NREL	National Renewable Energy Laboratory
FOWT	Floating Offshore Wind Turbines
HAWT	Horizontal Axis Wind Turbine
VAWT	Vertical Axis Wind Turbine
TLP	Tension Leg Platform
RNA	Rotor Nacelle Assembly
PID	Proportional Integral Derivative
LQR	Linear Quadratic Regulator
IBP	Individual Blade Pitch
DAC	Damage Accommodating Control
MPC	Model Predictive Control
LIDAR	Light Detection and Ranging
FAST	Fatigue, Aerodynamics, Structures and Turbulence
MAP	Mooring Analysis Program
BEM	Blade Element Momentum
JONSWAP	Joint North Sea Wave Project

FK	Froude Krylov
Hs	Significant Wave Height
Tp	Peak Time period
γ	Peak Shape Factor
RAO	Response Amplitude Operator
OES	Orbital Equilibrium State

TABLE OF CONTENTS

Page

LIST OF FIGURES

FIGURE Page

LIST OF TABLES

TABLE Page

1. INTRODUCTION AND LITERATURE REVIEW

1.1 Introduction

There is a growing need for energy in the world. Non-renewable sources of energy are depleting. There is a rising demand for more economic sources of renewable energy. One of the most promising sources of renewable energy is wind. There are numerous wind farms that have been built around the world. In the wind industry, it is well-known that the potential to tap wind energy is higher in the sea than on land. On this basis a number of companies have built offshore wind farms. For example, shown below is the Arkona Offshore Wind Farm, located 35km north-east of Rügen Island, in the Baltic Sea, Germany. This was developed by Statoil (now Equinor).

Figure 1.1: Arkona offshore wind farm (Reprinted from www.equinor.com [1])

Just like the oil industry, the wind industry is also moving further offshore into deeper waters. While it is economical to have ground fixed wind turbines in shallow water, when it comes to deep water, floating wind turbines are cheaper. Extensive research has been done over the years in developing Floating Offshore Wind Turbines (FOWTs). The first full scale operational FOWT was Hywind SPAR off the coast of Norway in the North Sea in September 2009. Recently, the world's first floating offshore wind farm was commissioned off the western coast of Norway in June 2017. This was also part of the Hywind project and developed by Statoil.

Texas is a leader in wind energy in the United States. Texas produces more wind energy than the next three states combined. Texas is also the leading consumer of electricity in the state using more than 10 percent of the power generated in US. There is a very fast growing population too, which calls for an increasing demand for power. Georgetown, near Austin in Texas, became one of the first cities in the US to be 100 percent powered by renewable energy. Houston which is the energy capital of the world is said to stay the energy capital of the world by focusing more on alternative sources of energy. Close to ninety percent of the energy demand in Houston is met by renewable energy. More than thirty percent of this energy demand is met by wind farms in west Texas.

Texas has a long coastline along the Gulf of Mexico. Most of the wind in Texas comes in from the GoM. Although Europe is leading in the context of Offshore Wind Power, Texas has a tremendous potential to develop technologies for deep water. With wind energy being proven to be reliable source of power, it is gaining recognition as a major contender for an alternative source of energy. In the near future, there will be need for cost effective solutions that work in the sea. This is where the concept of Floating Offshore Wind Turbines becomes favorable.

1.2 Floating Offshore Wind Turbines

Today's wind turbines are massive structures typically more than 90 m high (about the size of 28 story building). These have spinning blades with a mass equivalent to more than 25 cars. When these very structures are taken to water on a floating platform, the foundation also starts reacting to these loads.

There are 2 types of wind turbines that have been developed, Horizontal Axis Wind Turbines (HAWT) and Vertical Axis Wind Turbines. These are based on the axis of rotation of the blades. Each of them work based on very different aerodynamic principles. Historically HAWTs gained popularity owing to relatively constant wind loads on the blades, and several other advantages. Currently there is a renewed interest in VAWTs for use in FOWTs owing to the low Center of Gravity and ease of maintenance.

From a safety point of view, in the case of HAWTs, the dangers are way higher on floating platforms. The velocities and accelerations up there are amplified even for small platform pitching angular velocities because of the height at which the turbine shafts and generators are present. In such a situation, it is critical, that the motions of the platform be kept at a minimum.This is where extreme motion studies become important. Extensive research has been conducted on floating offshore structures for use in oil platforms such as Semisubmersibles, Tension Leg Platforms (TLPs) and SPARs. When it comes to FOWTs, new challenges arise. The loads are more at the top than from the bottom. The design philosophy needs to shift because of this. Conventionally, the weight of the equipment and all the drill strings and risers would act with relatively lower Center of Gravity. The goal was to stay afloat and stable. But in the case of FOWTs, there is very little need for equipment at deck level or below. The biggest load is the wind load that acts horizontally. A lot of this force goes to the mooring lines. This way the mooring lines contribute to a major chunk in the cost of the platform for FOWT.

Next, the major components involved in the analysis of FOWTs are described.

The wind turbine blades are long slender airfoil structures attached to a hub. They are typically 3 in number (sometimes 2). They are the main structures subject to aerodynamic loads as they rotate about the hub and generate power. Being long and slender, they are subject to bending in fore-aft direction, in the rotation direction as well as torsion along its own axis. The blade pitch can be controlled to change the angle of attack on the airfoil to modify the lift forces and subsequent power take off. The blades are connected to the hub which in turn is connected to the Nacelle assembly which houses the generator. The blades and hub form the Rotor and together with the Nacelle form the Rotor Nacelle Assembly (RNA). The generator inside the nacelle is connected to the hub through a shaft which also undergoes torsion loads. It is also connected to the brakes which control the rotation speed of the rotor. Various kinds of control servos are used to control the blade pitch and rotor speed. Generally rotors are controlled to rotate at constant rpm to ensure steady power and reducing load variation. The RNA could weigh about 350 MT. It can be rotated about the tower, so as to orient it along the wind direction.

The tower is generally a tapered cylinder. The height of the tower is adjusted based on the height required for the rotor hub (typically about 90m above sea level) Owing to the length, the tower acts as a cantilever free to bend in the fore-aft and side-side directions. The tower is fixed on the foundation floating platform. The platform is free to move in all 6 directions (3 translations and 3 rotations). The platform is held in place with the help of mooring lines.

The analysis of FOWTs presents many challenges. As described earlier, there are very complicated interactions between various components. The floating foundation itself is an engineering challenge. The whole structure is subjected to a lot of dynamic loading. These include aerodynamic, hydrodynamic, servo, structural and mooring loads. Being a relatively new field with very few prototypes installed, extensive simulations have to be

done on all that can go wrong.

1.3 FOWT Analysis Tools

With the resurgence in interest for Floating Wind Turbines came the need for good computer tools to analyze them. When Hydro Oil & Energy (now merged with Statoil) were analyzing the concept of Hywind SPAR, Skaare et al. [2] developed the coupled code SIMO/RIFLEX/HAWC2, in collaboration with Risø National Laboratory. Jonkman, in his doctoral thesis [3], incorporated a hydrodynamics module in the NREL wind turbine analysis computer program, FAST (Fatigue, Aerodynamics, Structures, and Turbulence). This enabled an easy method to analyze FOWTs. FAST has since then been extensively used as a platform to analyze various components of the FOWTs. It has also been coupled with better hydrodynamic analysis programs.

Shim & Kim [4] implemented FAST into their floater-mooring program CHARM3D to create a new integrated dynamic analysis tool. They used WAMIT as their pre-processor. This program was later further advanced by Bae [5]. Lackner & Rotea modified FAST to include Structural Control (FAST_SC) [6]. FAST was coupled with various other hydro and mooring codes such as SSODAC [7], Orcaflex [8], COUPLE [9]. Similarly SIMO/RIFLEX was also coupled with other codes such as AeroDyn [10] and TDHMILL [11]. Furthermore, there were others who developed their own FOWT analysis tools. These include WindFloat by Principle Power [12], aNySIM / PHATAS by ECN (Energy Research Centre of the Netherlands) and MARIN [13], CRAFT by Shanghai JiaoTong University [14], CALHYPSO by EDF Energy [15]

1.4 Need for Non-Linear Models

On top of the difficulties involved in the analysis of FOWTs, the new environment comes with the possibilities for instabilities and large amplitude motions. These kind of problems may not be adequately captured by simplified or linearized models. In the fol-

lowing paragraph we discuss the various problems that have been identified and discussed in the literature.

One of the main design criteria for any floating structure is survival in extreme sea and other environment states. Of this, of particular importance is survival in storms and hurricanes as discussed by Zambrano [16], Utsunomiya [17] and Kokubun [18]. Particular to Floating Offshore Wind Turbines is its susceptibility to controller malfunctions. Being a floating foundation, these malfunctions can prove detrimental. This is the case with negative damping [19]. There are also other instabilies such as those identified in platform yaw by Jonkman and Buhl[19], blade pitch control malfunction by Mizukami [20], and pitch actuator fault, grid loss, and shutdown by Bachynski [21]. Aerodynamic instabilities can also creep in, that can be dangerous as studied by Shen et. al.[22]. Structural fatigue of towers [23] and structural strength of mooring lines [24] also contribute to the overall design process. In the hydrodynamics side, our particular interest lies in phenomenon such as parametric excitation and resonance.

In the overall analysis of FOWT, all these factors have to be considered. Design of FOWTs involve range of criteria from which a controlling criteria is chosen [25]. When it comes to large amplitude platform motions, there are analytical models and higher fidelity simulation models. Thiagarajan [26] presented a simplified model for non-linear pitch decay. Lei and Sweetman [27] [28] studied theoretically the large amplitude motions of FOWTs. While these are useful in the initial design phase, higher fidelity tools as discussed in the previous section need to be used in the detailed design stage. Potential flow tools are good because of their lesser fidelity and higher accuracy in predicting forces and motions. In a random sea environment, approximations such as the Volterra series can capture the nonlinear memory effects as done by Somayajula [29].

1.5 Negative Damping in FOWT

In this work, the primary focus is on the phenomenon of negative damping. Conventional land based wind turbines controls focus on generating a constant power by adjusting blade pitch angle. But floating wind turbines are much more prone to platform pitching motion, as the foundation is not rigid. The wind causes the platform to pitch. The pitching motion results in a change in the relative velocity of the wind with respect to the blades due to correspondingly high horizontal motions at the blades. When conventional land based control is used, it acts as negative damping in platform pitch and adds energy to the system. This leads to unsteady platform pitch motions.

Nielsen, Hanson, & Skaare, 2006 [30] were the first to discover the phenomenon of negative damping when they conducted experiments using conventional land based wind turbine control. They were performing experiments of the Hywind Spar Wind Turbine concept in a model basin, in order to study the effect of waves and various controls. They also validated their results against their Code Simo/Riflex and a more simplified Matlab code - HywindSim. The experiments indicated large resonant motions for wind velocity above rated, but not as high as was predicted by the codes. They attributed this to the lower damping estimates used in their code, compared to that observed in experiments.

Jonkman and Buhl [19] demonstrated the susceptibility of floating offshore wind turbines to excessive pitching motions using FAST, a dynamics analysis tool for wind turbines, in which they incorporated hydrodynamic and mooring modules. Jonkman [31] later came up with an analytical evaluation of what happens during negative damping. In this same work, he studied the effect of 3 other conventional wind turbine controllers on the pitch motion of the platform.

Bir and Jonkman [32] suggested that a system having negative damping could lead to exponential growth in platform motion, which is classified as an instability as opposed

to a resonance. Resonant motion requires external excitation, grow linearly and occur at discrete frequencies. However, instabilities are self-excited and can occur over a range of design or operating conditions. They can grow exponentially, but may settle to a limit cycle high amplitude oscillations.

Larsen and Hanson [33] looked at the negative damping phenomenon from a controls perspective, deriving analytic expressions relating the blade pitch control to the aerodynamic torque. They tuned the controller gains so that controls acted slower than the natural pitching frequency in order to provide positive aerodynamic damping. While it is effective in controlling platform pitch motion, the generator rotational speed and power vary much more (i.e., up to 30%).

There are numerous controllers that were developed following these works. Karimirad and Moan [34] continued further on the work of Larsen and Hansen[33]. They compared the Parked Wave only case, Parked Wave-Wind and Operating Wave-Wind cases in various wind speed conditions. They noted that the motion response of the platform to the waves was not modified by the presence of wind. In particular, they also noted that, while the platform pitch motion was the dominant platform response in over-rated wind speeds, it was the surge motion that dominated at the rated speed. Furthermore, they developed a controller similar to Larsen and Hansen [33] which involved tuning the controller gains. This way, the platform pitch motion was arrested a great deal at over-rated wind speed. However the platform surge motion in the tuned condition was still significantly high in the rated wind speed.

It is proposed that the reason for the surge motion is not just to do with the negative damping. The platform surge motion occurs due to the sudden change in control algorithm at the rated wind speed of 11.4 m/s. At this speed, the control algorithm changes from maximum power to a constant power approach, which involves a change of blade pitch angle. Initially, the platform starts oscillating either in platform surge or platform

pitch mode. This causes a change in relative velocity at the blades in turn causing an oscillating wind speed. Oscillating wind speed causes the control to keep switching algorithms quickly. This can be compared to a person on a swing folding legs at one end to increase the amplitude. This causes a parametric excitation in surge direction, causing the vessel to surge in a large amplitude limit cycle. The results of this effect are studied in Section 4.3.

1.6 Controls to Address Negative Damping

Initially the focus was on shifting from a constant power to constant torque approach. This was worked upon by Larsen & Hanson, 2007 [33]. Constant torque approach reduced the platform pitch significantly. However, with this approach there was a high fluctuation in power. Then there was work on optimizing a balance between constant power against constant torque [31]. Lackner, 2009 [35] advocated relatively simpler PID (Proportional Integral Derivative) controller over complicated multivariable LQR (Linear-Quadratic Regulator) control. While most of the controls were based on Collective Blade pitch control, Namik & Stol, 2009 [36] suggested the use of Individual Blade pitch (IBP) Controller and worked extensively on them. IBP is very useful in reducing platform pitching loads. Namik & Stol, 2009 [37] also suggested the use of Disturbance Accommodating Control (DAC) to compensate for the disturbance caused by wind and waves. Chaaban & Fritzen, 2014 [38] came up with a Model Predictive Control (MPC) which uses the information about incoming wind and waves to forecast the system behavior and send control inputs accordingly.

MPC has a problem of power fluctuation. This problem can be offset to a good degree by installing a wind farm that has a more regulated overall power output. With technologies such as LIDAR being used to forecast the incoming waves [39] [40] it will soon be possible to have easy to implement tools for incoming wave data. System Identification is another upcoming field being used to predict motions [41]. Also, currently the control

is for just the turbine blade pitch. MPC has the potential to be expanded to include other more effective controls. It may be used in conjunction with other active positioning systems [42] or semi- active tuned damping tools, which can be added to the control loop. Faster computers have been helping reduce the simulation time. Using SimDyn, MDL HydroD etc it's possible to get very accurate results within a reasonable time scale. This helps in giving sufficient time in actuating the controls. In this scenario it is apt to develop an integrated control tool that is capable of using the incoming wave and wind data, analyzing the platform behavior and generating control outputs that can preemptively avoid excessive platform motions. This is much like the Dynamic Positioning System in use today.

1.7 Research at MDL

In this section, we will talk about the the research being performed in at MDL, Texas A&M University. Guha [43] developed the computer program MDL HydroDyn, making use of a 3D frequency domain Green's method in infinite water depth, for predicting hydrodynamic coefficients, wave induced forces and motions. This was later developed to include added resistance in ships [44] [45] and forward speed effects [46] [47]. Somayajula [48] worked on a time domain tool, SIMDYN for simulating large amplitude motion of marine and offshore structures. His work was focused on the occurrence of parametric roll in ships [44] [29], roll damping [49] and System Identification [50]. Liu advanced the work done by Guha on Frequency domain methods. He enabled irregular frequency removal methods [51] [52] [53] and also did significant research on interaction between multiple ships in non-zero speeds [54]. A part of the work presented in this thesis is also being presented in the ASME conference [55].

1.8 Objective

The literature review shows us that there are various extreme motion scenarios possible for FOWTs. There are also many who have developed tools to analyze FOWTs. FAST is one of the main tools for FOWT analysis available today. MDL has its expertise on analysis of floating structures. SIMDYN was one main time domain analysis tool developed in MDL, with its own unique capabilities in analyzing large amplitude motions. Negative damping is a classic instability that has been studied in the literature. There have been many controllers developed to address it. But the main issue with most of them is that the controllers do not take into account the system properties.

The objective of this project is to create a FOWT analysis tool, by coupling FAST and SIMDYN codes. This would enable the capability of analyzing the role of non-linear Froude Krylov and non-linear hydrostatic forces on the motions of FOWTs. This is to be used to study the phenomenon of negative damping. A comparison would be made between a linear and a non-linear analysis. If they prove to be significantly different, then it would show that non-linear forces do need to be considered while designing for extreme scenarios.

2. THEORY

2.1 FAST theory

Beginning with FAST v8, NREL follows a modularized approach in dealing with the motions and controls in FAST. It follows a state space representation of modules. Each component of a FOWT, be it the wind turbine aerodynamics, wind turbine controls, structural bending of the wind turbine blades and tower, floating hydrodynamics of platform or loads on mooring lines, they are computed as independent modules using FAST as a platform. The modules communicate between themselves sending data in the form of Inputs, Outputs, Continuous, Discrete and Constraint States, and Parameters. Extensive work has been done in this regard by NREL to come about with this new approach. [56]

2.1.1 FAST modules

- Elastodyn - It is main overall time domain solver of FAST. All the other modules pass the forces acting on the structure at different points at each time step. Elastodyn integrates the differential equation using solvers such as Runge Kutta 4th Order or Adams-Bashforth methods. It takes as input the hydrodynamic loads, aerodynamic loads, substructure reactions, and control commands. It solves for all the degrees of freedom of the FOWT, which includes the platform motions (Surge, Sway, Heave, Roll, Pitch and Yaw)

- BeamDyn - This module takes care of the turbine blade structural dynamics. It uses geometrically exact beam theory (GEBT) to solve for these.

- Aerodyn - This is the main module that calculates the aerodynamic loads on the turbine blades. It has a few options on how this is done, one of them being the Blade Element Momentum theory.

- Hydrodyn - This module is responsible for the hydrodynamic loads acting on the platform. This usually takes input from WAMIT, a commercial code that does frequency domain analysis of the platform and generates the hydrodynamic coefficients.

- MAP/ FEAMooring/MoorDyn - These are some of the options for the mooring modules that can be used for the analysis, depending on the fidelity required.

- ServoDyn - This serves to control the blade pitch angle, generator speed, brakes and a few other parameters depending on the controller algorithm being followed.

- SubDyn - This is applicable to earth fixed wind turbines, including those offshore. These are used to account for the foundation reaction loads under the soil.

- IceDyn - This is used in very specific applications where there is occurrence of ice that needs to be accounted for.

2.1.2 The State Space Model Used in FAST

Following is a description of the various kinds of variables and data that are passed between modules. Each of them are vectors or 1 dimensional arrays.

- Inputs (identified by u) - These are the initial input variables such as position, velocity and acceleration that is supplied to the module, to do the calculations.

- Outputs (y) - Theses are the final outputs that are calculated by the module such as forces.

- States are generally internal to a specific module. They are sort of the intermediate variables being used between inputs and outputs. In a state space representation, Inputs are related to states by linear first order differential equations, in the case of

continuous states and linear difference equations in the case of discrete equations. While the outputs are linearly dependent on the inputs and states.

  - Continuous states (x) - These are, just as the name suggests, analog or continuous time states. They can be integrated. In the case of floating structures, state space based radiation "memory" is one such example.
  - Discrete states (x^d) - These are states such as digital control signals which have jumps and are defined in steps.
  - Constraint states (z) - These are used to define constraints between inputs, other states and outputs. These are algebraic variables which are not differentiated or discrete.

- Parameters (p) These are variables that are totally independent of the inputs, outputs and states. They can be fully defined at initialization. Examples are mass, inertia, hydrodynamic coefficients and undisturbed incident waves.

Now let us discuss about the 2 main approaches used in FAST in coupling modules, loose and tight coupling. In tight coupling, all the inputs, outputs and states relations are set by the modules and the integration to obtain the new time step inputs is done together. While in loose coupling, the individual modules are responsible for tracking their states and integrating using their solvers. This is shown in Figure 2.1.

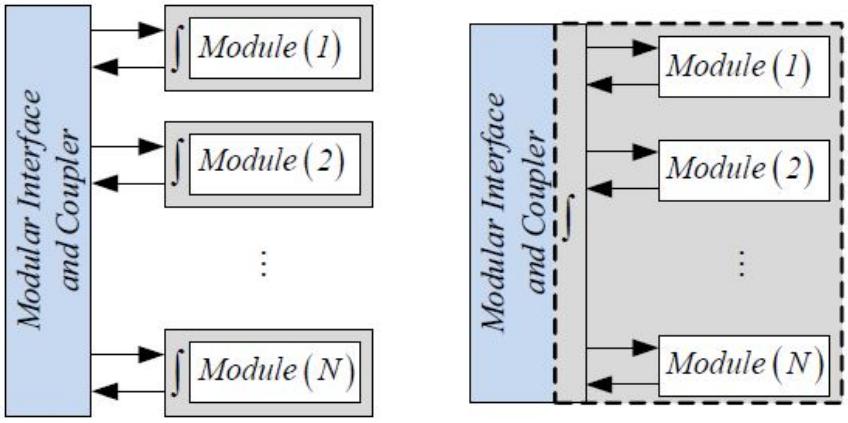

Figure 2.1: Loose and tight coupling schemes in FAST (Reprinted from Jonkman, 2013 [56])

In a tightly coupled scheme, the algebraic equations connecting the inputs, outputs and states will be as shoen in Equations 2.1a-d. Note here that Z is a constraint equation relating the states, inputs and time. Similarly Y relates outputs to the states, inputs and time. These are algebraic expressions and not differential equations. FAST uses efficient mathematical solvers to satisfy these constitutive equations and update the input for next time step.

$$\dot{x} = X(x, x^d, z, u, t) \tag{2.1a}$$

$$x^d[n+1] = X^d(x|_{t=n\Delta t}, x^d[n], z|_{t=n\Delta t}, u|_{t=n\Delta t}, t|_{t=n\Delta t}) \tag{2.1b}$$

$$0 = Z(x, x^d, z, u, t) \quad \text{with} \quad \left(\left|\frac{\partial Z}{\partial z}\right|\right) \neq 0 \tag{2.1c}$$

$$y = Y(x, x^d, z, u, t) \tag{2.1d}$$

If there are N modules being used, then the inputs (u), outputs (y) and states (x, x^d,z) are vectors obtained by combining the corresponding vectors in the individual modules, as

shown below.

$$u = \begin{Bmatrix} u^{(1)} \\ u^{(2)} \\ \vdots \\ u^{(\mathrm{N})} \end{Bmatrix} \quad \text{and} \quad y = \begin{Bmatrix} y^{(1)} \\ y^{(2)} \\ \vdots \\ y^{(\mathrm{N})} \end{Bmatrix} \tag{2.2}$$

$$x = \begin{Bmatrix} x^{(1)} \\ x^{(2)} \\ \vdots \\ x^{(\mathrm{N})} \end{Bmatrix} \quad , \quad x^{\mathrm{d}} = \begin{Bmatrix} x^{\mathrm{d}(1)} \\ x^{\mathrm{d}(2)} \\ \vdots \\ x^{\mathrm{d}(\mathrm{N})} \end{Bmatrix} \quad \text{and} \quad z = \begin{Bmatrix} z^{(1)} \\ z^{(2)} \\ \vdots \\ z^{(\mathrm{N})} \end{Bmatrix} \tag{2.3}$$

In general, for both tight and loose coupling, input-output relation equation can be written as,

$$0 = U(u, y, t) \quad \text{with} \quad \left| \frac{\partial U}{\partial \tilde{u}} \right| \neq 0 \tag{2.4}$$

where $\tilde{u}$ is a reduced order 1D matrix with same variables as u removing all the repetitions. There may be a few inputs which are repeated across modules. Here, this is kind of the main equation that is solved by the FAST solver.

Before we discuss the loose coupling, let us define these notations used in the constitutive relations in both loose as well as tight coupling above. The state and output functions are also combined across all modules into vectors as shown below.

$$X = \begin{Bmatrix} X^{(1)} \\ X^{(2)} \\ \vdots \\ X^{(\mathrm{N})} \end{Bmatrix} \quad , \quad X^{\mathrm{d}} = \begin{Bmatrix} X^{d(1)} \\ X^{d(2)} \\ \vdots \\ X^{d(N)} \end{Bmatrix} \quad , \quad Z = \begin{Bmatrix} Z^{(1)} \\ Z^{(2)} \\ \vdots \\ Z^{(\mathrm{N})} \end{Bmatrix} \quad \text{and} \quad Y = \begin{Bmatrix} Y^{(1)} \\ Y^{(2)} \\ \vdots \\ Y^{(\mathrm{N})} \end{Bmatrix} \tag{2.5}$$

In loose coupling, the states, inputs and outputs are related by the following expressions. Note that, U here acts as a constraint equation across modules as opposed to Z

which acts as a constraint equation within a module. Together U and Z are used by the solver in FAST to complete a feedback loop.

$$\dot{x} = X(x, x^d, z, u, t) \tag{2.6a}$$

$$x^d[n+1] = X^d(x|_{t=n\Delta t}, x^d[n], z|_{t=n\Delta t}, u|_{t=n\Delta t}, t|_{t=n\Delta t}) \tag{2.6b}$$

$$\begin{Bmatrix} 0 \\ 0 \end{Bmatrix} = \begin{Bmatrix} Z(x, x^{\mathrm{d}}, z, u, t) \\ U(x, x^{\mathrm{d}}, z, u, t) \end{Bmatrix} \quad \text{with} \quad \left| \begin{bmatrix} \dfrac{\partial Z}{\partial z} & \dfrac{\partial Z}{\partial u} \\ \dfrac{\partial U}{\partial z} & \dfrac{\partial U}{\partial u} \end{bmatrix} \right| \neq 0 \tag{2.6c}$$

$$y = Y(x, x^d, z, u, t) \tag{2.6d}$$

In HydroDyn, the acceleration, velocity and position serve as inputs to the module. Hydrodyn module then calculates forces and outputs them. Elastodyn takes this as input and integrates to give the new position, velocity and acceleration. This global analysis uses Kane's dynamics [57]. In the meantime, Hydrodyn takes care of the integration of all the intermediate states used within the module.

The time domain analysis is described in greater detail in the Methodology section. This involves initialization, time simulation and end.

2.2 Hydrodynamic Loads

All floating structures in the ocean are subjected to a number of hydrodynamic forces. These include the diffraction forces (F_D), radiation forces (F_{Rad}), viscous forces (F_V) and restoring forces (F_{Res}). The diffraction loads are those induced by incoming waves. These are composed of the incoming Froude Krylov forces (F_{FK}) and scattering forces (F_{Scat}). The radiation forces are created by the motion of the floating body, which creates waves. Viscous forces are generated by the viscosity of the fluid (sea water). Restoring forces are caused by the stiffness due to the difference in the weight and buoyancy. Thus the total force can be expressed as follows.

$$\{F\} = \left\{ \begin{array}{c} \text{F} \\ \\ \text{M} \end{array} \right\} = \{F_D\} + \{F_{Rad}\} + \{F_V\} + \{F_{Res}\} \tag{2.7}$$

where,

F_D = Diffracted Wave Force

F_{Rad} = Radiated Wave Force

F_V = Viscous Force

F_{Res} = Restoring Force

$$\{F_D\} = \{F_{FK}\} + \{F_{Scat}\} \tag{2.8}$$

where,

F_{FK} = Wave induced Froude Krylov Force

F_{Scat} = Scattered Wave Force

2.2.1 Frequency Domain Analysis

Frequency domain analysis needs to be performed first before performing a time domain analysis. Certain forces such as wave and radiation are frequency dependent. A complex velocity potential can be defined under the assumption of inviscid, incompressible and irrotational fluid as:

$$\Phi(\vec{x}, t) = [-Ux + \phi_S(\vec{x})] + \left[\phi_I(\vec{x}, \beta, \omega_I) + \phi_D(\vec{x}, \beta, \omega_I) + \sum_{j=1}^{6} \eta_j \phi_j(\vec{x}, U, \omega_e)\right] e^{i\omega_e t} \tag{2.9}$$

where,

ω_e = encounter frequency, which is same as wave frequency ω for zero speed case as inthe case of FOWTs

ϕ_S = perturbation potential due to steady translation

ϕ_I = incident wave potential; ϕ_D is the diffracted wave potential

ϕ_j and η_j = radiation potential due to unit motion and vessel motion amplitude respectively in the jth direction

The incident wave potential ϕ_I, diffraction potential ϕ_D and radiation potential ϕ_j are determined by solving the following boundary value problem as described by Guha,2016 [47]

Once the radiation velocity potential is obtained, the zero speed hydrodynamic coefficients are given by:

$$A^0_{jk} = -\frac{\rho}{\omega_e}\int_S Im(\phi_k)n_j ds \tag{2.10}$$

$$B^0_{jk} = -\rho\int_S Re(\phi_k)n_j ds \tag{2.11}$$

The pressure on the hull can be found using the Bernoulli's equation:

$$P = \frac{1}{2}\rho U^2 - \rho\frac{\partial\Phi}{\partial t} - \frac{1}{2}\rho|\nabla\Phi|^2 - \rho g z \tag{2.12}$$

The incident wave excitation force also known as the Froude Krylov force is given by:

$$F_I = i\omega_I\rho\int_S \phi_I n_j ds \tag{2.13}$$

and the diffraction wave excitation force is

$$\begin{aligned} F_D &= \rho \int_S (i\omega_e n_j - U m_j)\phi_D ds \\ &= -\rho \int_S \phi_j^0 \frac{\partial \phi_I}{\partial n} ds \qquad \text{for } j = 1, 2, 3, 4 \\ &= -\rho \int_S \phi_j^0 \frac{\partial \phi_I}{\partial n} ds + \frac{\rho U}{i\omega_e} \int_S \phi_3^0 \frac{\partial \phi_I}{\partial n} ds \qquad \text{for } j = 5 \\ &= -\rho \int_S \phi_j^0 \frac{\partial \phi_I}{\partial n} ds - \frac{\rho U}{i\omega_e} \int_S \phi_2^0 \frac{\partial \phi_I}{\partial n} ds \qquad \text{for } j = 6 \end{aligned} \tag{2.14}$$

Response Amplitude Operator (RAO) are the transfer function that relate the motion or force response spectra to the amplitude of waves. Frequency domain programs can be used to evaluate the forces and motions for regular wave cases in a range of wave frequency, and hence be used to obtain the RAOs.

$$H(\omega) = \left| \frac{z_a}{\zeta_a}(\omega) \right| \tag{2.15}$$

where,

$H(\omega)$ = RAO/ transfer function

z_a = Motion amplitude response (eg:- Heave)

ζ_a = Wave amplitude

2.2.2 Hydrodynamic Loads in FAST

In FAST, the Global coordinate system is set at the mean sea level, the center of the structure, with Z axis positive upward. The positive X axis is along the nominal (zero-degree) wave propagation direction. The Y axis can be found assuming a right-handed Cartesian coordinate system [58]. Shown in Figure 2.2 is the same concept. The Hydro-Dyn module uses the same origin and axis for the local coordinate system.

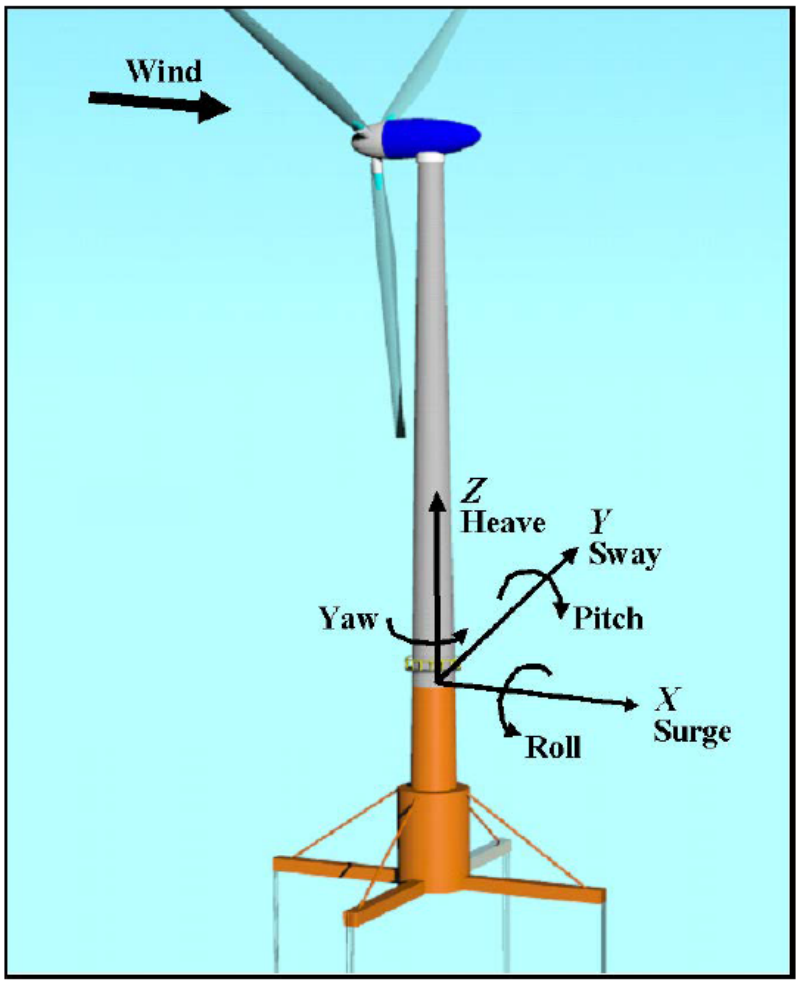

Figure 2.2: FAST Coordinate system (Reprinted from Jonkman, 2014 [58])

Hydrodyn module in FAST does all the hydrodynamic calculations. In this section we discuss the theory used in potential flow option.

The external load on the support platform is estimated using the following formula.

$$F_i^{Platform} = -A_{ij}\ddot{q}_j + F_i^{Hydro} + F_i^{Lines} \tag{2.16}$$

Where $F_i^{Platform}$ is the total of external loads, F_i^{Hydro} is the hydrodynamic load and F_i^{Lines} is the mooring lines load. A_{ij} (i,j) component of the sum of impulsive hydrodynamic added

mass and Mass matrix M_{ij} [3]

The hydrodynamic forces, applied at the reference point have the following components.

$$\boldsymbol{F}_{WRP} = \boldsymbol{F}_W + \boldsymbol{F}_{HS} + \boldsymbol{F}_{RD_n} + \boldsymbol{F}_{AM} \tag{2.17}$$

Wave diffraction force F_W is given by

$$\boldsymbol{F}_W = \frac{1}{N} \sum_{k=-\frac{N}{2}-1}^{\frac{N}{2}} W[k] \sqrt{\frac{2\pi}{\Delta t} S_\zeta^{2-Sided}(\omega)} X(\omega, \beta)|_{\omega=k\Delta\omega} e^{j\frac{2\pi kn}{N}} \tag{2.18}$$

where $S_\zeta^{2-Sided}$ is defined based on the choice of JONSWAP or Pierson Moskowitz spectrum, W[k] is the Fourier transform of a standard normal distribution time series and X is the wave excitation force per unit wave amplitude (Wave RAO).

Hydrostatic Force is given by

$$\boldsymbol{F}_{HS} = \rho g V_0 \left(\{\delta\}_3 + y^{CB} \{\delta\}_4 - x^{CB} \{\delta\}_5 \right) - C^{Hydrostatic} x \tag{2.19}$$

Radiation convolution integral is discretized and calculated as

$$\boldsymbol{F}_{RD_n} = -t_{RD} \sum_{i=n-N_{RD}}^{n-1} K_{n-i-1} \dot{x}_i \tag{2.20}$$

2.2.3 Hydrodynamic Loads in SIMDYN

SIMDYN uses 3 different coordinate systems based on the force being calculated, the global earth fixed coordinates system (GCS), steady moving coordinate system (SMCS) and body fixed moving system (BCS) [59]. In the case of a floating wind turbine which is not moving with a steady forward speed, the GCS and SMCS are the same. In our case, the origin is fixed at the mean sea level at the body center. We follow the same convention

as used in FAST. Figure 2.3 shows this.

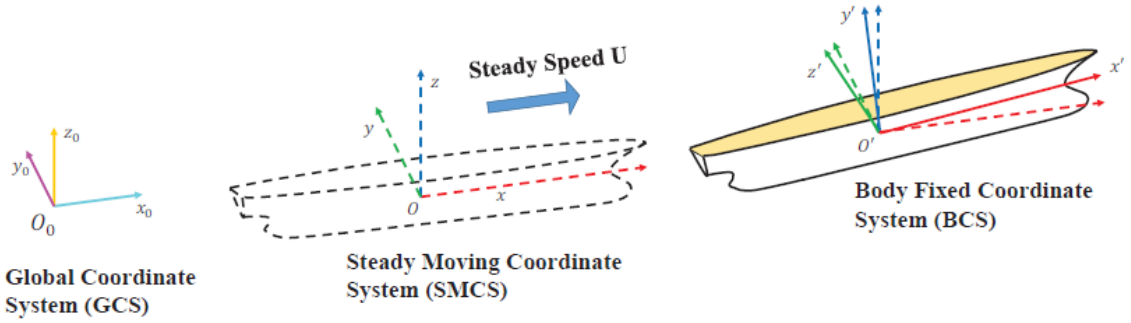

Figure 2.3: SIMDYN Coordinate system (Reprinted from Somayajula,2017 [59])

Wave induced non-linear Froude Krylov forces are obtained, incorporating Wheeler stretching up to the instantaneous waterline. The underwater pressure is given by

$$p(t,x,y,z) = -\rho\frac{\partial\phi_I}{\partial t}(t,x,y,z-\eta) \quad \text{for} \quad z \leq \eta(t,x,y) \tag{2.21}$$

$$= -\sum_{i=1}^{N} a_i g e^{k_i(z-\eta)} \sin(k_i(\cos(\beta) + y\sin(\beta)) - \omega_i t + \epsilon_i) \tag{2.22}$$

Force and moment are obtained by integration of the pressure over the instantaneous wetted surface area S_B

$$\boldsymbol{F}_I(t) = \int_{S_B} p(t,x,y,z).\boldsymbol{n}dS \tag{2.23}$$

$$\boldsymbol{M}_I(t) = \int_{S_B} p(t,x,y,z).(\boldsymbol{x}\times\boldsymbol{n})dS \tag{2.24}$$

The scattering wave force is obtained using the wave force RAO (F_{S_j}) calculated in

a standard frequency domain program. Fourier transform of the incident wave is used to obtain Force, first in frequency domain and then converted back to time domain.

$$F_{S_j}(t) = \mathscr{F}^{-1}[F_{S_j}(\omega) \times \mathscr{F}[\eta(t)]] \tag{2.25}$$

For a single wave excitation frequency, Radiation force has 2 components, one due to added mass and other radiation damping.

$$\{F_{Rad}\} = -[A(\omega)]\{\ddot{\xi}\} - [B(\omega)]\{\dot{\xi}\} \tag{2.26}$$

However for an irregular wave, which consists of multiple frequencies, the expression involves a convolution integral.

$$\{F_{Rad}\} = -[A(\infty)]\{\ddot{\xi}\} - [B(\infty)]\{\dot{\xi}\} - \int_0^\infty [K(\tau)]\{\dot{\xi}(t-\tau)\}d\tau \tag{2.27}$$

where [A(∞)] and [B(∞)] are 6×6 infinite frequency added mass and radiation damping matrices.

[K(τ)] is the 6×6 matrix of retardation functions which is evaluated as follows.

$$[K(\tau)] = \frac{2}{\pi}\int_0^\infty [B(\omega) - B(\infty)]\cos(\omega\tau)d\omega \tag{2.28}$$

Restoring forces are obtained using the instantaneous buoyancy and weight of the vessel.

$$\boldsymbol{F} = \int_{S_B} -\rho g z.\boldsymbol{n}dS + \boldsymbol{W} \tag{2.29}$$

$$\boldsymbol{M} = \int_{S_B} -\rho g z.(\boldsymbol{x} \times \boldsymbol{n}) dS + \boldsymbol{x_G} \times \boldsymbol{W} \tag{2.30}$$

$$\boldsymbol{W} = -mg\hat{k} \tag{2.31}$$

Viscous forces consists of 5 diffferent components, wave damping (B_W), skin friction damping (B_F), eddy damping (B_E), lift damping (B_L) and bilge keel damping (B_{BK})

$$B_{eq} = B_W + B_F + B_E + B_L + B_{BK} \tag{2.32}$$

3.1 ITI Energy Barge

ITI Barge was a floating wind turbine concept which consists of a wind turbine mounted on a square barge with a moonpool that acts as a Oscillating Water Column (OWC) Wave Energy Converter. This barge was chosen as this was used in the literature to study the phenomenon of negative damping. Figure 3.1 shows a model of this concept. The main specifications of the barge are summarized in Table 3.1.

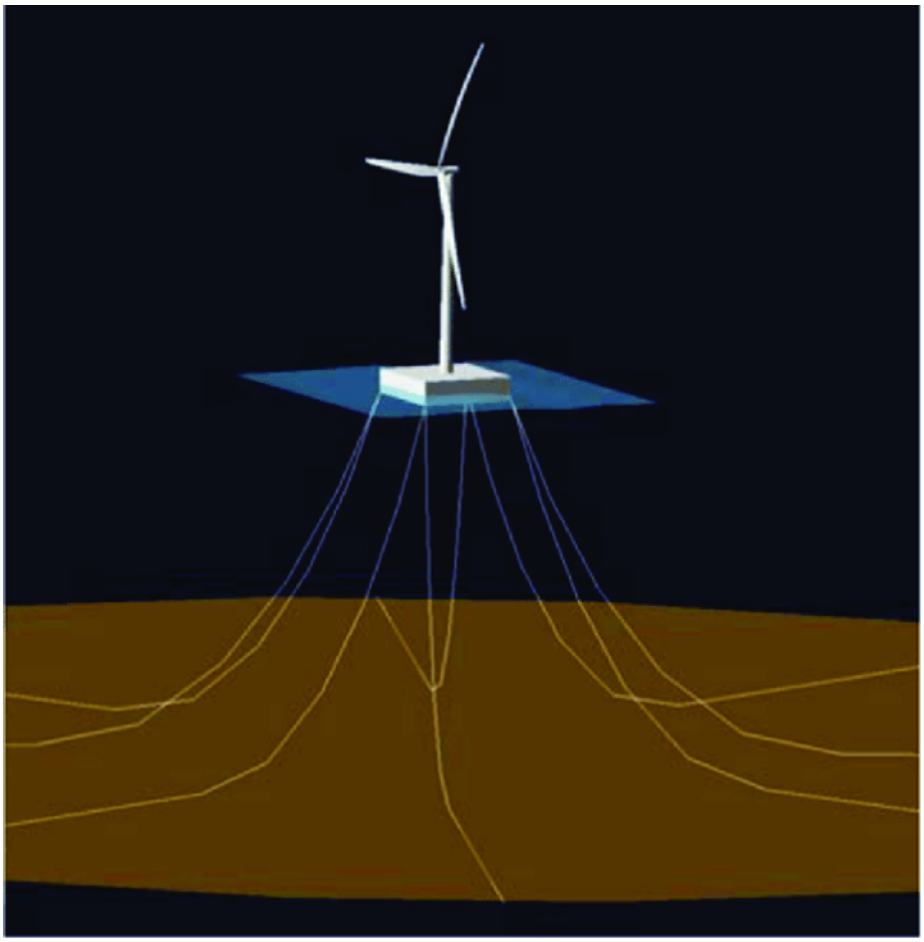

Figure 3.1: ITI Energy Barge (Reprinted from Jonkman, 2007 [3])

Size (W $\times$ L $\times$ H)	40 m $\times$ 40 m $\times$ 10 m
Moon pool (W $\times$ L $\times$ H)	10 m $\times$ 10 m $\times$ 10 m
Draft, Freeboard	4 m, 6 m
Water Displacement	6,000 m^3
Mass, Including Ballast	5,452,000 kg
CM Location below SWL	0.281768 m
Roll Inertia about CM	726,900,000 $kg.m^2$
Pitch Inertia about CM	726,900,000 $kg.m^2$
Yaw Inertia about CM	1,453,900,000 $kg.m^2$
Anchor (Water) Depth	150 m
Separation between Opposing Anchors	773.8 m
Unstretched Line Length	473.3 m
Neutral Line Length Resting on Seabed	250 m
Line Diameter	0.0809 m
Line Mass Density	130.4 kg/m
Line Extensional Stiffness	589,000,000 N

Table 3.1: ITI Energy Barge Parameters. based on Jonkman et.al, 2007 [3]

Before the frequency domain analysis, the mass inertia properties of the ITI Energy Barge were calculated. The mass, center of gravity and local moment of inertia of the individual components of the wind turbine was based on the NREL 5MW reference wind turbine definition [60]. It was calculated about the origin (Mean Waterline Line, Barge Center). Table 3.2 shows the results.

Component	**m(MT)**	**x_{cg}(m)**	**y_{cg}(m)**	**z_{cg}(m)**	**I_x(kg m^2)**	**I_x(kg m^2)**	**I_x(kg m^2)**
Platform	5,452	0.00	0.00	-0.28	7.3E+08	7.3E+08	1.5E+09
Tower	348	0.00	0.00	38.23	7.2E+08	7.2E+08	0.0E+00
Nacelle	240	-1.90	0.00	89.35	0	0	2.6E+06
Hub	57	5.00	0.00	90.00	1.2E+05	0.0E+00	0.0E+00
Rotor Blades	53	5.00	0.00	90.00	3.5E+07	3.5E+07	1.3E+06
Total	**6,150**	**0.02**	**0.00**	**7.01**	**4.8E+09**	**4.8E+09**	**1.5E+09**

Table 3.2: ITI Energy Barge mass inertia properties.

Radius of Gyration k_{xx} = 27.93 m ; k_{yy} = 27.94 m ; k_{zz} = 15.42 m ;

3.2 Potential Flow Frequency Domain Analysis

The first step in the process of analyzing hydrodynamic loads was to do a frequency domain analysis of the platform using commercial code WAMIT v5 and MDL codes HydroD and MULTIDYN. The commercial software Rhinoceros was used to generate a panel mesh of the underwater surface of the ITI Barge. A mesh size of 1m was used to generate the mesh. This size was found to give optimum convergence and computation speed. Shown in Figure 3.2 is the mesh generated by Rhinoceros software. This was stored as a gdf (geometry definition file).

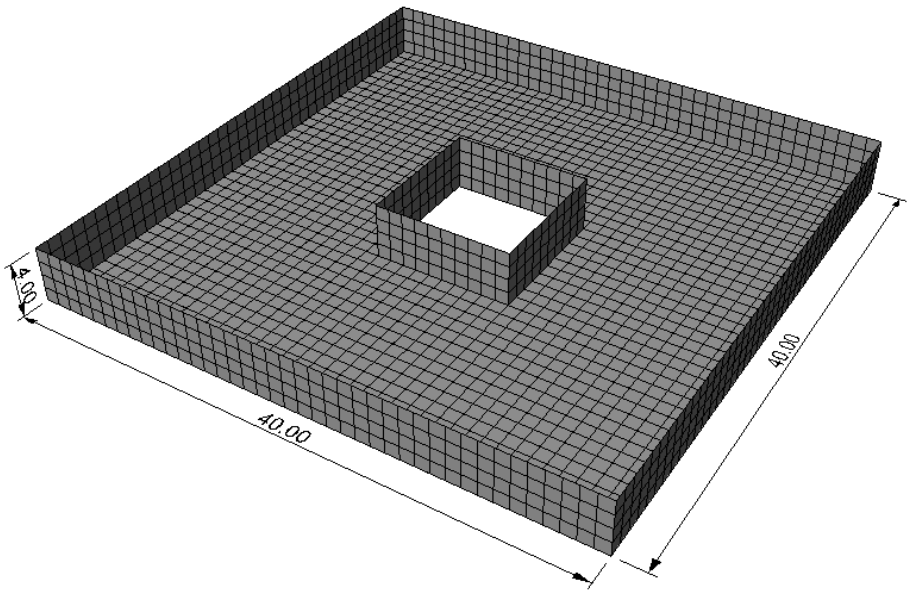

Figure 3.2: ITI Energy Barge Rhino Model without Moonpool lid

The depth of the water in which we analyze this barge is 150m. We approximate this as deep water for ease of computation. We use the infinite depth case which uses the infinite depth green function, and infinite depth approximation for waves and bottom boundary condition.

We analyze for frequency range of 0.05 to 2.20 rad/s (3 to 125 s). This includes the general wave frequency range (3 to 15 s). The frequency domain programs were run for incident wave angles ranging from 0 to 180 deg at steps of 22.5 deg.

Initially an analysis was performed without placing a lid in the moonpool. The added mass and radiation damping generated by the 3 programs (MDL HydroD, MDL MULTIDYN and WAMIT v5) are plotted out in the Appendix A Figures A.1 to A.10. Only A11 and B11 are shown here in Figure 3.3. The results show good agreement with each other. The results from MDL HydroD and MDL MultiDyn are almost on top of each other. However they also show a jump in different modes at particular frequencies. This

was identified to be caused by the excitation of the sloshing modes in the moonpool at certain frequencies. The sloshing in the moonpool acts a source of dissipation at certain frequencies.

Bandas and Falzarano[61] have previously worked on the sloshing problem for a T-Craft vessel. Liu [62] has worked on multi body problems, which involve the fluid between the bodies, using MDL MULTIDYN. The sloshing problem is to be incorporated in a future version of MDL MULTIDYN.

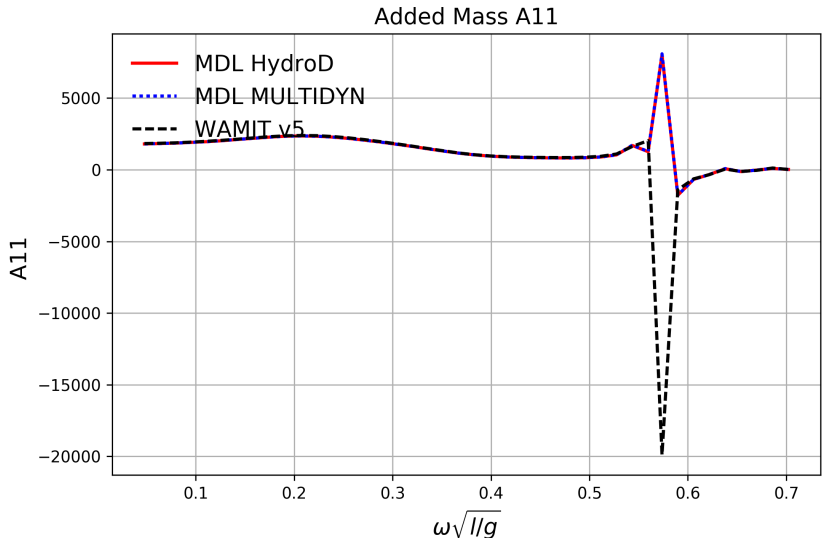

(a) Radiation Added Mass A11

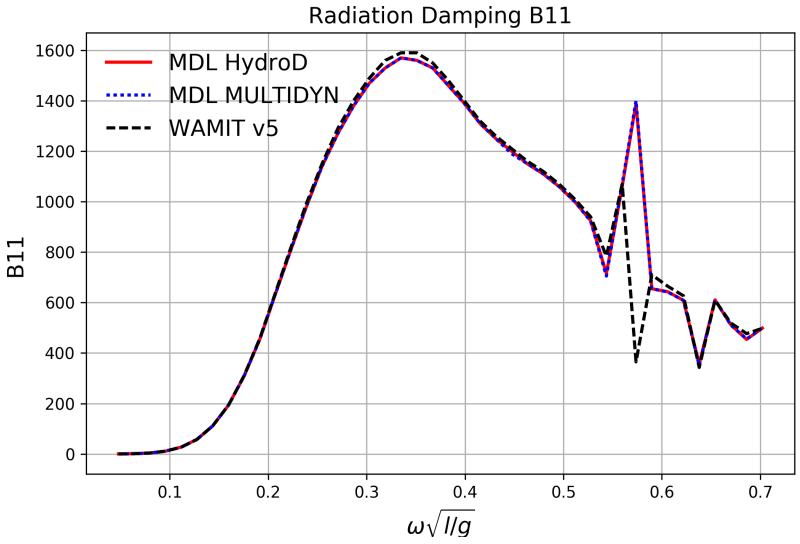

(b) Radiation Damping B11

Figure 3.3: Added Mass, Radiation Damping comparison using WAMIT, MDL HydroD and MDL MULTIDYN

Jonkman in his PhD dissertation handled the problem of sloshing by placing a lid at 0.01 m below the water surface inside the moonpool. This suppressed the sloshing modes.

Following this approach, the geometry file was modified to what can be seen in Figure 3.4. It included a lid in the moonpool at 0.01m below the water free surface.

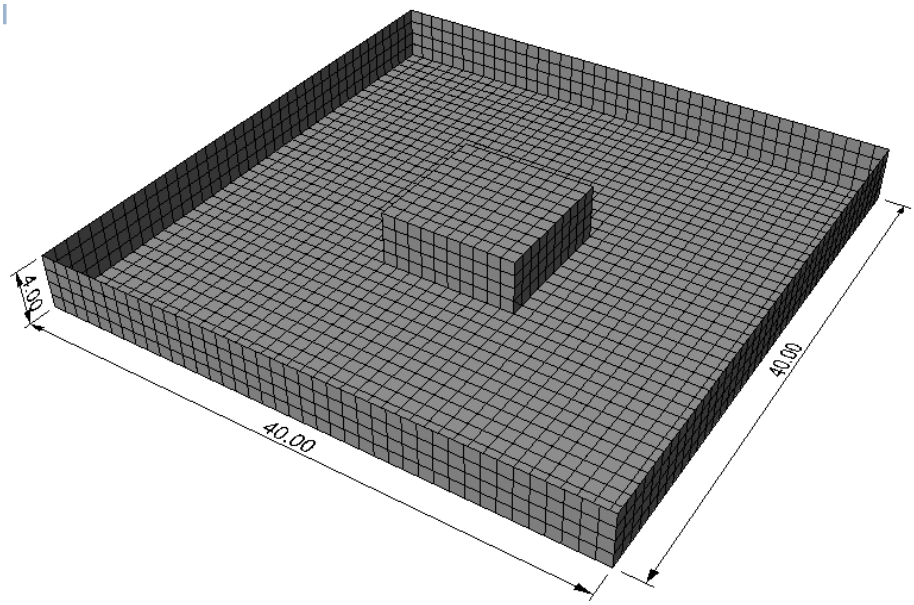

Figure 3.4: ITI Energy Barge Rhino Model with Moonpool lid

MDL HydroD was not designed to handle vessel surfaces too close to the water free surface. Doing so created numerical instabilities that resulted in incorrect results in a range of frequencies. WAMIT on the other hand has a feature called ILOG that can be set to 1, in order to handle such instabilities. MDL MULTIDYN can handle a lid problem by default.

Hence, it was decided to carry out the analysis using WAMIT and MDL MULTIDYN. These results we compared against the results obtained by Jonkman [3]. The certified test cases provided by NREL along with the FAST package includes the input files for ITI Energy Barge. This was used in obtaining the plots. These results are plotted in Appendix Figures A.11-A.20. Figure 3.5 demonstrates the results obtained for A11 and B11.

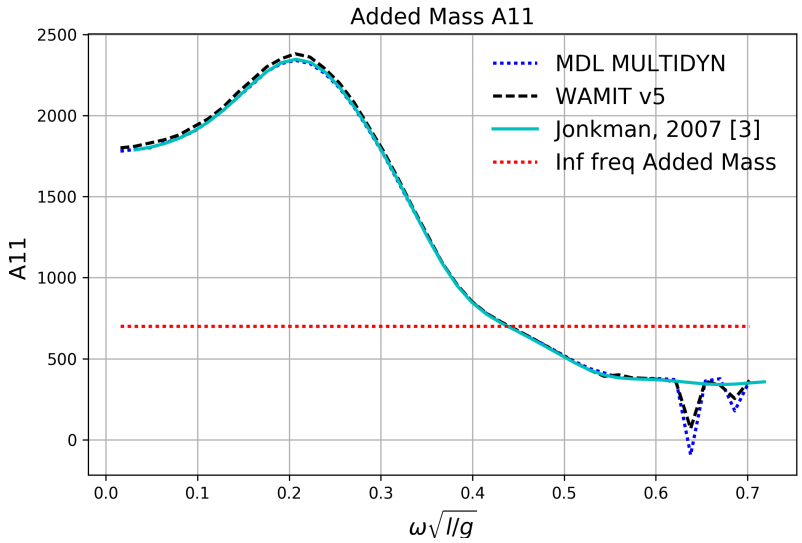

(a) Radiation Added Mass A11

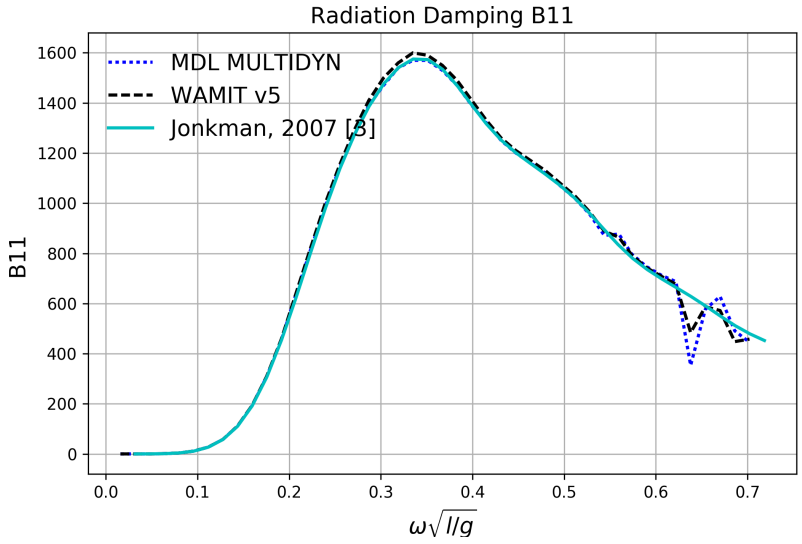

(b) Radiation Damping B11

Figure 3.5: Added Mass, Radiation Damping comparison using WAMIT, MDL MULTIDYN and published result

The following were the output files generated by MDL MULTIDYN that were used as input for the time domain simulations using SIMDYN and the coupled code FAST-

SIMDYN.

- PanelProperties.csv- Panel Properties file is a file generated by MDL MULTIDYN to indicate the numbering of panels, along with their properties
- AddedMassDamping.csv The radiation added mass and radiation damping when multiplied by motion acceleration and velocity respectively give the forces by the waves generated due to vessel motion. Section 3.1 describes how this was obtained and validated in detail.
- RAO.csv - Response Amplitude Operator as shown in 2.2.1 are the transfer functions between motion response and incident wave amplitude.
- ForceDiffraction.csv - Generated as force calculated by diffraction potential
- RadiationPressure.csv - This is the pressure on each panel for the entire vessel obtained using the radiation potential for each mode of motion
- DiffractionPressure.csv - Diffraction Pressure includes only the modification induced by the body due to incident wave obtained from the diffraction potential as described in section 2.2.1
- ForceFroudeKrylov.csv - Incident wave force obtained by integration of pressure over the hull surface. This can be used in the linear analysis of wave forces.

The geometry file for SIMDYN was redefined to include the above water portion as shown in Figure 3.6. The mesh was refined close to the free surface, to have a more accurate estimation of the nonlinear forces near the free surface.

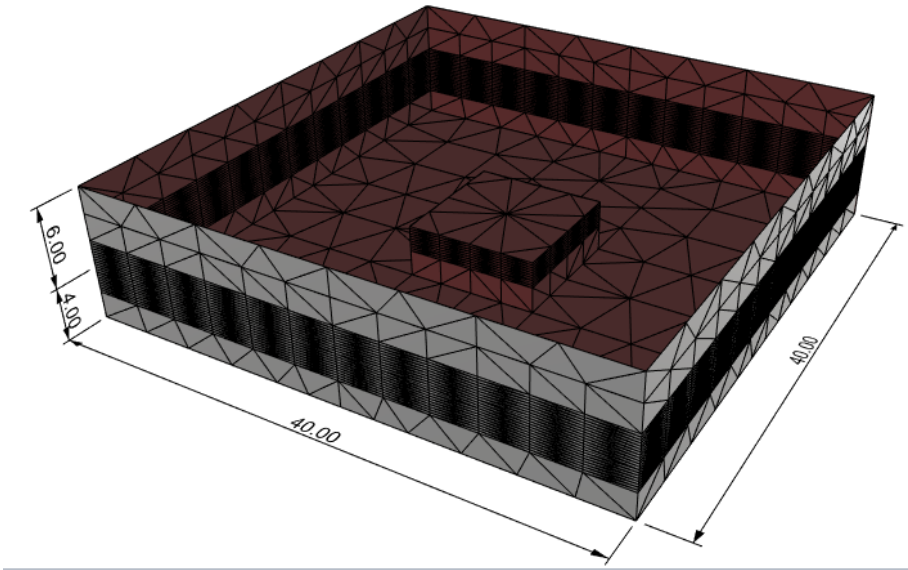

Figure 3.6: ITI Energy Barge Rhino Model used for SIMDYN

3.3 Coupling of FAST and SIMDYN

One of the longest steps was understanding how the two programs were written. They involved use of multiple modules connected to each other. SIMDYN and FAST used very different algorithms. FAST is highly modularized, with one of the modules (ie.Elastodyn) acting as the primary time domain solver. There is a lot of passing of data between modules at each time step that is carried out by another module. While SIMDYN does use modules, the main time domain solver acted as the central place which called the various modules at each step. So for the coupling to be done, it was decided to use the FAST Elastodyn as the primary time domain solver. Figures 3.7 to 3.11 show a snapshot of the overall algorithm followed in the two programs.

Both the programs had 3 common steps

- Intialization - This involved the declaration of variables, initialization of default values, and solving the zero time step. In FAST this is done as shown in Figure 3.7.

In SIMDYN, this was done in the portion shown in the blue and yellow portions in Figure 3.11.

- Time Simulation - This is the main simulation where the motions were integrated over time based on the various forces and moments acting on the platform. In FAST this involved both an intermediate step involving states shown in Figure 3.8 and the main calculation as shown in Figure 3.9. In SIMDYN, it is the green portion of Figure 3.11.

- End - This is were the variables declared are destroyed and all the open files are saved and closed. In FAST this is as shown in Figure 3.10. In SIMDYN, it is done as shown in the orange portion of Figure 3.11.

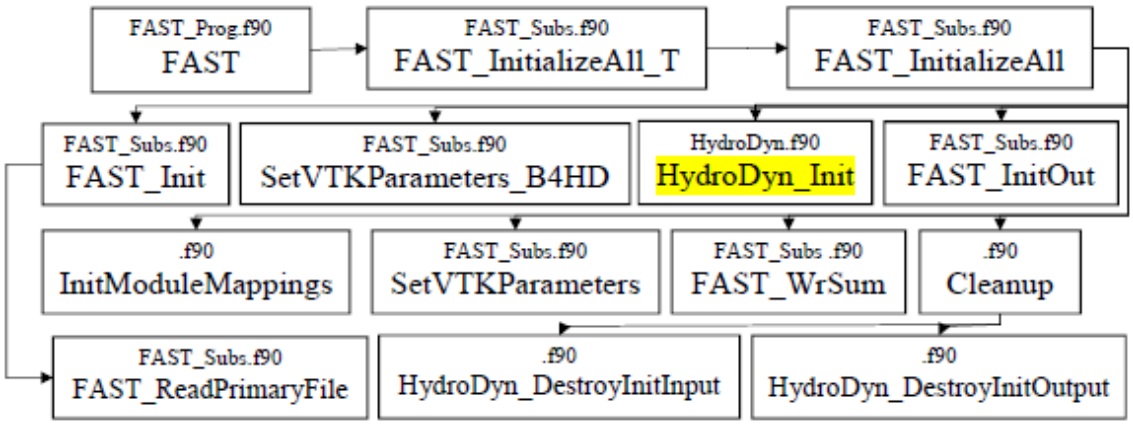

Figure 3.7: FAST Hydrodyn Initialization

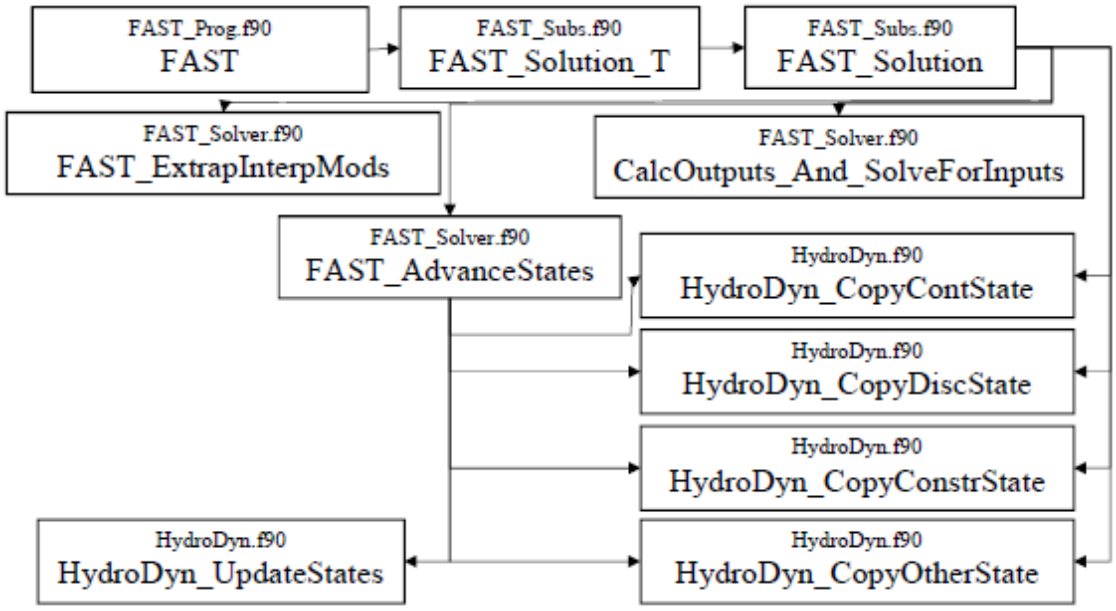

Figure 3.8: FAST Hydrodyn intermediate steps before calculations

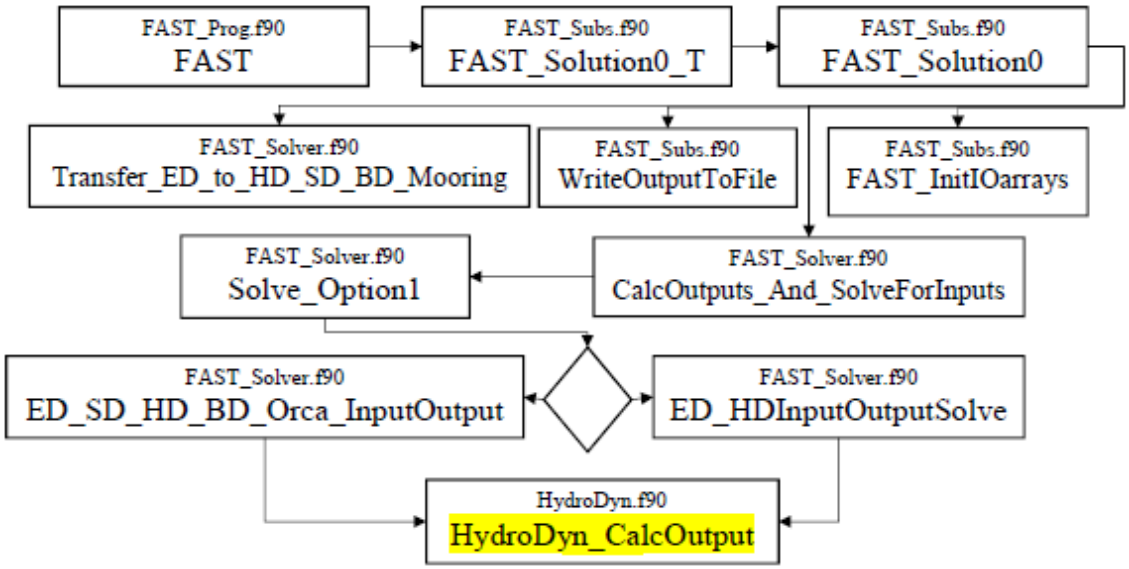

Figure 3.9: FAST Hydrodyn main time simulation Forces calculation

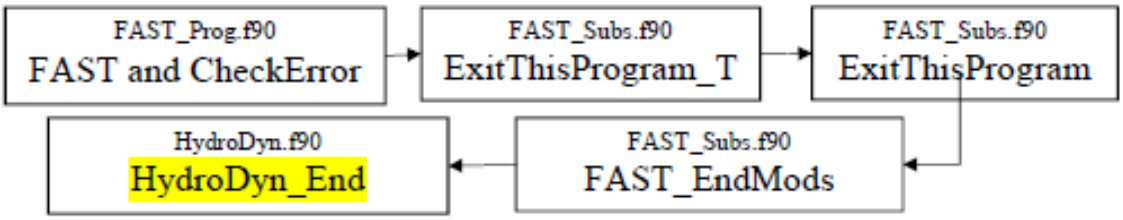

Figure 3.10: FAST Hydrodyn End

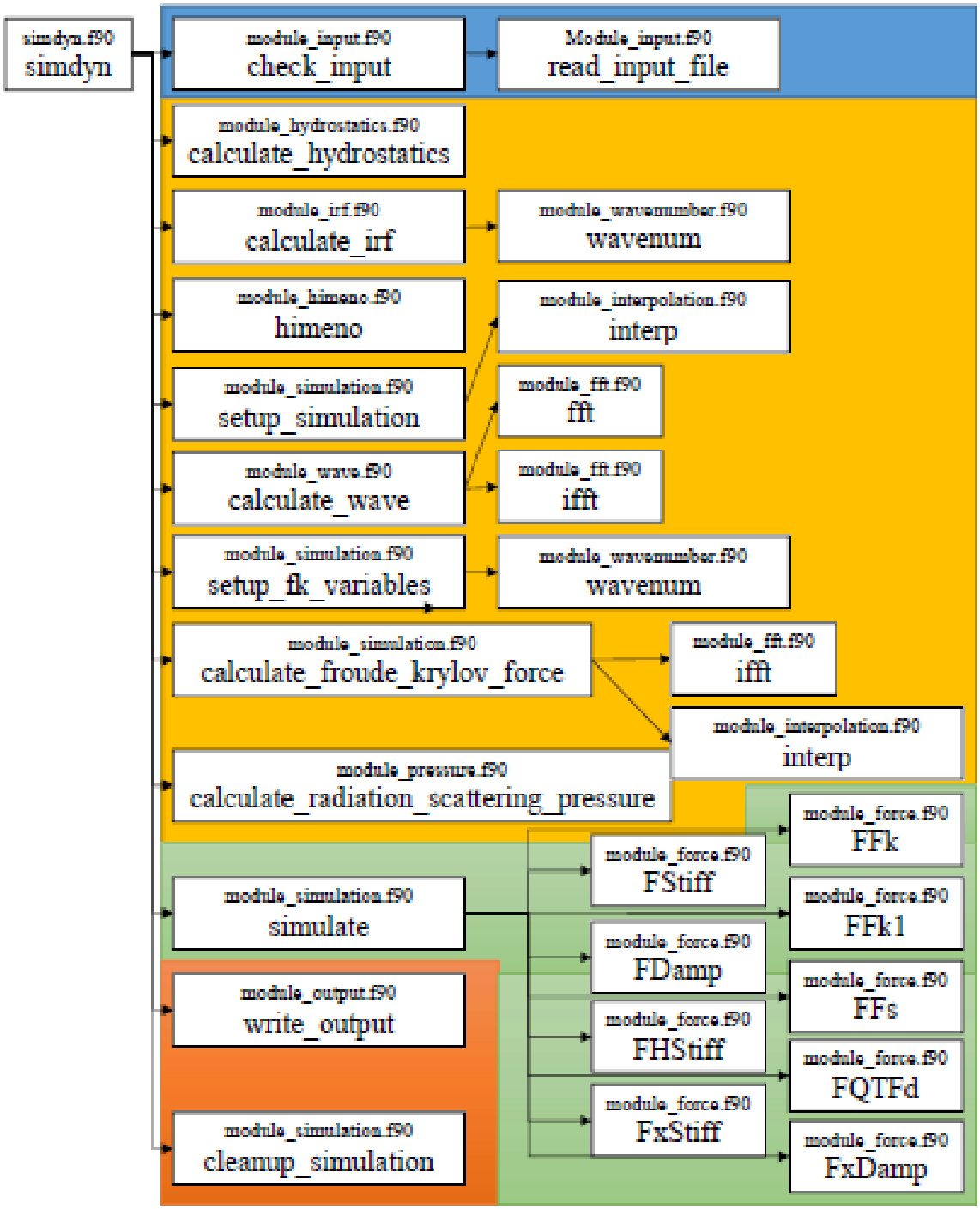

Figure 3.11: SIMDYN algorithm

The SIMDYN code was modified and grafted onto the Hydrodyn module of FAST. A number of validations were done to ensure the correctness of the coupling. This is discussed in the following section.

Both FAST and FAST-SIMDYN take the environment conditions of wind and waves as inputs along with other parameters and geometry files. The outputs are the time history of the various motions, forces and moments.

3.4 Validation of Coupling

Initially an effort was made to match the programs SIMDYN and FAST-SIMDYN, in the absence of mooring lines. Doing this would ensure that the coupling was done correctly. This way we would know that if FAST-SIMDYN gave the same results as given by SIMDYN then, we would only have to concentrate on ensuring that the input to SIMDYN was correct. These cases are shown in the Appendix. The first case was without wind or waves. This is shown in Figure B.1 and B.2. This was followed by cases with regular and irregular (JONSWAP) waves as described in Table 3.3.

The mass matrix definition and weight were accounted for in both SIMDYN and FAST-SIMDYN. This proved to be of critical importance. In SIMDYN, it was defined in the input file, and the coding was done accordingly. In the coupled program, FAST-SIMDYN, this had to be modified in order for FAST to take care of this part without double counting the mass anywhere. In essence, in FAST-SIMDYN, only the hydrostatic and hydrodynamic loads at the instantaneous position of the vessel is calculated by SIMDYN. The physical mass and inertia are accounted by FAST.

One of the other issue was that FAST was used as the main time domain solver, instead of SIMDYN. FAST used Kane's Dynamics [57] to transfer forces and moments between different modules. The main program in SIMDYN was in itself a time domain solver. So in order to couple, the original SIMDYN program had to be altered so that only the

hydrodynamic loads had been input in the same manner as Hydrodyn module in FAST. For instance the radiation added mass term had to be taken to the right hand side. The small time step used in FAST and possibly the algorithm used in the time domain solver ensured a stable solution even after doing this.

By now, it was ensured that the time integration of the motions in SIMDYN and FAST-SIMDYN, in the absence of mooring was established right. Next step was to ensure that the coupled code compared well against FAST at least in the linear case. Initially the mooring module to be used needed to be chosen. The results from MAP (Mooring Analysis Program) was compared with those from FEAMooring (another module for Mooring which involved more resolution). The results from FEAMooring looked more reasonable, as the surge motions using MAP was higher. Hence FEAMooring was chosen. Again, to validate FAST and FAST-SIMDYN results were compared for cases without wind, in zero wave, regular wave and irregular wave. These are summarized in Table 3.3 and the plots are shown in the appendix.

The controller used in the default input file had modified the controller gains to avoid the occurrence of negative damping [63]. This was modified back to the original values for the purpose of demonstration of negative damping.

Initially the zero load case caused the vessel to heave down a little due to the mooring lines. This was offset to zero, because the frequency domain analysis was conducted for a zero trim and heave equilibrium case.

Some of these cases that were used for validation are shown in the appendix as listed in Table 3.3. Then, the cases with the presence of uniform steady wind (uniform in space, steady in time) were studied systematically.

Case	Figure	Mooring?	Wind speed (m/s)	Regular/ JONSWAP	Wave Height (m)	Wave Period (s)	Description
1	B.1 & B.2	No	0	Regular	zero	-	SIMDYN vs FAST-SIMDYN
2	B.3 & B.4	No	0	Regular	1	7	SIMDYN vs FAST-SIMDYN
3	B.5 & B.6	No	0	JONSWAP	1	7	SIMDYN vs FAST-SIMDYN
4	B.7 & B.8	MAP/ FEA	0	Regular	1	7	MAP vs FEA
5	B.9 & B.10	FEA	0	Regular	zero	-	FAST vs FAST-SIMDYN
6	B.11 & B.12	FEA	0	Regular	1	7	FAST vs FAST-SIMDYN
7	B.13 & B.14	FEA	0	JONSWAP	1	7	FAST vs FAST-SIMDYN
8	B.15 & B.16	FEA	7	Regular	1	7	FAST vs FAST-SIMDYN
9	B.17 & B.18	FEA	11.4	Regular	1	7	FAST vs FAST-SIMDYN
10	B.19 & B.20	FEA	17	Regular	1	7	FAST vs FAST-SIMDYN
11	B.21 & B.22	FEA	17	Regular	2	7	lin vs nonlin FK

Table 3.3: List of validation plots in Appendix

4.1 Background

In this chapter, we introduce the concept of negative damping and describe how it is relevant to FOWT and study the role of wave and wind on the motions caused by it.

Figure 4.1 shows the plot of the traditional control used in wind turbines. This is from the definition of 5 MW wind turbine by NREL for use in offshore environment [60]. As wind speed increases until the rated wind speed, the controller leaves the blade pitch angle to zero and operates to generate maximum power. Above the rated wind speed, the controller saturates the power output by adjusting the blade pitch and thereby reducing the wind force on the blades.

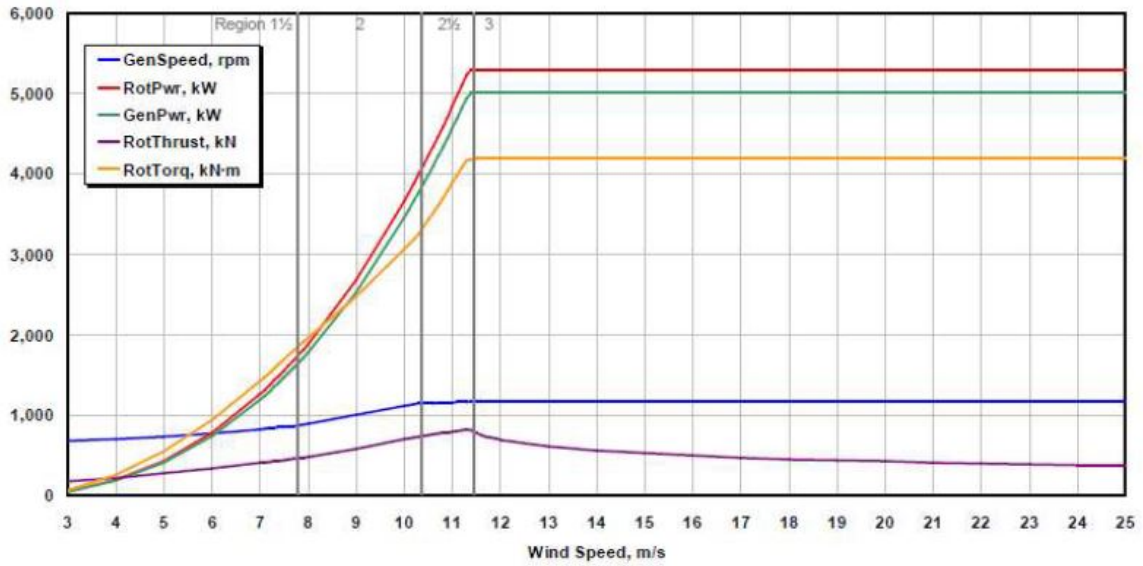

Figure 4.1: Control definition for NREL 5MW Wind Turbine (Reprinted from Jonkman et.al, 2009 [60]

4.2 Negative Damping Using FAST-SIMDYN

Constant power generation controller when applied to floating wind turbines results in instability as demonstrated below. In our study, only the effect of a steady uniform wind is being studied. For wind speeds below the rated wind speed, motions of the platform are dominated by waves. But above the rated wind speed of about 11.4 m/s, negative damping starts exciting the platform pitch natural mode of motion. Shown in Figure 4.2-4.3, are the motions of the barge in the presence of a 7s wave period 1m wave height regular wave in varying wind speeds. For low wind speeds, wind only causes static offsets in surge and pitch modes of motion. At these low wind speeds, waves dominate the dynamic motion response in all modes as can be seen.

But above the rated wind speed, the controller starts to excite the platform pitch mode of motion. Due to the coupling between platform pitch and platform surge modes, even the surge mode oscillates at the natural frequency of pitch. The Heave mode, however, is virtually unaffected by wind.

The power generated by the wind turbine is dependent on the wind speed experienced at the rotor. Traditional shore based controllers try to maintain a constant power supply to the grid. In order to achieve this, the blade pitch angle is adjusted so that the lift generated by the blades provides the required power. In the process, there is a horizontal force exerted by the wind on the rotor hub and on the tower. This force is related to the wind speed at the rotor hub. In the case of floating wind turbines, this force acts as a platform pitching moment. As it is floating, the platform begins undergoing pitching motions. The platform pitching motion causes a change in the relative wind speed experienced at the rotor hub. This is directly related to the pitching motion angular velocity and the surge velocity. The pitching moment applied by the wind also starts to vary due to a controllers that try to maintain constant power. This platform pitching moment is therefore related

to the platform pitching velocity. It serves to increase the motions. That is why this phenomenon came to be called negative damping. An analytical analysis, as described above, was done by Jonkman [31].

When we take a closer look at the energy spectrum in Figures 4.4-4.5, it is interesting to note that the contribution of waves to the motion of the barge remains unchanged with a change in wind speed and control. The spectrum in all the cases shows a distinct unchanging peak at the wave frequency (i.e. 0.14 Hz).

In the negatively damped cases for wind speeds above the rated (11.4m/s), the response spectra indicates the presence of a new peak at the pitch natural frequency (about 0.06 Hz). Again the surge mode also shows a peak at the same frequency. The spectrum shows a very strong coupling between the platform pitch and surge motions. This is understandable as there is very little stiffness in the surge direction. However the pitch mode has significant stiffness induced by the restoring moment from the water. This results in a transfer of energy to the surge mode.

It was also noted that above wind speed of 16m/s, the motions suddenly go to a smaller steady state motion as compared to those between 12 and 16 m/s. This phenomenon was investigated in Section 4.4.

As discussed in the introduction, there was an idea that there is a possibility of high surge motions near the rated wind speed. This is investigated in the following section 4.3.

The platform sway, roll and yaw are not as significant, in the cases being analysed in our study. Therefore in the following sections, we will be showing only the results for platform surge, heave and pitch motions.

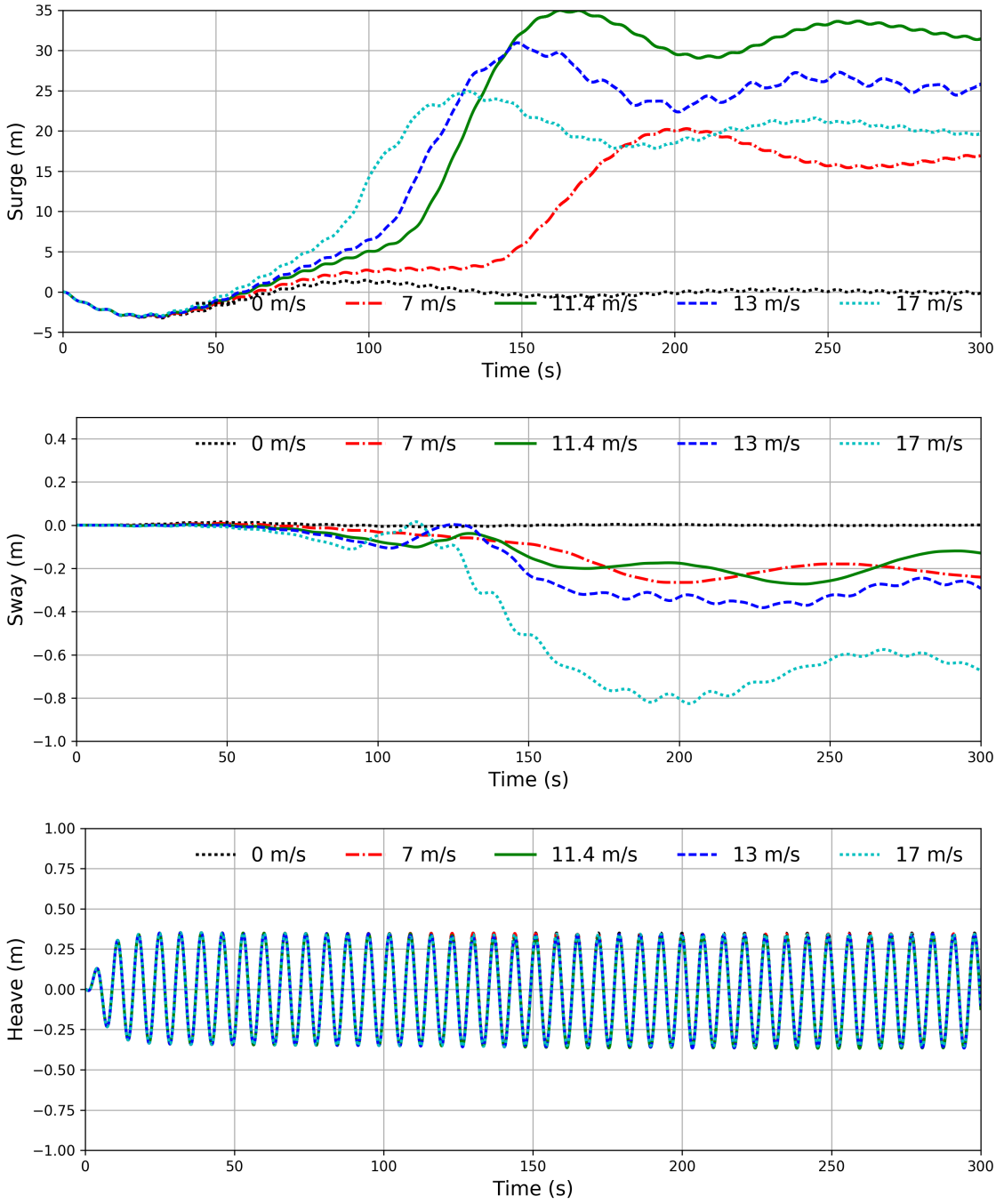

Figure 4.2: Translation motion response in 0 to 17 m/s wind 1m 7s regular wave Linear Hydrodynamics

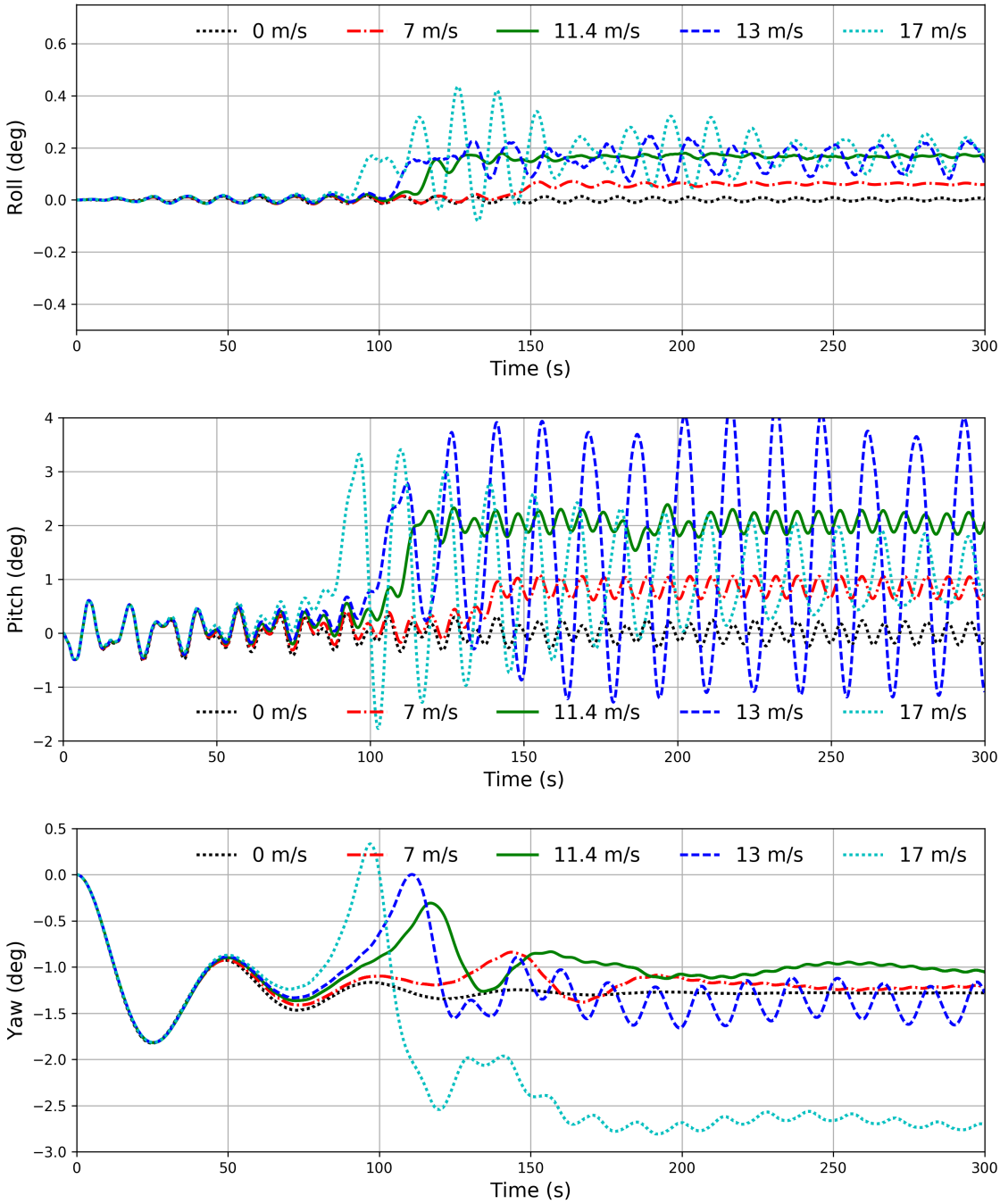

Figure 4.3: Rotation motion response in 0 to 17 m/s wind 1m 7s regular wave Linear Hydrodynamics

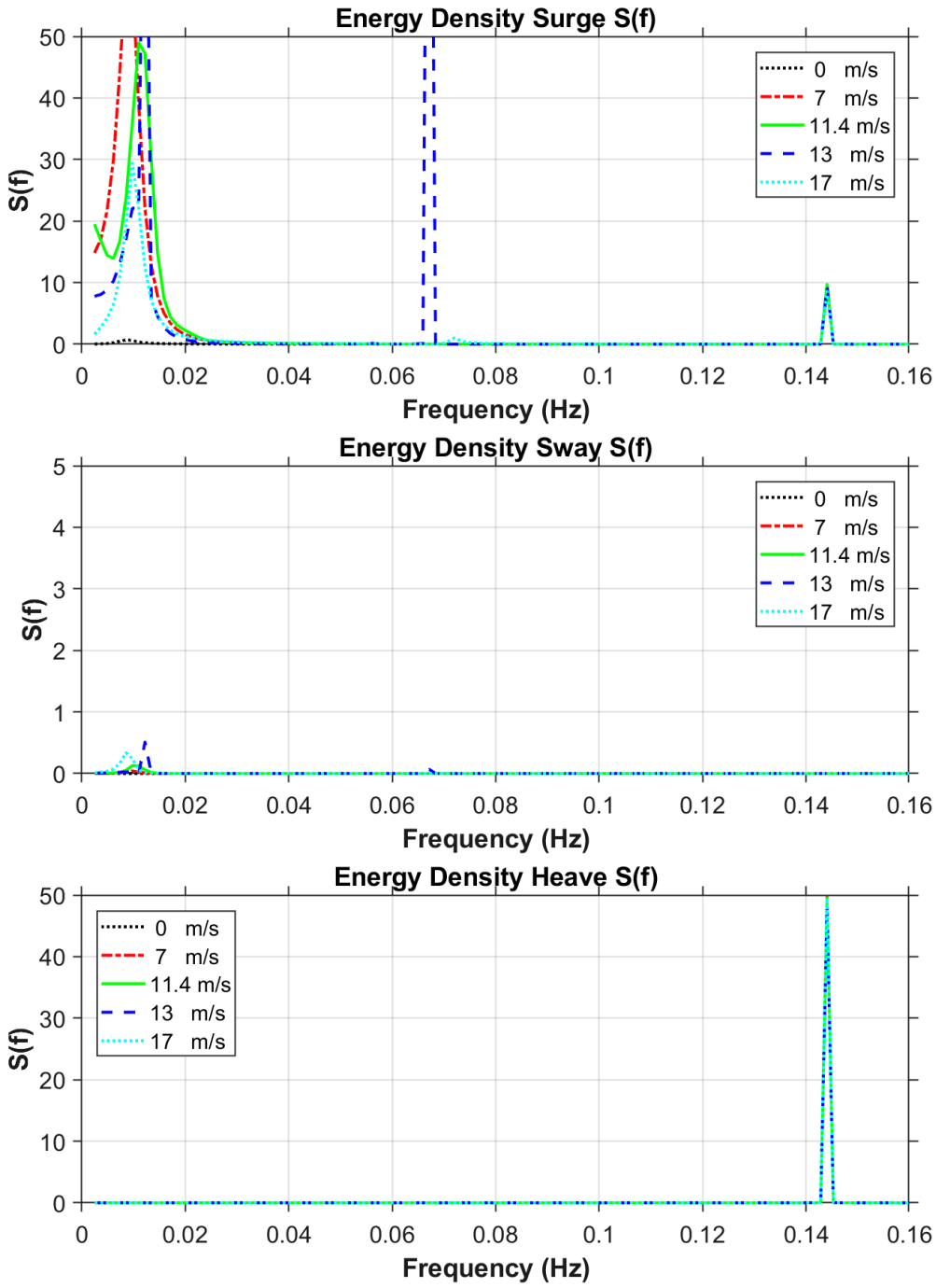

Figure 4.4: Development of negative damping Surge, Sway, Heave Spectrum Linear Hydrodynamics

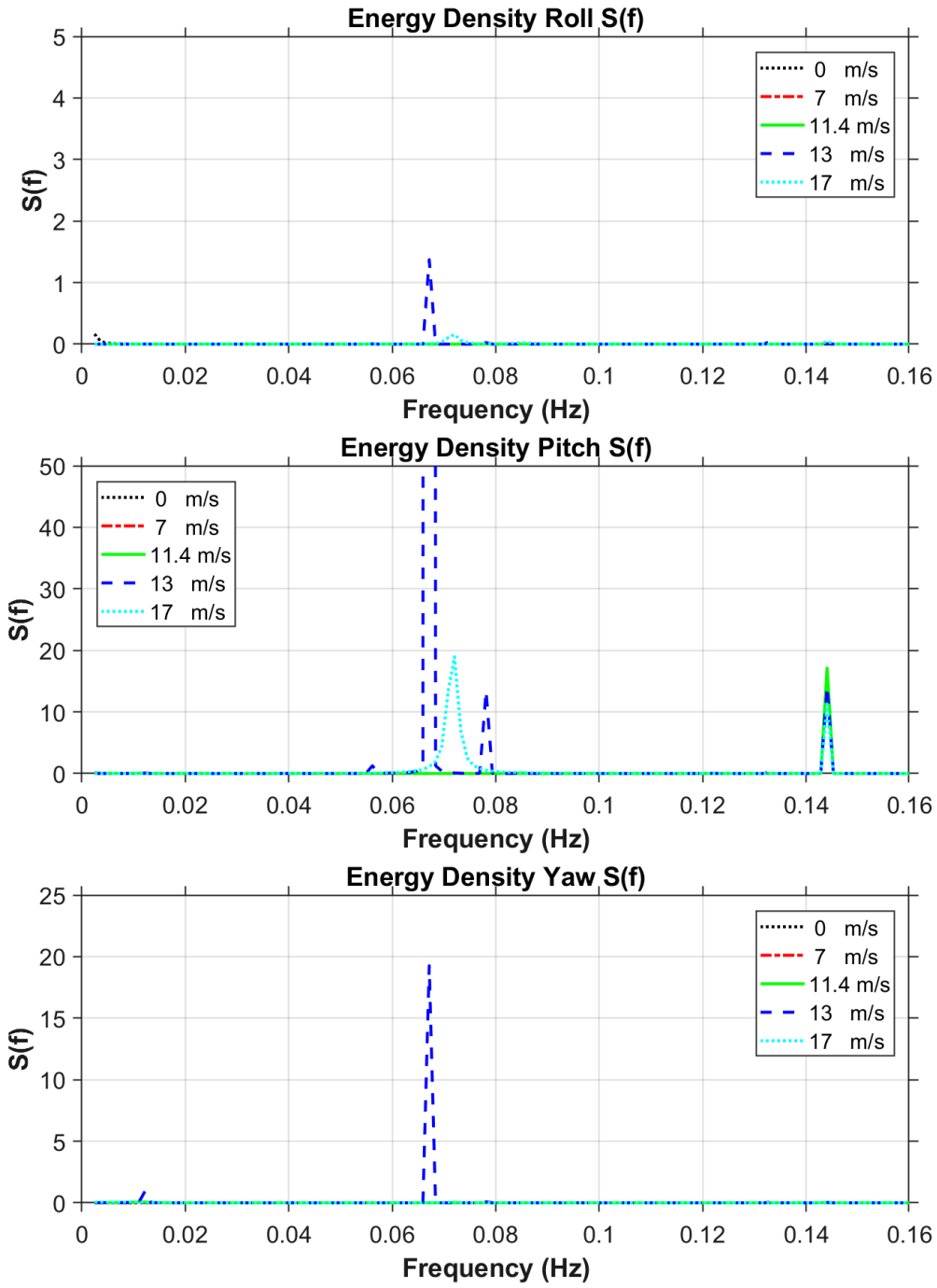

Figure 4.5: Development of negative damping Roll, Pitch, Yaw Spectrum Linear Hydrodynamics

4.3 Large Surge Motions Near Rated Speed

The relative velocity at the wind turbine hub keeps changing due to the pitching motion due to the waves. In the frequency range close to the rated wind speed, this change causes the controllers to switch between the maximum power and the constant power control. This periodic switching acts as an exciting factor for the surge motion. The switching acts like a push given to a swing at the end of each oscillation causing the amplitude to constantly rise. This explains the peak in surge at the surge natural frequency (0.01 Hz) for wind speeds close to rated wind speed (11.4 m/s).

To demonstrate this effect, simulations were carried out for wind speeds between 11 and 12 m/s at steps of 0.2 m/s. The results are shown in Figures 4.6 an 4.7. At wind speed 11.6m/s there is sharp increase in the surge motions. It is evident that the surge motions die down above and below this speed. Hence, the controllers have to be modified to have a smooth transition from one control algorithm to another.

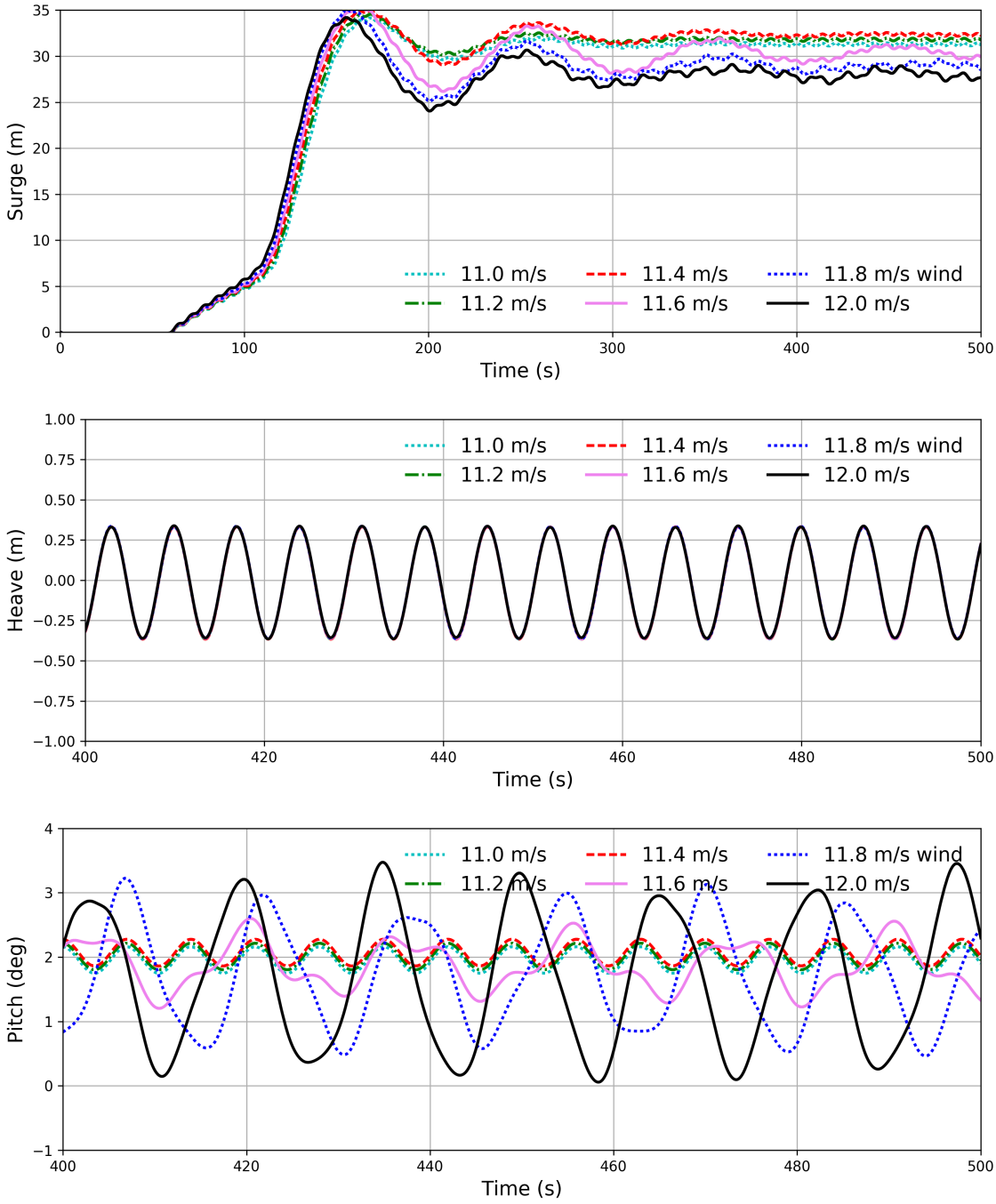

Figure 4.6: Surge, Heave, Pitch motion response in 11 to 12 m/s wind 1m 7s regular wave

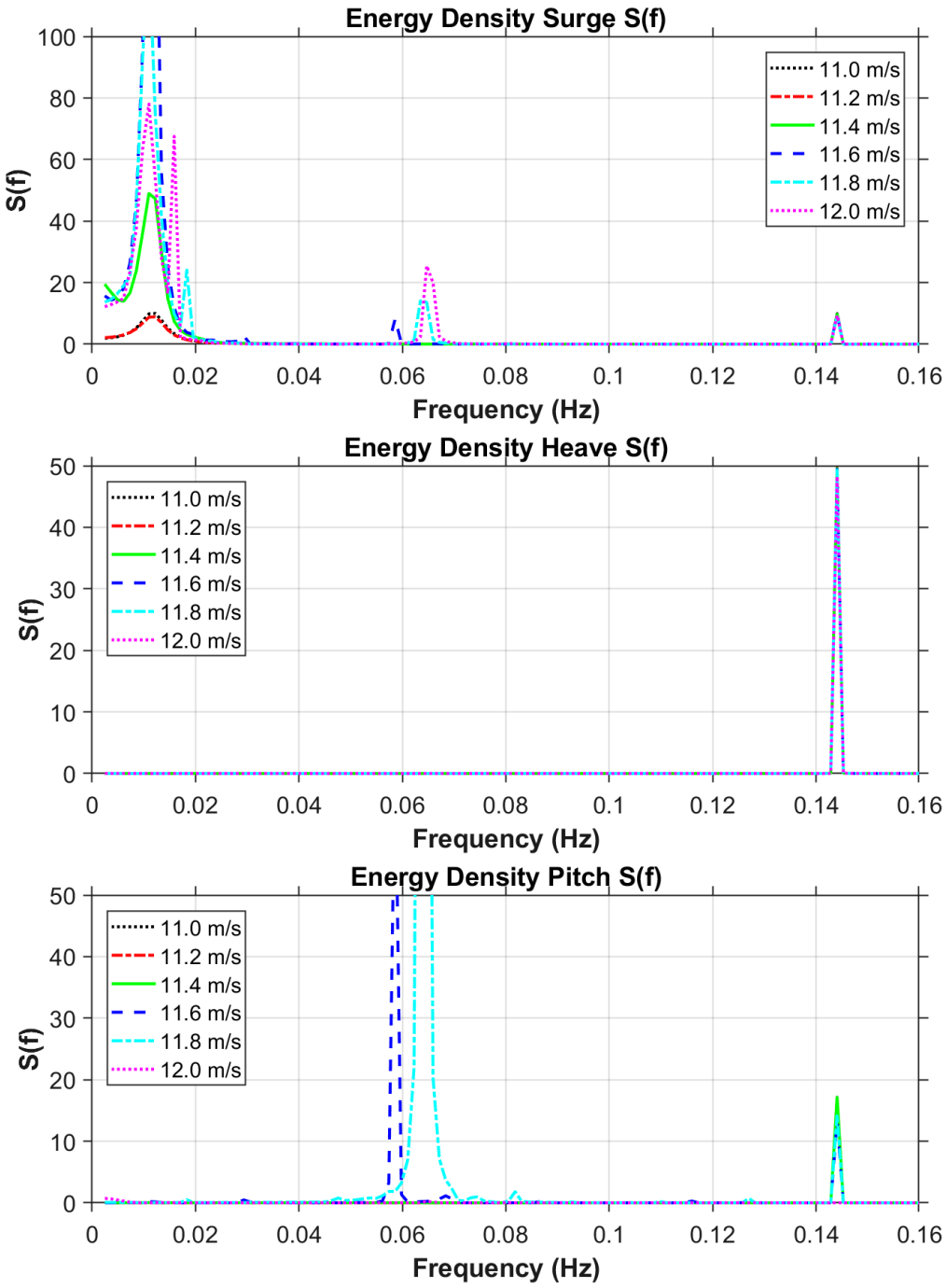

Figure 4.7: Surge, Sway, Heave Spectrum near rated wind speed

4.4 Jump Bifurcation

In section 4.2, we observed that the platform pitch amplitude for a wind speed of 13 m/s at steady state was significantly higher than that observed for 17m/s. In order to understand this a detailed analysis was conducted in the range of wind speeds between 12 and 17 m/s. Shown in Figure 4.8 are the time series of the simulations in the same range (12 - 17 m/s wind speed). We are primarily concerned about the platform surge and platform pitch. As was observed earlier, the coupling between the two is very significant.

The time series show that there is a significant difference in the pitch motion amplitudes exhibited by wind speeds from 12 to 15 m/s, compared to 16 and 17 m/s. This is confirmed by the spectrum in Figure 4.9. The energy in the platform pitch natural mode, as well as that in platform surge at pitch natural frequency are significantly higher in 12-15 m/s compared to 16-17 m/s. Based on our discussion in Section 4.2, we ask the question of whether the switching of controller algorithms at 11.4 m/s affects the platform pitch mode as well in the said range.

In order to study this, we need to first understand that controllers operate based on wind speed at the rotor hub. A pitching motion of the platform, combined with the surge motions would invariably change the relative speed of wind experienced at the rotor hub. Shown in Figures 4.10 and 4.11 are the changes in relative velocity at the hub due to the platform pitch and surge motions for 13 m/s wind and 16 m/s wind speed respectively. In the case of wind speed 13 m/s, the relative wind speed falls below the rated wind speed (11.4 m/s) every once in a while. This causes a change in controller algorithm and destabilizes it to a large amplitude pitch oscillations. But by the time the wind speed reaches 16 m/s, it is free from the controller transition zone. There is still negative damping occurring, which excites the platform pitch frequency, but it is significantly lower than that caused by the transition zone.

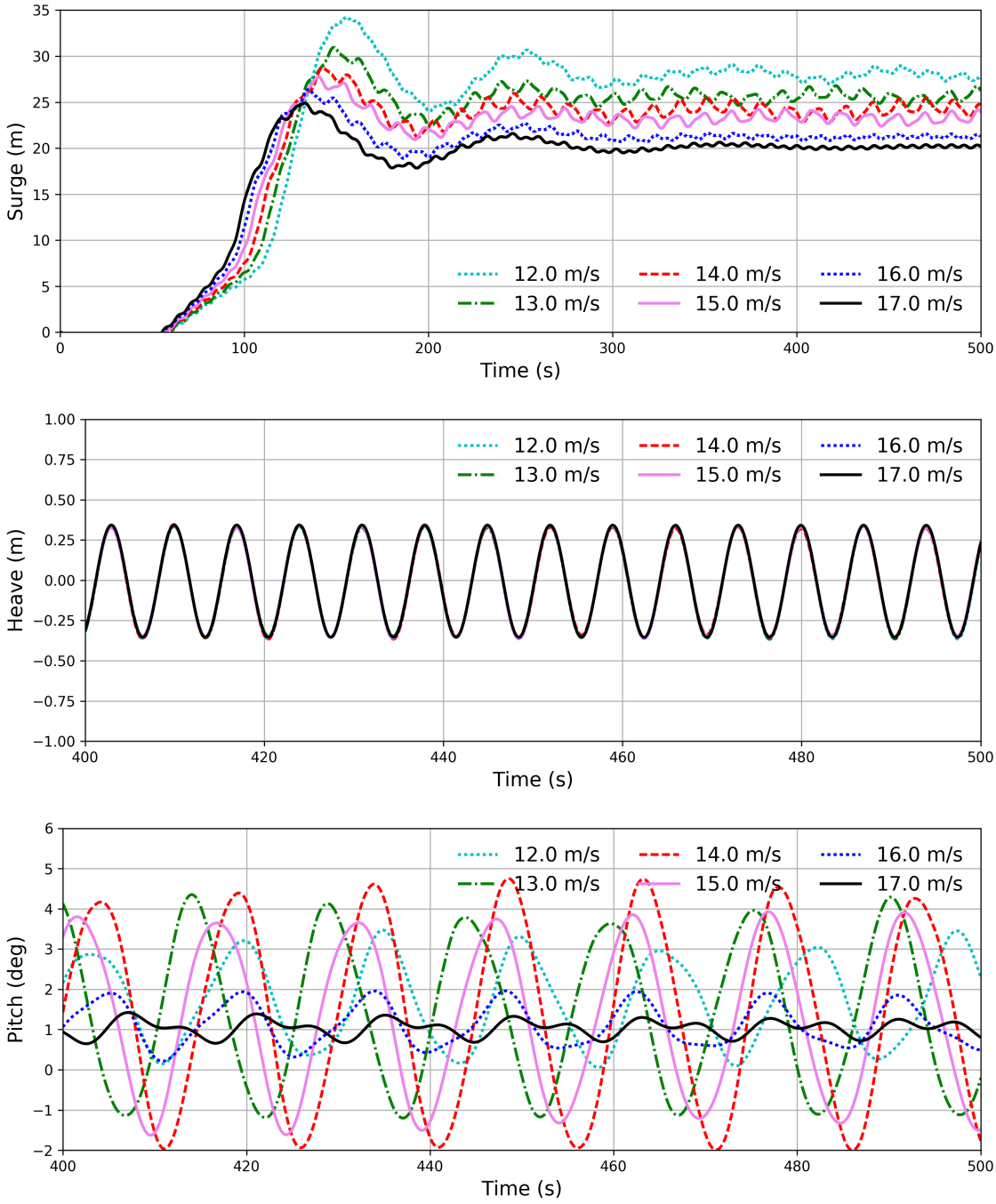

Figure 4.8: Surge, Heave Pitch motion response in 12 to 17 m/s wind 1m 7s regular wave

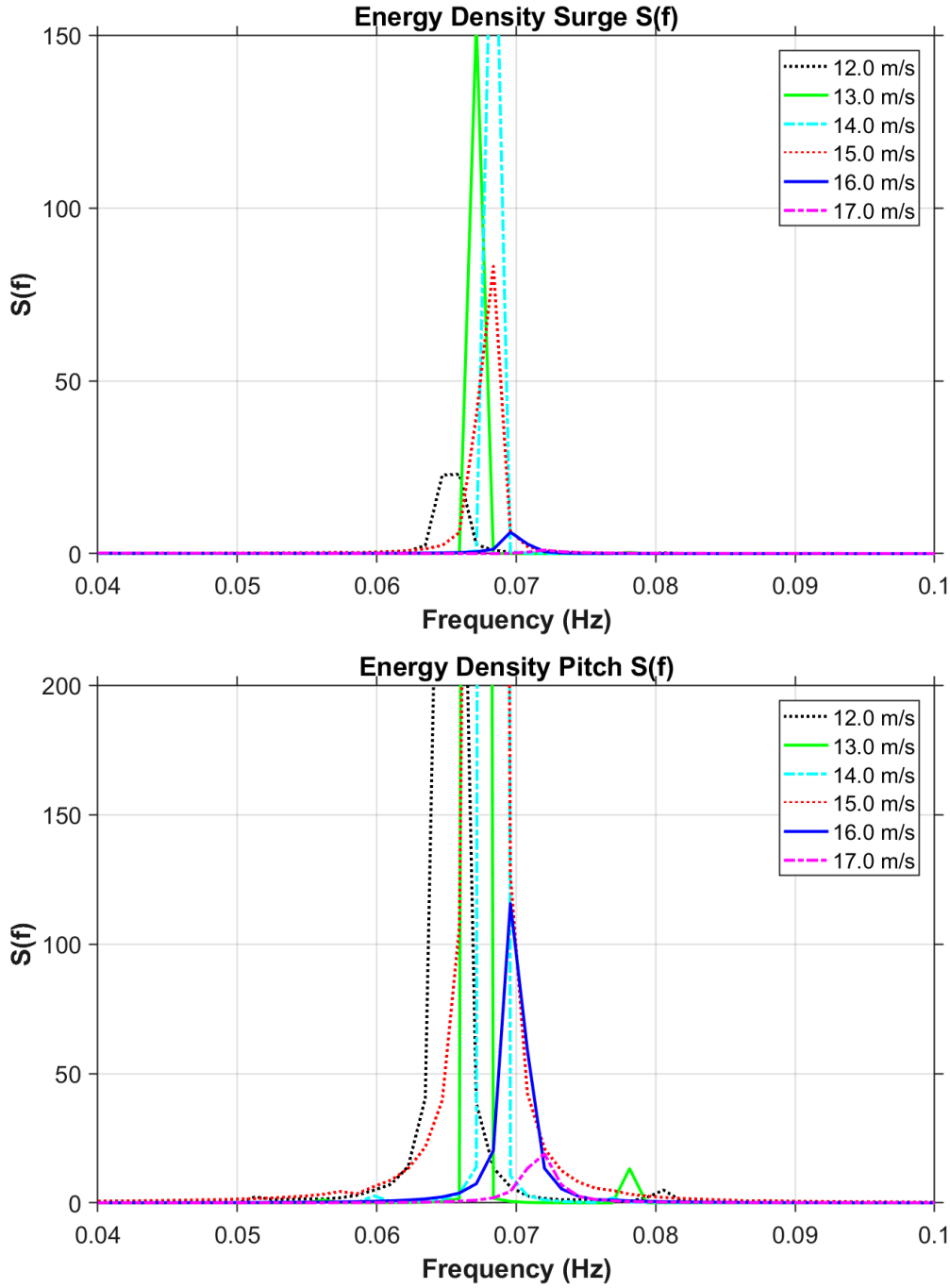

Figure 4.9: Surge, Pitch Spectrum 12-17m/s wind

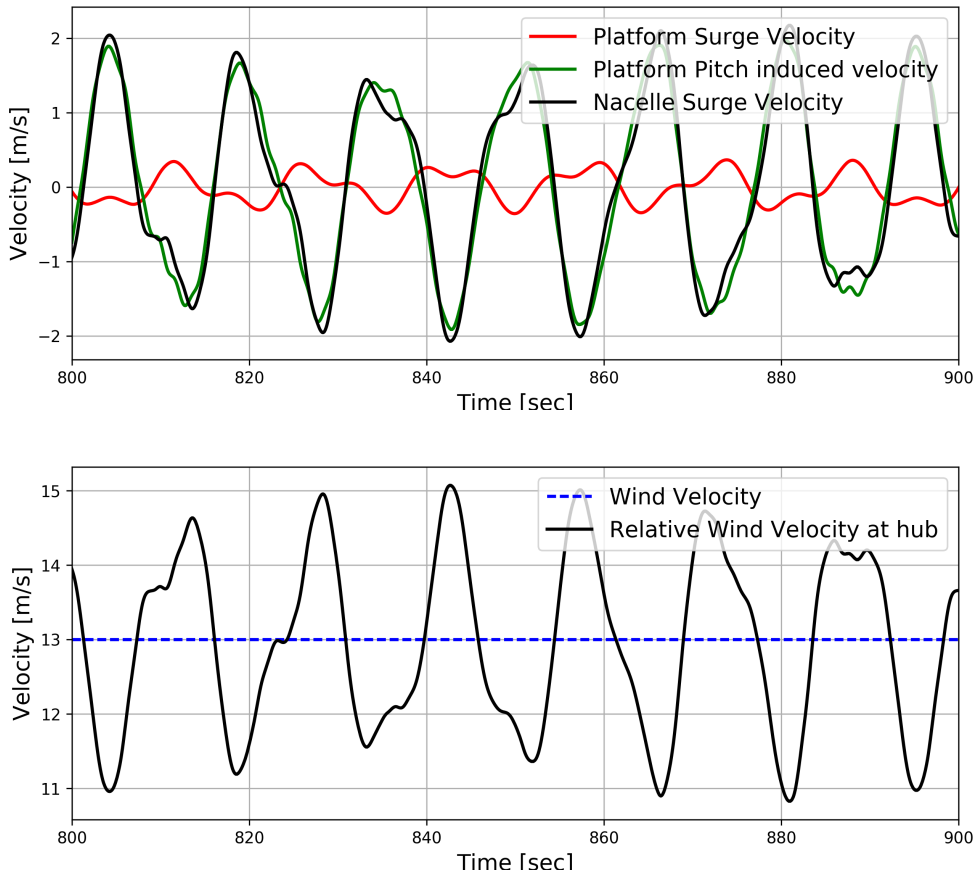

Figure 4.10: Platform Surge, Pitch induced relative velocity change at Rotor hub 13.0 m/s wind

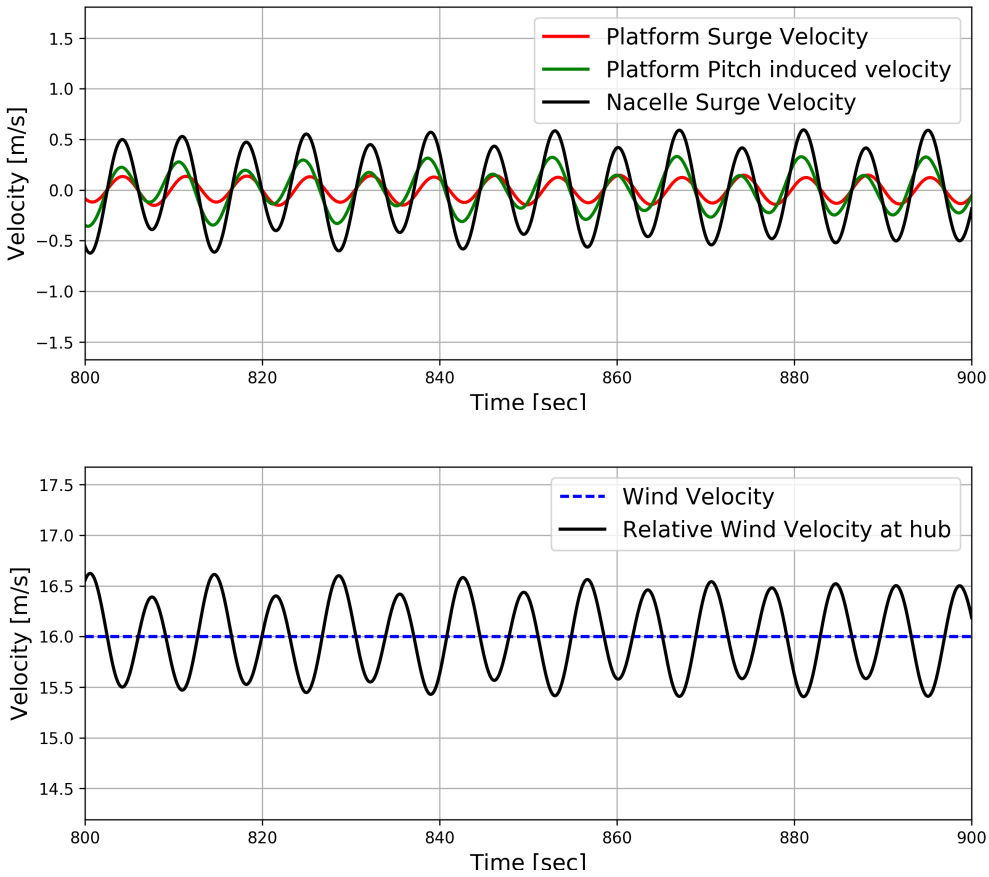

Figure 4.11: Platform Surge, Pitch induced relative velocity change at Rotor hub 16.0 m/s wind

Linear systems show distinct resonance frequencies as shown in Figure 4.12a. They occur at a single frequency, and depending on the damping, may result in high amplitude motions close to the resonance frequency. The system behavior is very much dependent on the frequency of excitation and system natural frequency. But there are some systems like the duffing oscillator, which shows a hardening spring behavior as shown in Figure 4.12b. The backbone of the resonance peak, compared to an equivalent linear system, is bent. As can be seen there is range of frequencies over which there are 3 possible amplitudes of vibration, 2 of which can be stable. These are called Orbital Equilibrium States (OES). If

there are 2 stable OES for the same frequency, then the OES at which the system vibrates or oscillates depends on the initial conditions.

The jump phenomenon or jump bifurcation is observed when we vary the frequency of excitation. As shown in Figure 4.12b, if we start at a low frequency and keep increasing the frequency of excitation, at a certain point, the amplitude of oscillation suddenly jumps down. Similarly, if we approach in the opposite direction, i.e. decrease the frequency of excitation, there is a jump up at a different frequency. So, the amplitude of system vibration depends on the initial path through which it was excited. Depending on that, the system oscillation amplitude can be one or the other.

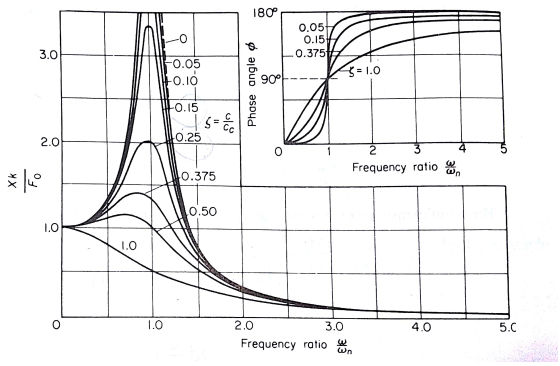

(a) Linear

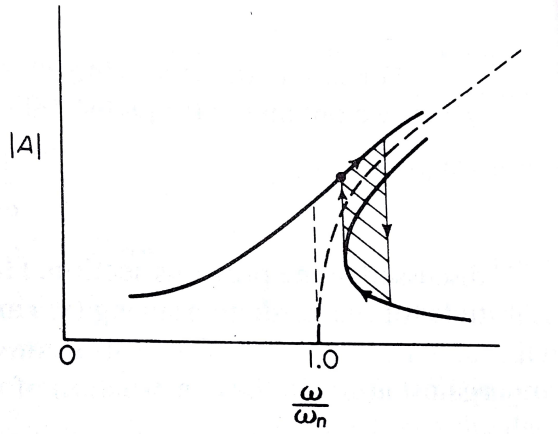

(b) Non-linear: Jump phenomenon in a hardening spring

Figure 4.12: Linear vs Non-linear dynamic amplification curves (Reprinted from Thomson and Dahleh 1998 [64])

In our case, we expect a similar behavior, except, the parameter used is wind velocity instead of frequency. What we were interested in is if we could observe a jump type bifurcation as shown in Figure 4.13. If we begin our system excitation at a low wind velocity, we expect it to go to the higher amplitude OES. But if we decrease the wind velocity from a high enough value, we expect the system to go to a low amplitude OES over a larger range of wind speeds. The sudden jump in the amplitude of platform pitch oscillation

between 15 and 16 m/s in Figures 4.8-4.9 is what suggested a jump type bifurcation.

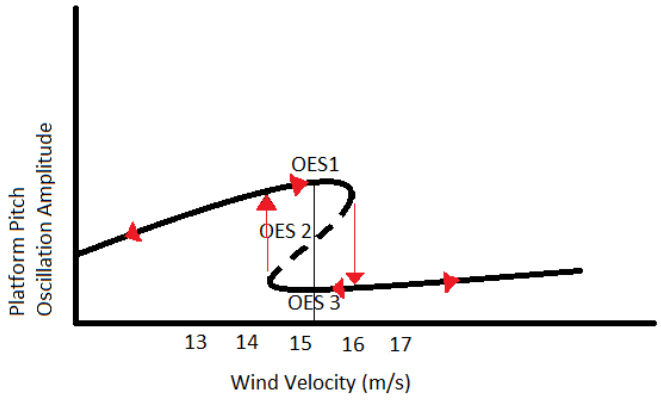

Figure 4.13: Expected Bifurcation

In all the cases we analyzed previously, we used an initial ramp for the wind speed in which the wind speed would steadily increase from 0 to the required speed in a certain amount of time (100s). This would make the platform go through the controller transition phase every time. This would cause large platform excitations for wind speeds as high as 15 m/s, which is quite far from the controller transition zone. In order to investigate, we analyzed 2 cases. The first one is a steadily, slowly increasing wind speed and the second is a case with slowly decreasing speed. These are shown in Figures 4.14 and 4.15 respectively.

As is evident from the plots, in the region between 11 m/s and 20 m/s wind speed, there is significant difference in the motions observed, depending on whether the relative wind speed passes through the controller transition zone. As long as the platform is initially undergoing steady motions which are low amplitude, the platform pitching velocity does not trigger the transition of controller. Once the controller transition is triggered at any

point there is a very high possibility of the system jumping into the higher amplitude stable OES.

Figure 4.14 shows a large region over which the motions are of high amplitude. This is because the wind speed passes through the controller transition zone. It dies down eventually when the wind speed is high enough above the rated wind speed. In Figure 4.15, after the initial transients, the motions are very low. These stay low for a larger range of wind speeds. The platform pitching picks up again at wind speed very close to the rated wind speed. Below the rated wind speed, the motions die down again.

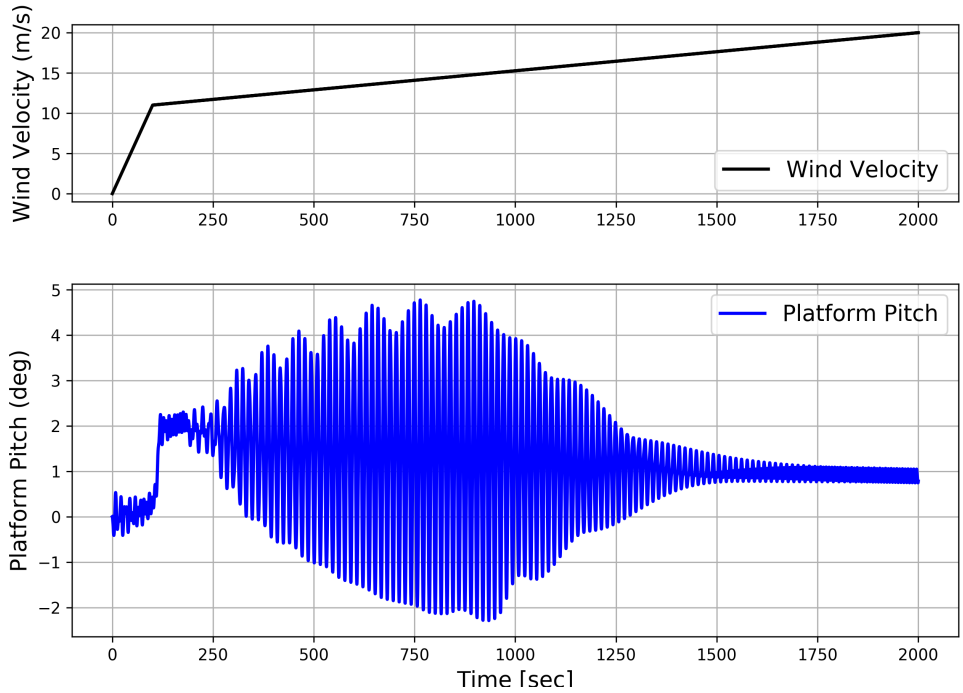

Figure 4.14: Platform Pitch variation with wind speed increasing from 11 to 20 m/s

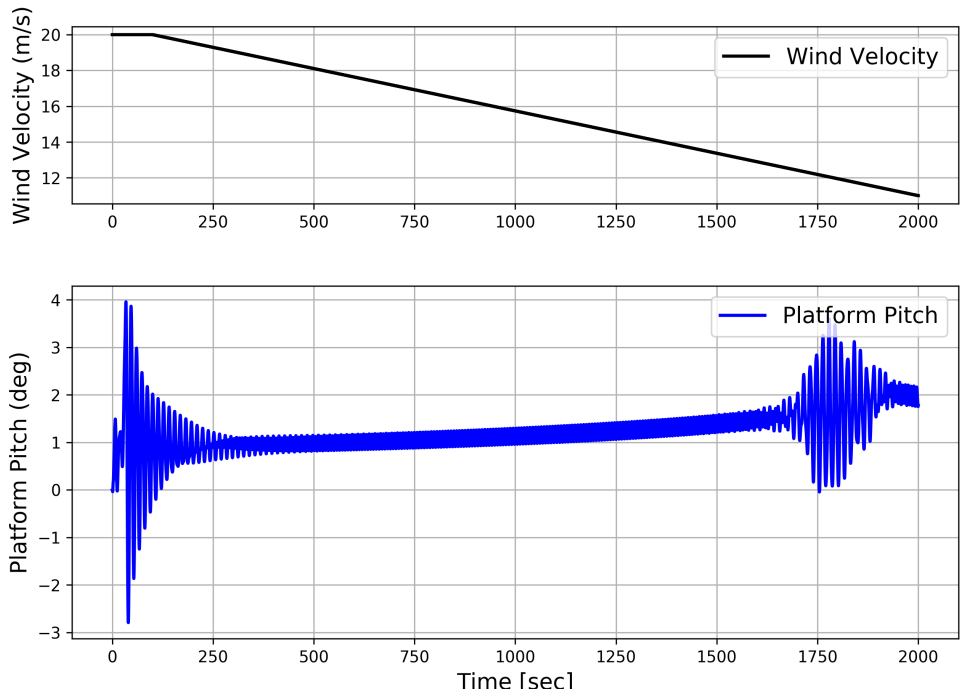

Figure 4.15: Platform Pitch variation with wind speed increasing from 20 to 11 m/s

To confirm this theory we need to find a wind speed that exhibits 2 stable orbital equilibrium states as expected from the discussion before. Such a wind speed was 15 m/s. Figures 4.16 and 4.17 show the 2 distinct steady state behaviors observed for the same wind speed. When the wind approaches from 0 m/s it the platform jumps to a higher amplitude OES. But, when the wind speed approaches from 20 m/s, the platform goes to a lower amplitude OES instead. The lower amplitude OES (1 deg platform pitch amplitude) is about 5 times less compared to the higher amplitude OES (5 deg platform pitch amplitude). Hence our theory is validated.

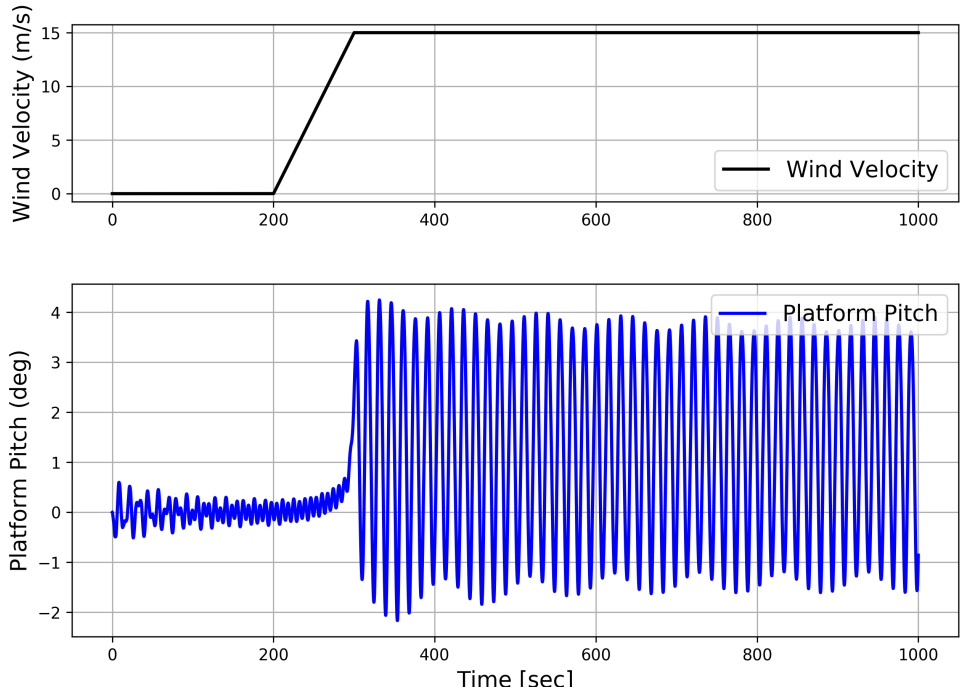

Figure 4.16: Platform Pitch at 15 m/s wind speed with wind approaching from 0 m/s

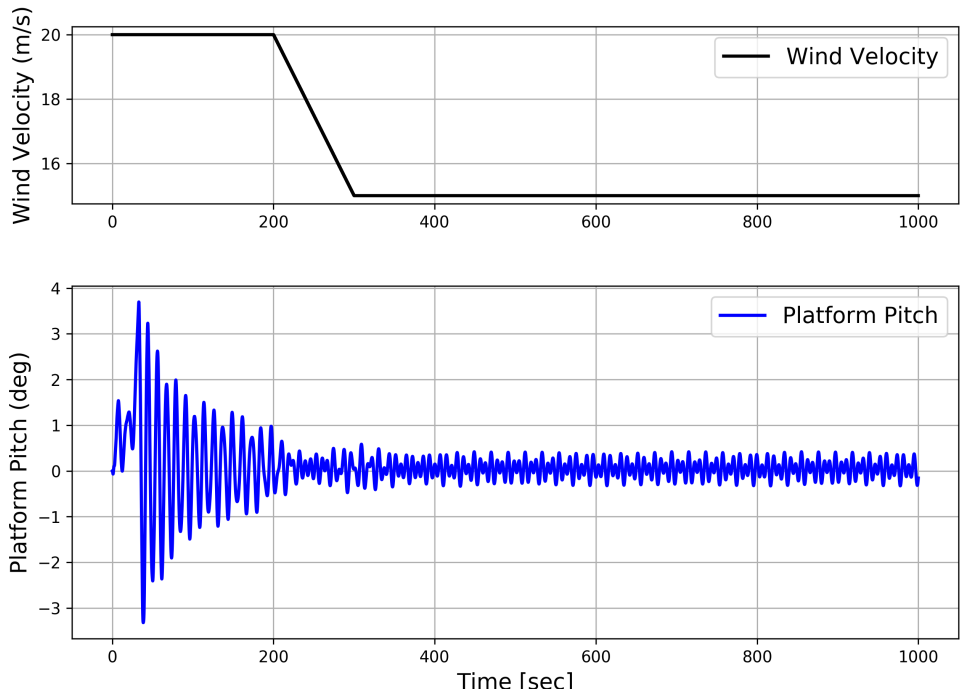

Figure 4.17: Platform Pitch at 15 m/s wind speed with wind approaching from 20 m/s

We discussed primarily what happens when we vary the wind speed. There is also the case on what happens when we start at a wind speed of say 15 m/s. The system response in this case depends on the initial velocity and position of the system. There are basins of attraction for each of the Orbital Equilibrium States discussed above. In a certain range of initial velocity and positions, the system tends to settle at OES 1, while for certain other initial conditions it settles for OES 3. OES 2 is an unstable saddle, because of which it is physically hard to realize. This concept is illustrated in the case of ship rolling by Falzarano, 1995 [65]. This is something that can be investigated further.

A duffing oscillator can be mathematically represented by Equation 4.1. Here, x is the position, ω_n the system natural frequency,μ the cubic stiffness coefficient, F the external forcing amplitude, ω the forcing frequency and ϕ the phase. When $\mu > 0$, the system behaves as a hardening spring, where the stiffness is related to the cube of displacement.

Our wind turbine system also has an underlying mathematical structure. This needs to be studied further.

$$m\ddot{x} + \omega_n^2 x + \mu x^3 = F cos(\omega t + \phi) \tag{4.1}$$

Most of the controls addressed in section 1.6 such as the PID, LQR and IBP, do not take into account the system nature, that exhibits a bifurcation due to the controller algorithm. Therefore new controllers have to be designed taking care of this system property.

4.5 Effect of Waves

Based on our findings in section 4.4, we have separately studied the role of waves in the cases of 13 m/s wind and 17 m/s wind. 13 m/s wind speed case is a representative of the higher amplitude OES, while 17m/s is that of the lower amplitude OES. Figures 4.18-4.21 represent the effect of wave period using regular waves. Figures 4.22-4.25 are used to study the effect of irregular waves generated using a JONSWAP spectrum.

In Section 1.2, we discussed briefly about the effect of waves observed during the occurrence of negative damping phenomenon. The platform pitch natural frequency gets excited heavily. Surge motions are also excited, and they die down very slowly. The heave mode of oscillation is not affected by the negative damping. The heave motions are governed only by the waves.

Figures 4.17-4.18 compare the time series and spectrum of motions induced by a steady 13 m/s wind in the presence of regular waves of time period 6 s (0.17 Hz), 7 s (0.14 Hz), and 9 s (0.11 Hz). The spectrum shows that the amplitude of pitch natural frequency of excitation is unaffected by change in wave time period. There are distinct peaks observed at the wave frequencies. The variation observed in surge natural frequency (0.01Hz) cannot be used to draw suitable conclusions.

Figures 4.19-4.20 does the same analysis for a wind speed of 17 m/s. In this case the energy in the pitch natural frequency is very much comparable to the energy in the wave

frequency. Interestingly, higher frequency causes larger platform pitch natural frequency and surge natural frequency excitation. For the same amplitude of pitch oscillations, higher frequency, has a higher velocity variation induced at the rotor hub. This would cause the controller to trigger more energy being pumped to the pitch natural frequency.

The results are more clear in the case of 17 m/s wind speed compared to 13 m/s. This is because, at 17 m/s wind speed, it is a stable steady state affected only by a single controller algorithm. In the case of 13 m/s there is a switching happening that makes the behavior more erratic.

Next, we analyze the role of an irregular sea. Figures 4.22-4.25 show the effect of a JONSWAP sea, compared to a regular wave sea. A JONSWAP spectrum with a significant wave height 1m, peak period 7s and peak shape factor of 1.0 was used for the analysis. Both 13 m/s and 17 m/s wind speeds are studied. This was compared against the corresponding motion response in regular waves of the same wave height and period.

In the case of 13 m/s wind it can be seen that the irregular seas do not alter the surge and pitch motion, but it affects the heave motion significantly. In the case of 17 m/s wind speed, irregular seas tend to pump in more energy into the pitch and surge natural modes of oscillations.

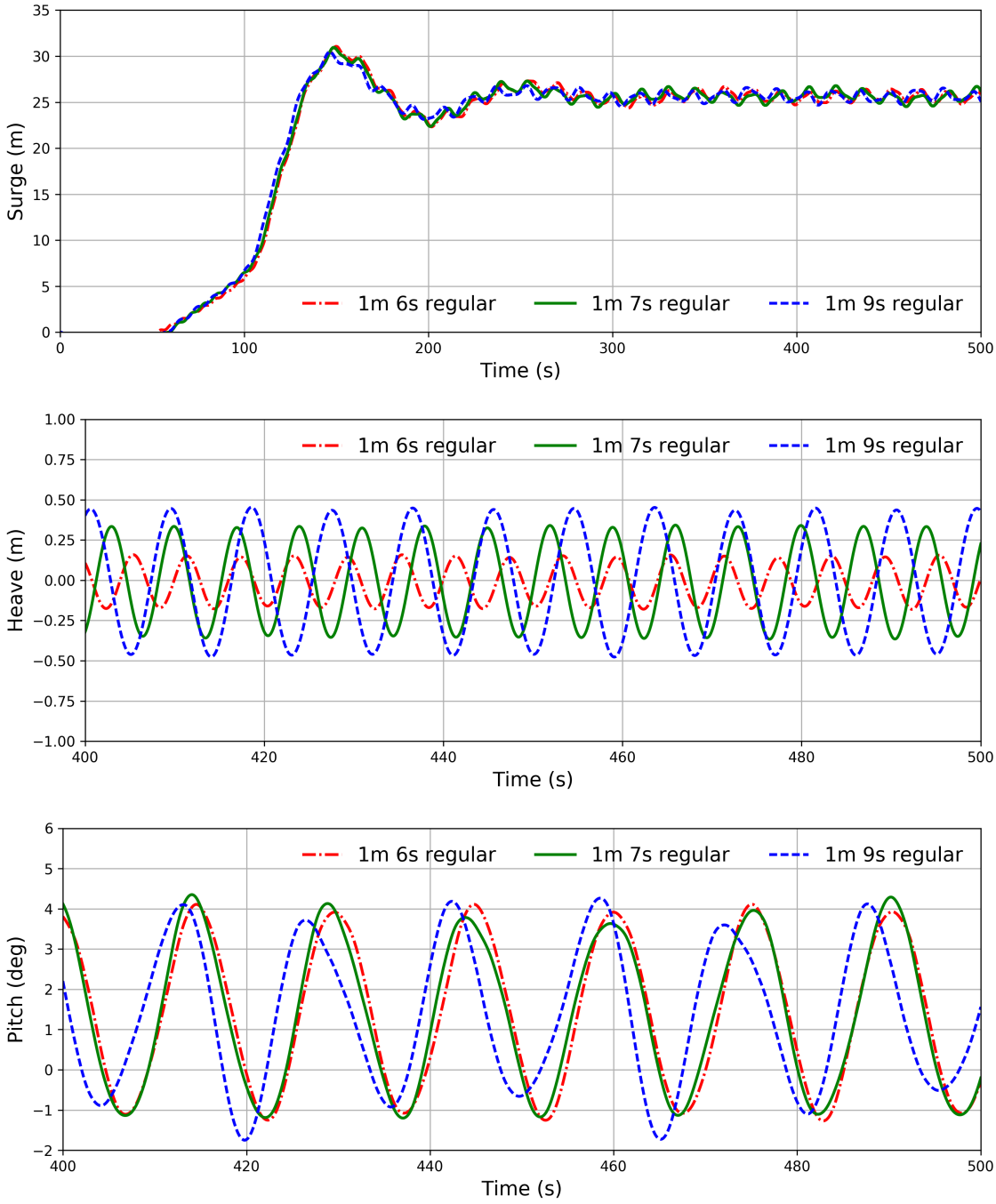

Figure 4.18: Surge, Heave, Pitch response in 13 m/s wind 1m 6s,7s,9s regular wave

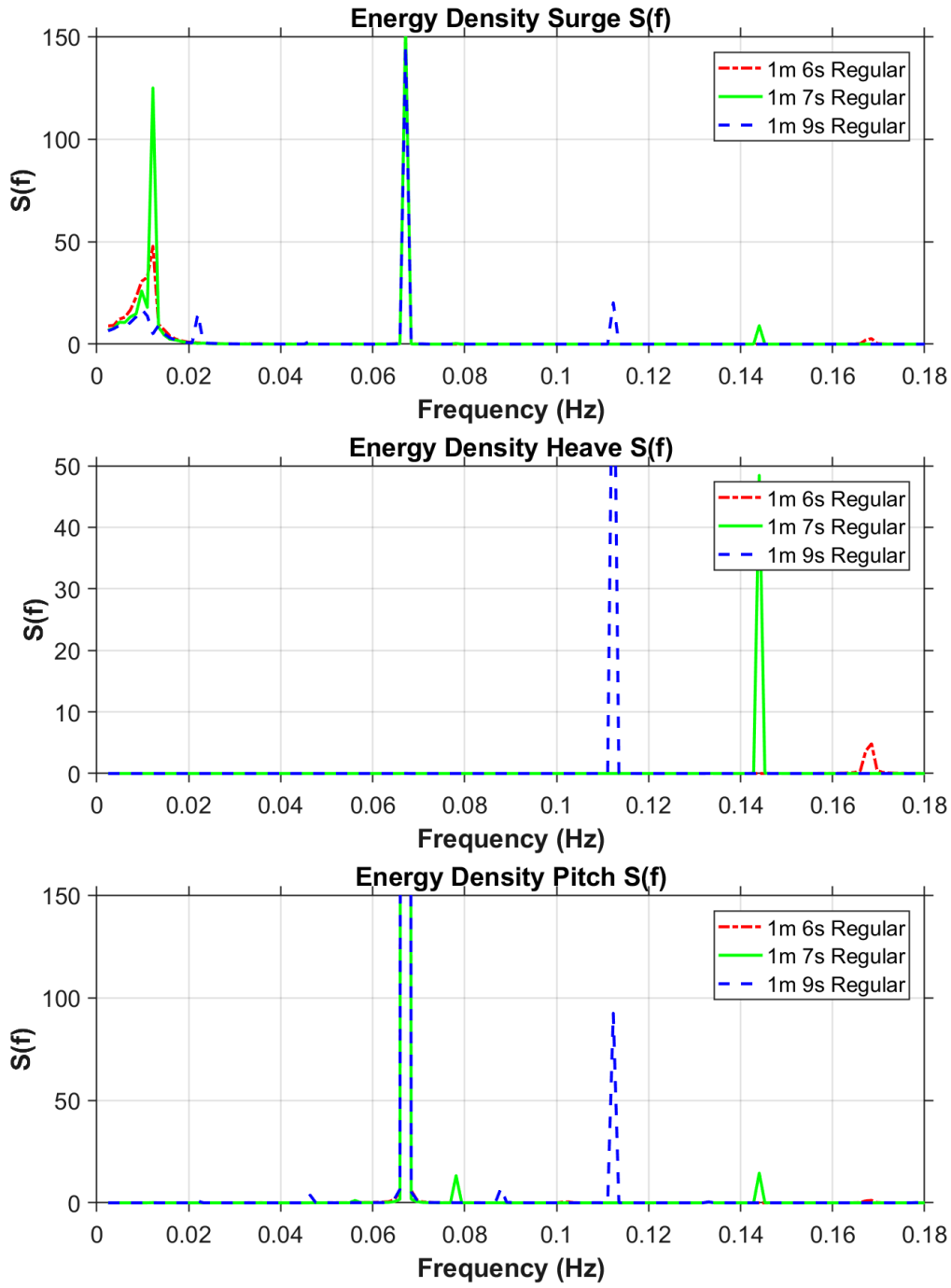

Figure 4.19: Surge, Heave, Pitch Spectrum 13m/s wind 1m 6s,7s,9s regular wave

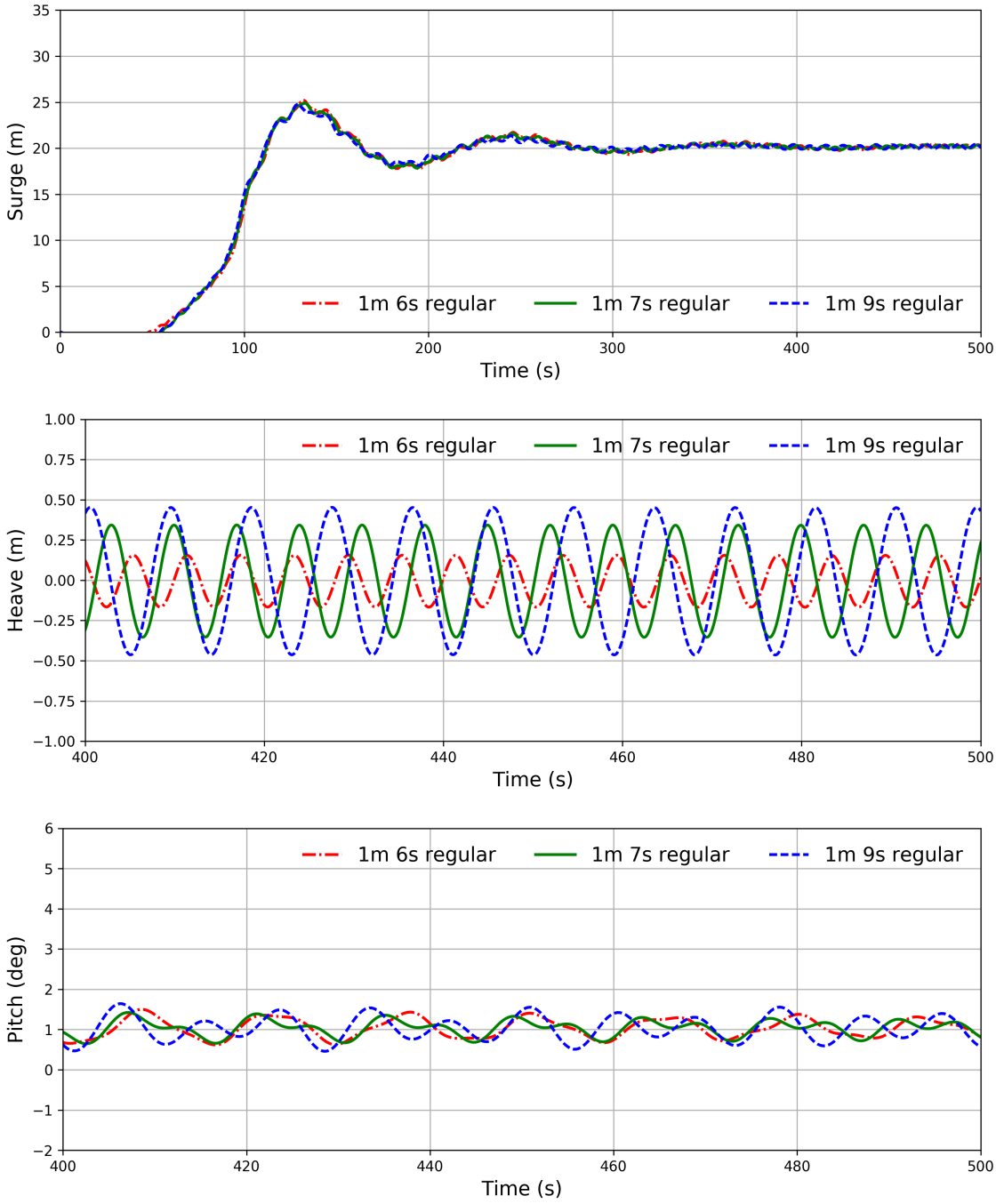

Figure 4.20: Surge, Heave, Pitch response in 17 m/s wind 1m 6s,7s,9s regular wave

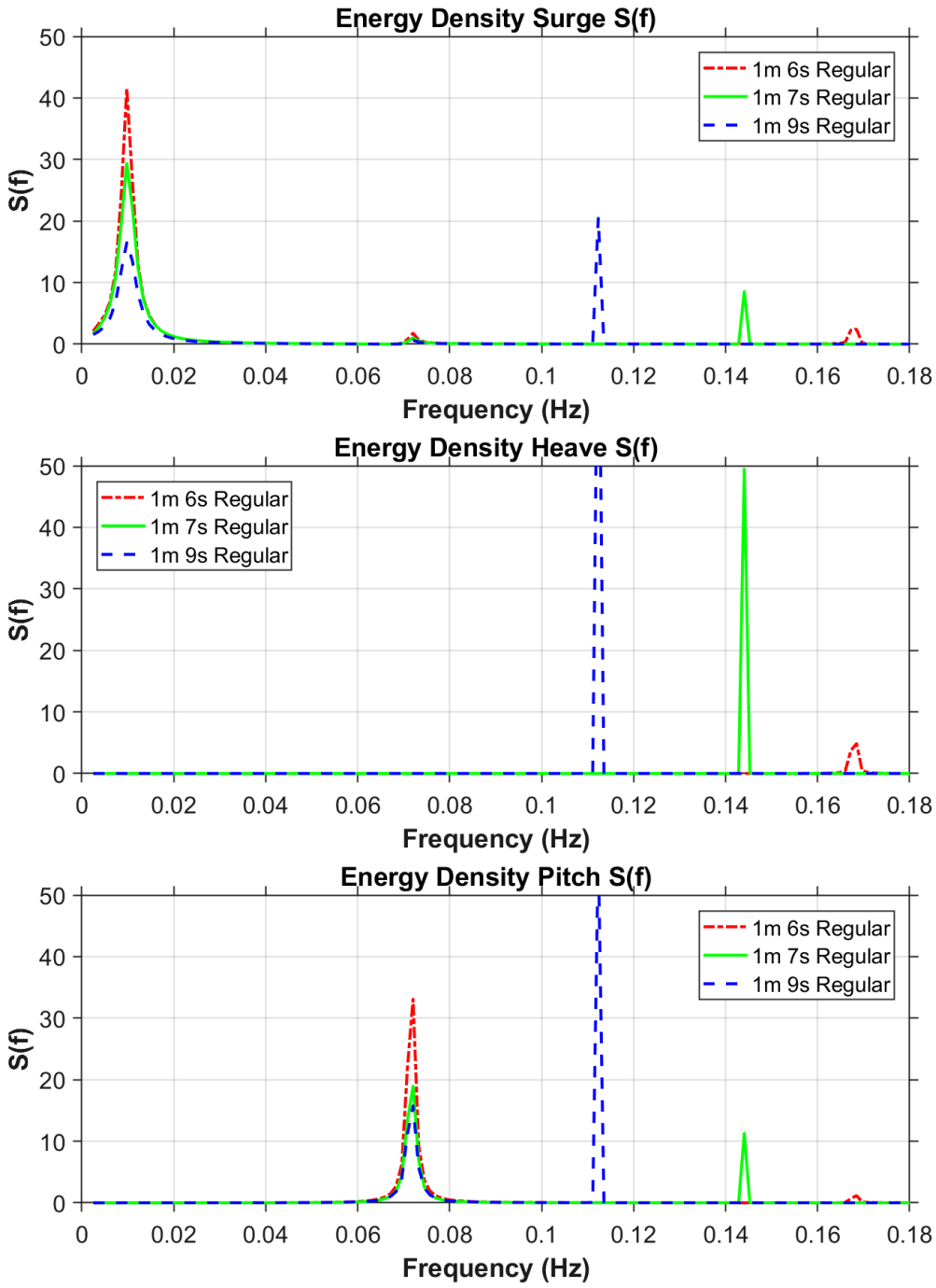

Figure 4.21: Surge, Heave, Pitch Spectrum 17m/s wind 1m 6s,7s,9s regular wave

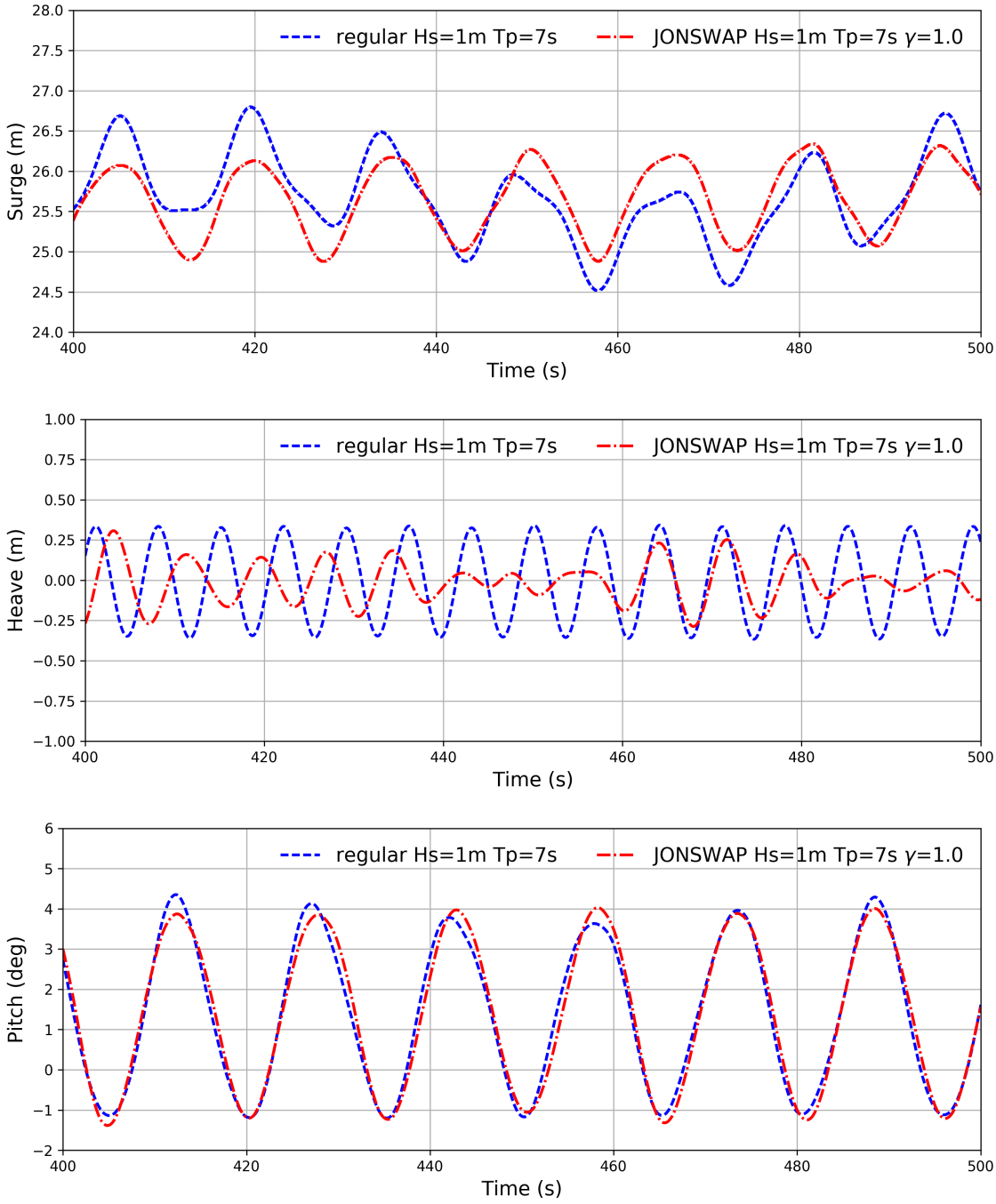

Figure 4.22: Surge, Heave, Pitch motion response in 13 m/s wind 1m 7s regular vs 1m 7s JONSWAP wave

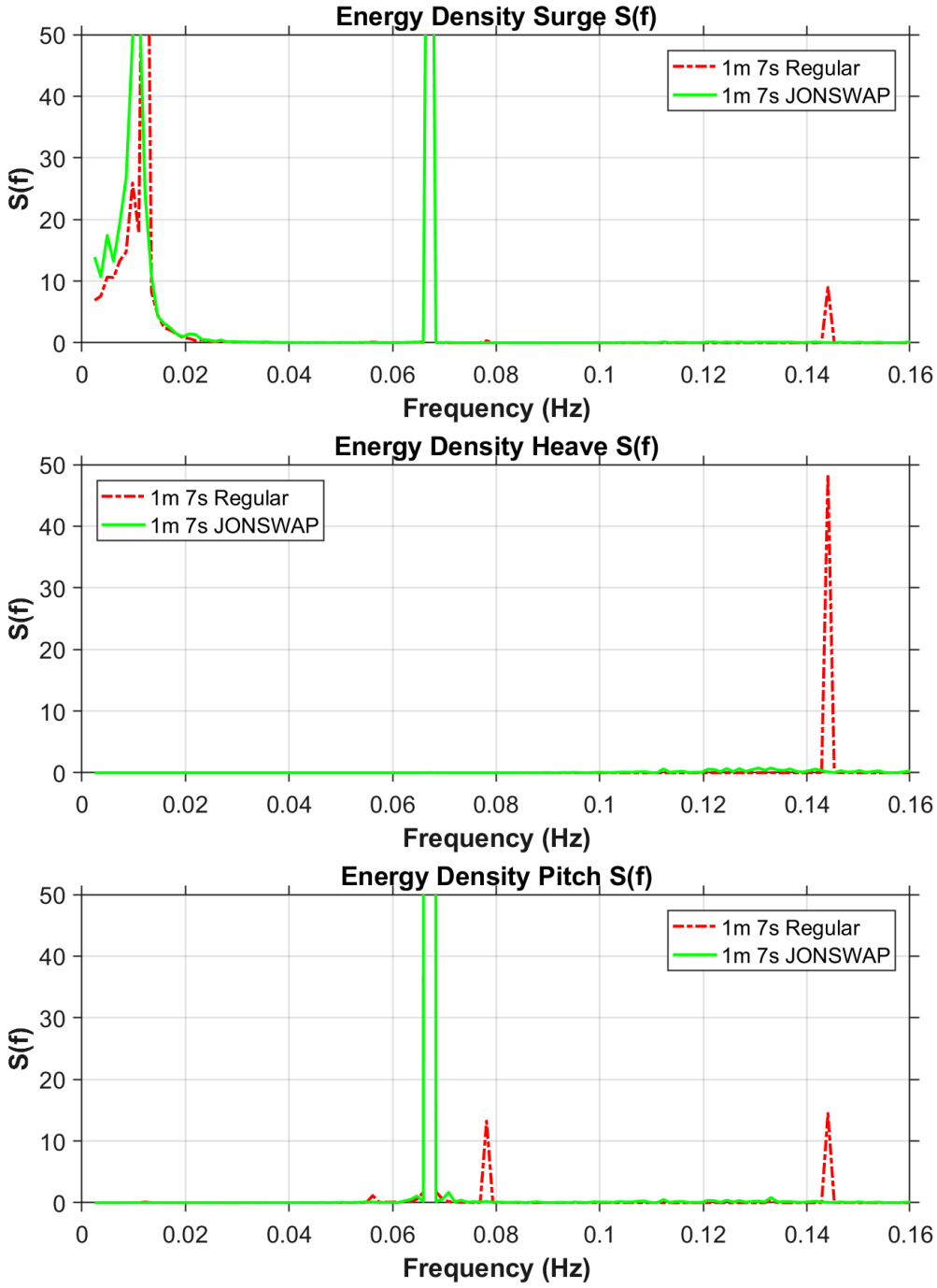

Figure 4.23: Surge, Sway, Heave Spectrum 13m/s wind 1m 7s regular vs JONSWAP wave

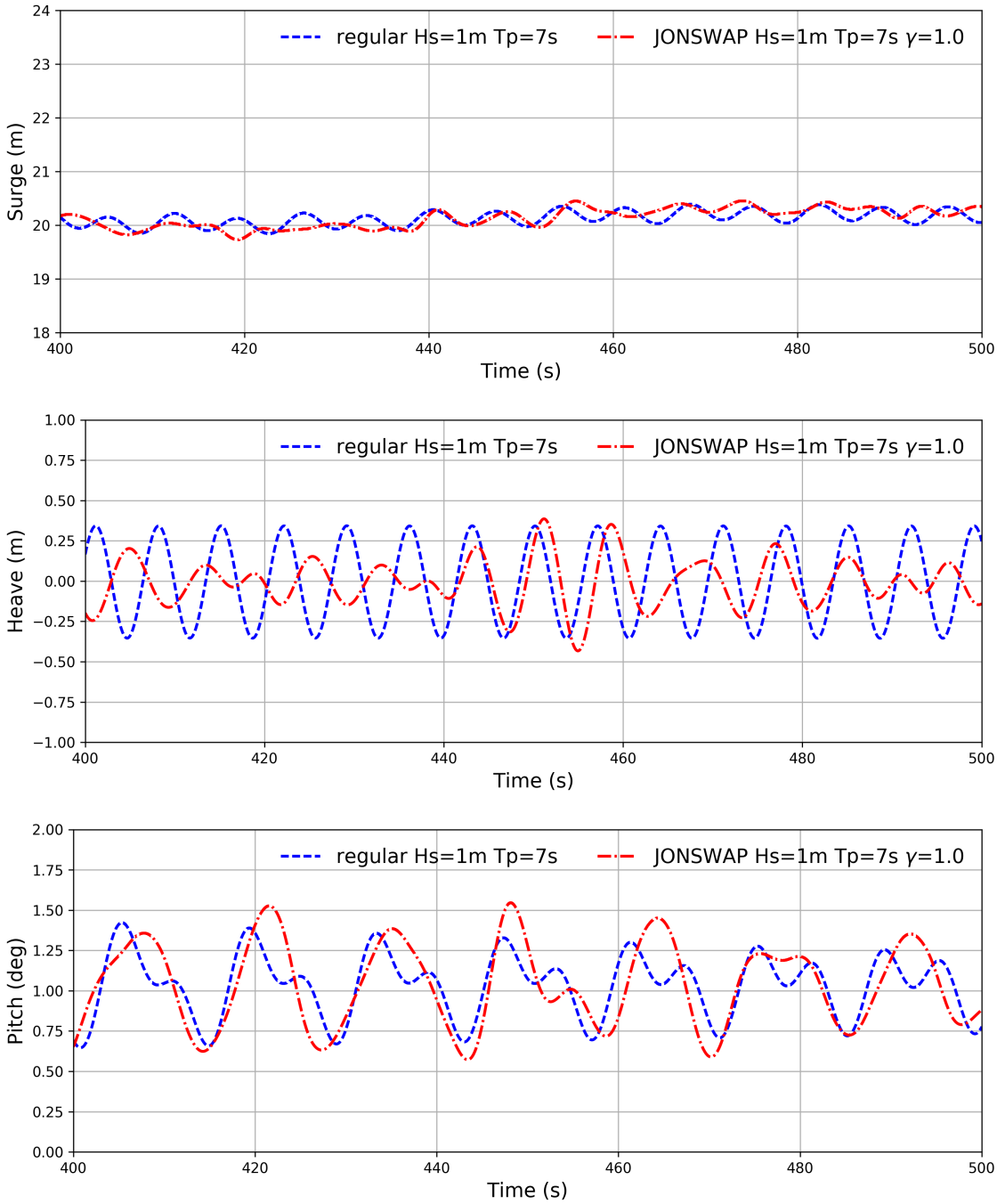

Figure 4.24: Translation motion response in 17 m/s wind 1m 7s regular vs 1m 7s JONSWAP wave

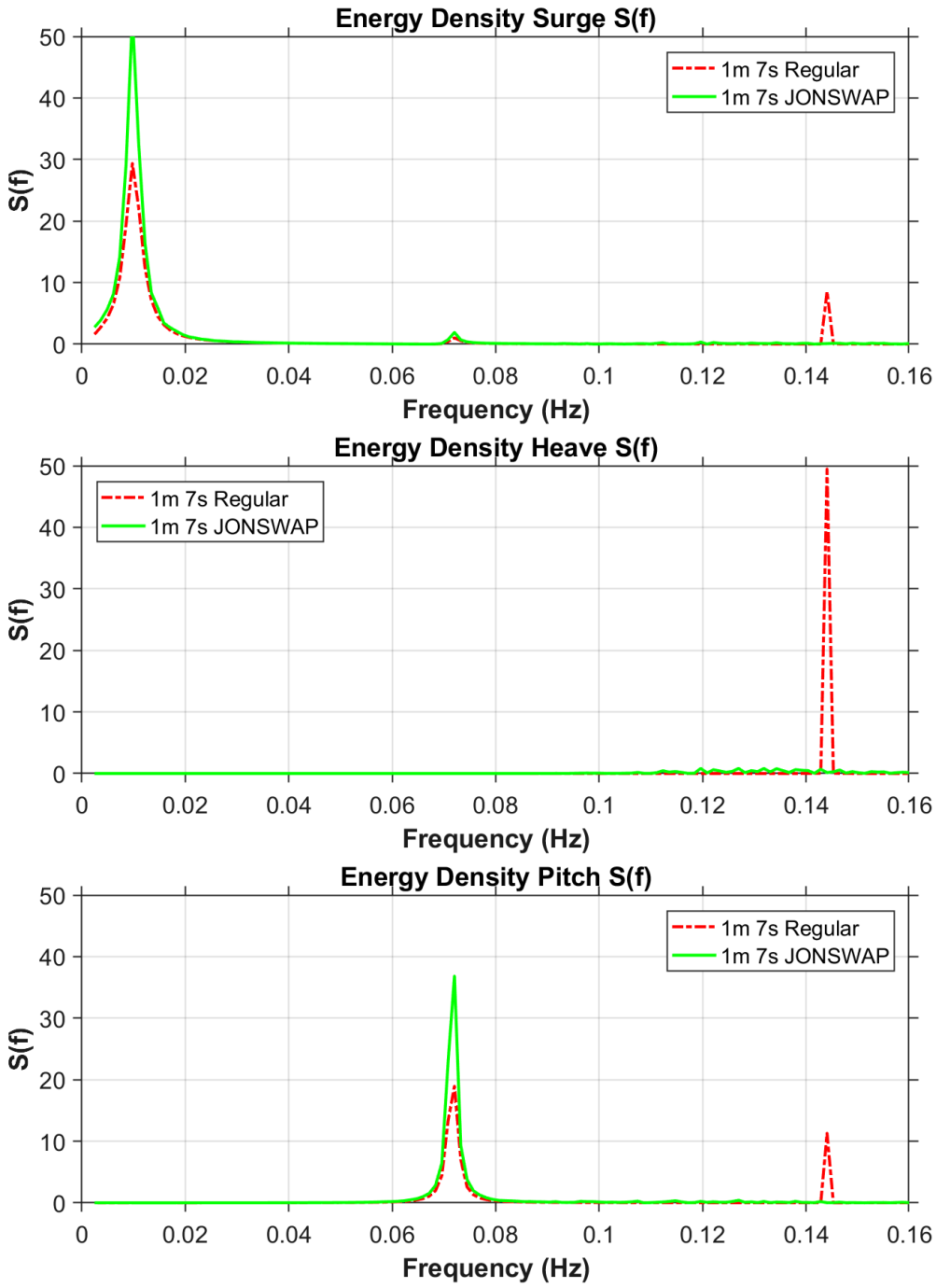

Figure 4.25: Surge, Sway, Heave Spectrum 17m/s wind 1m 7s regular vs JONSWAP wave

4.6 Linear vs Non-linear Froude Krylov and Non-linear Restoring Forces

Non-linear Froude Krylov and non-linear hydrostatic restoring forces do play an important role when it comes to large amplitude motions. Fig 4.25 to 4.28 show the comparison of motions estimated using linear as compared to such a non-linear analysis. The non-linear forces estimate a higher heave motion in comparison to the linear estimation for all cases. Heave motions are wave dominated. Therefore, accounting for the wave forces up to exact free surface can make a significant change in the estimation of forces.

In our case we are analysing a 7s wave which has a wavelength of about 76m. The barge we are analysing is 40 m long. So the barge is close to half the wave length and subject to high pitching. The wave length is about twice the barge natural pitching frequency. The non-linear analysis shows a lot higher pitching motion especially where the wave component is significant. In the case of wind speeds 13 m/s and 15m/s, it was shown earlier that they are near the transition zone with high natural pitch frequency motions. Because of this, the role of the wave forces is not seen as significantly.

But in the case of 17m/s wind speed, where the wave contribution is comparable to that from negative damping, the pitching motion predicted by non-linear analysis is higher than that from linear.

Figures 4.29 and 4.30 summarize the occurrence of negative damping as expected from an analysis using non-linear Froude-Krylov and non-linear hydrostatic restoring force calculation.

There are other non-linearities such as non-linear scattering forces. However, non-linear Froude-Krylov and non-linear hydrostatics are the main contributors of the non-linearity and are able to capture most of the system behavior.

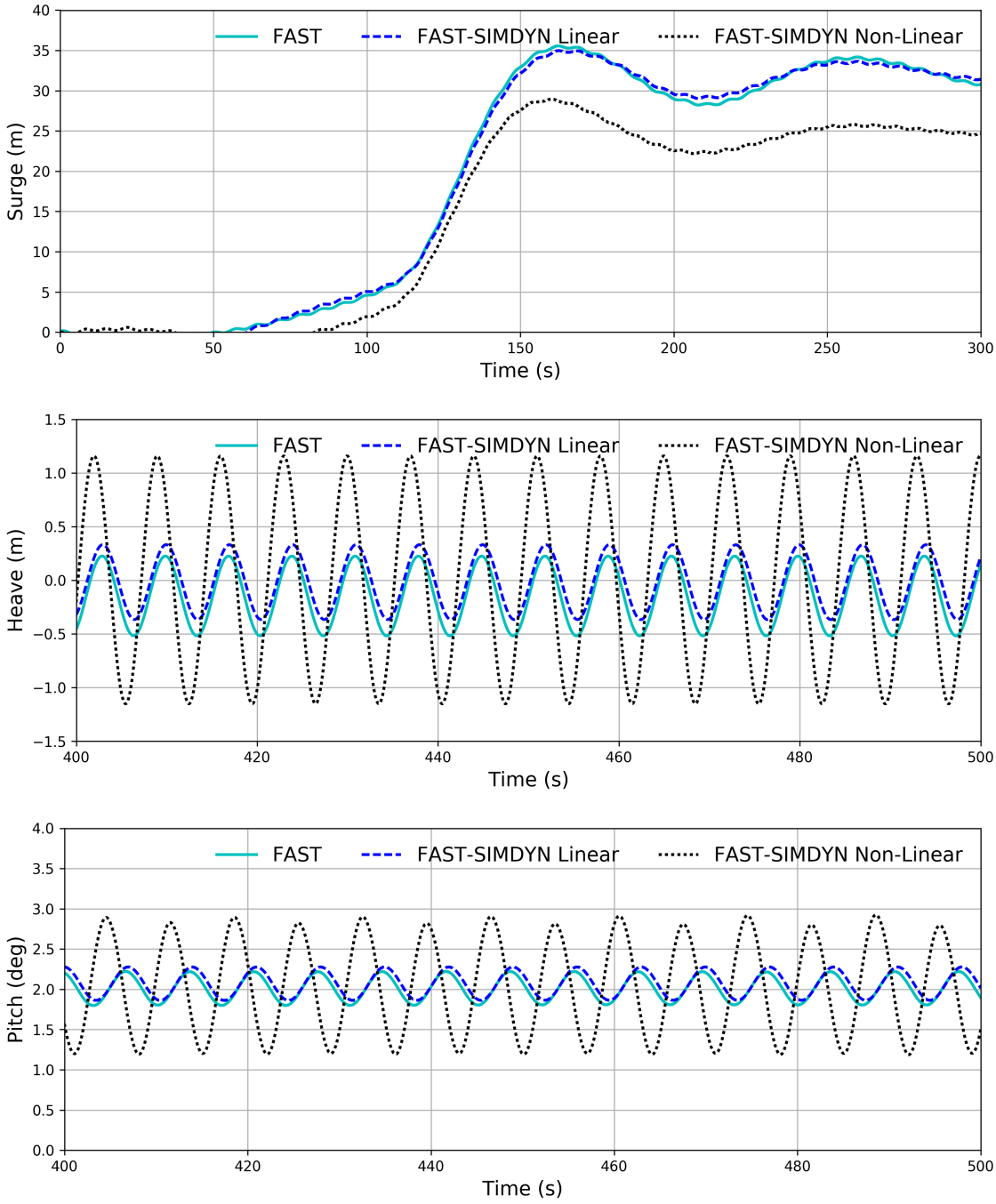

Figure 4.26: Surge, Heave, Pitch motion response in 11.4 m/s wind 1m 7s regular wave Linear vs Non-Linear Froude Krylov

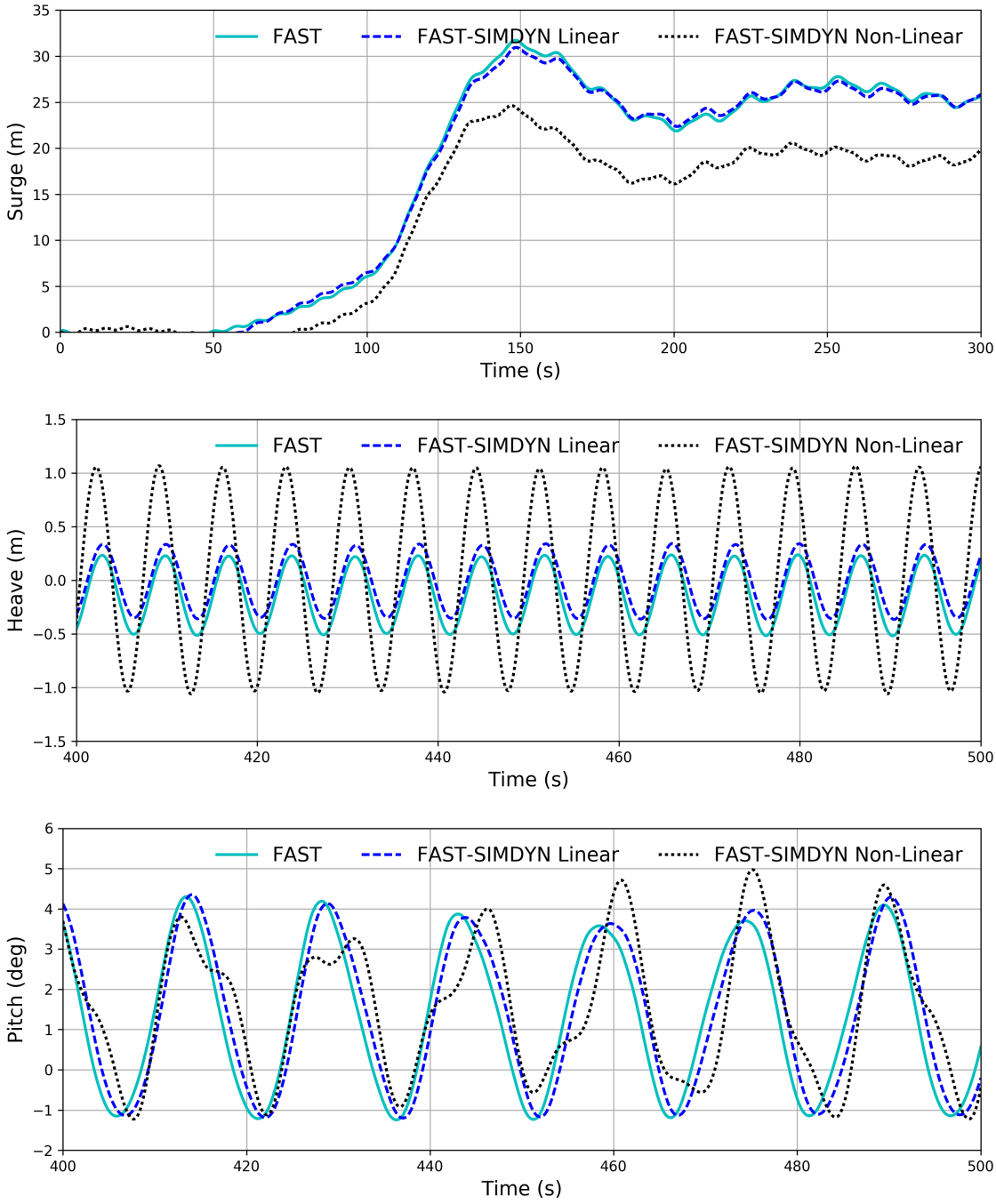

Figure 4.27: Surge, Heave, Pitch motion response in 13 m/s wind 1m 7s regular wave Linear vs Non-Linear Froude Krylov

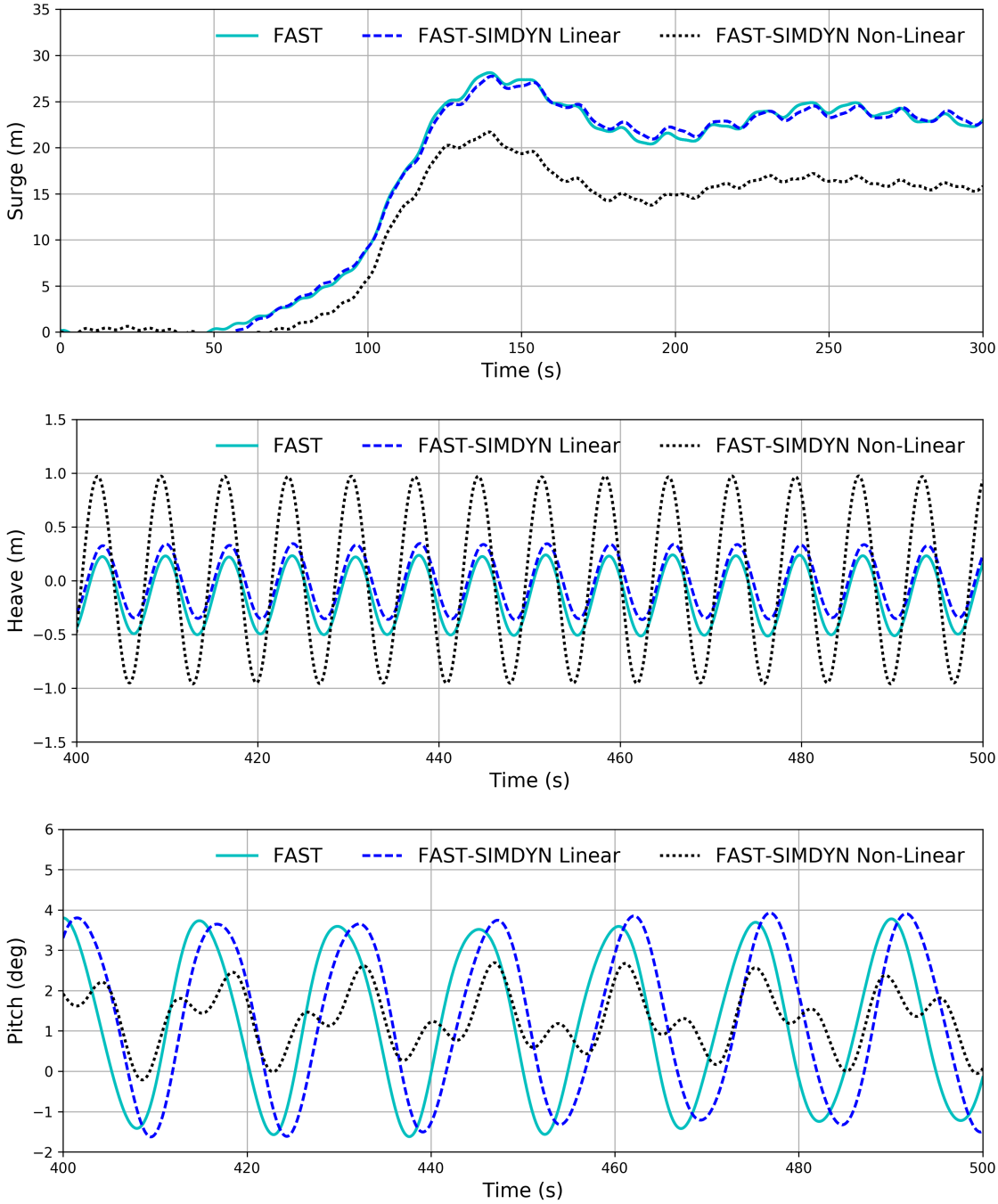

Figure 4.28: Surge, Heave, Pitch motion response in 15 m/s wind 1m 7s regular wave Linear vs Non-Linear Froude Krylov

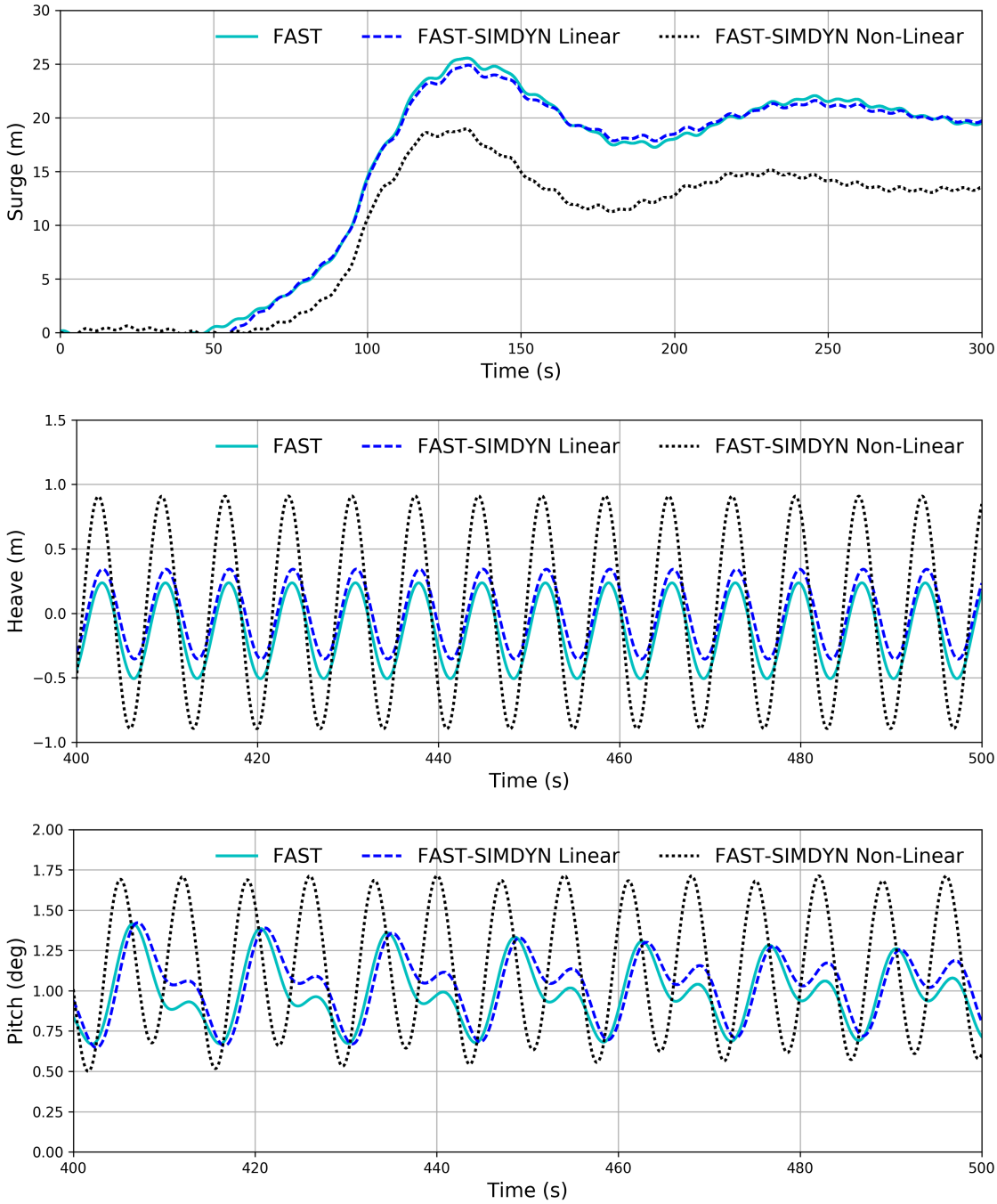

Figure 4.29: Surge, Heave, Pitch motion response in 17 m/s wind 1m 7s regular wave Linear vs Non-Linear Froude Krylov

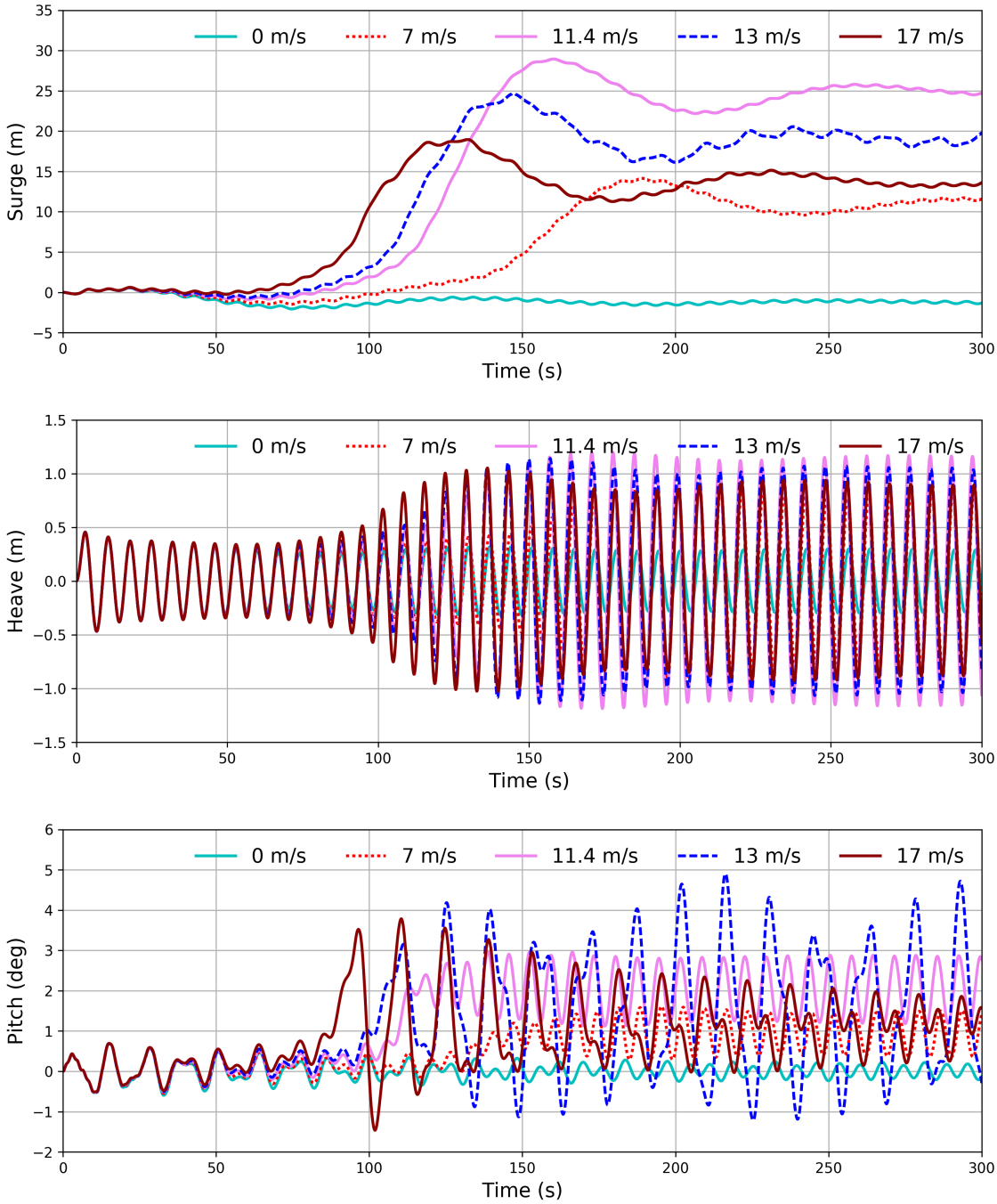

Figure 4.30: Surge, Heave, Pitch motion response in 0 to 17 m/s wind 1m 7s regular wave Non-linear

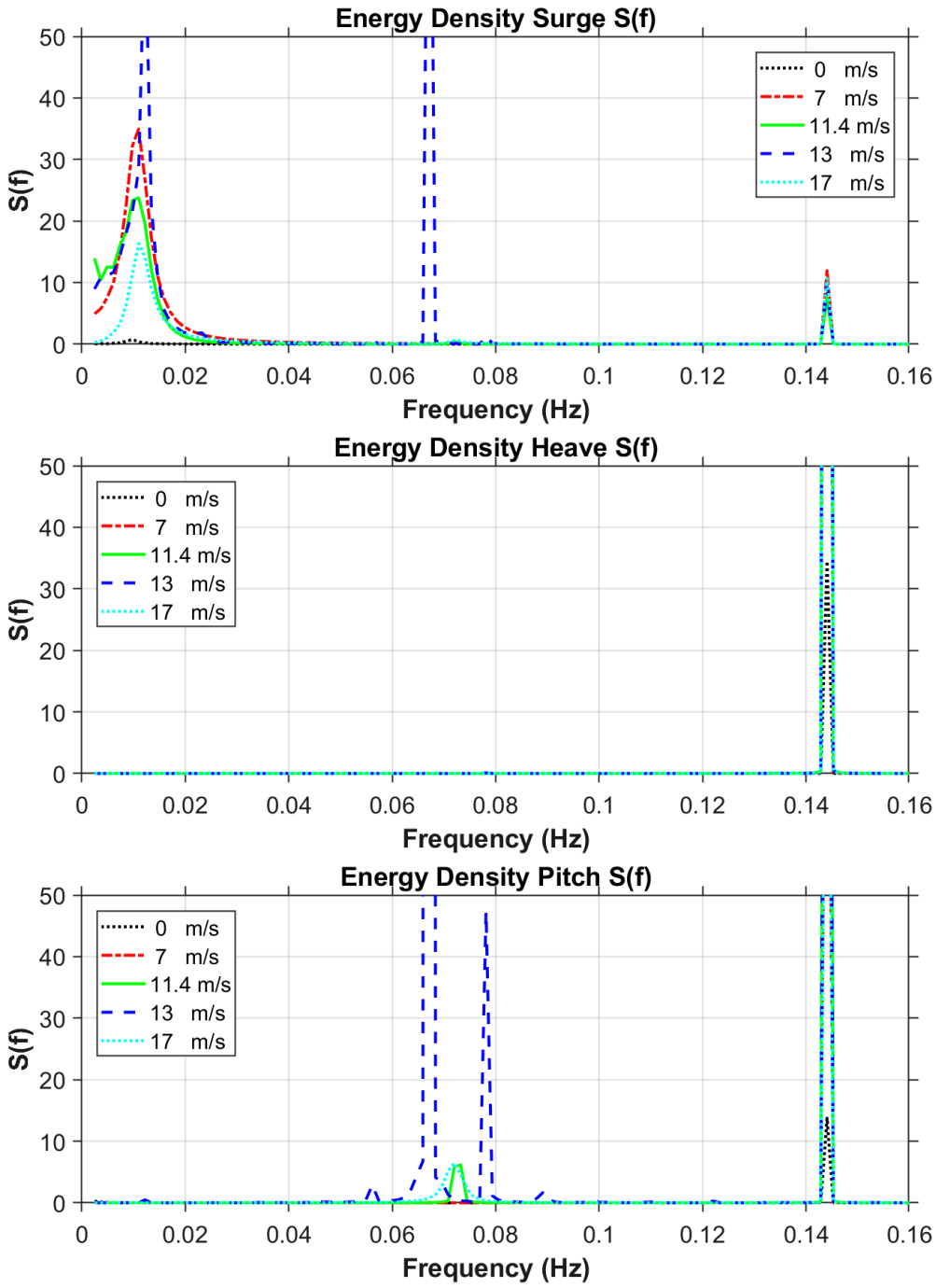

Figure 4.31: Surge, Heave, Pitch Spectrum near rated wind speed

5. CONCLUSIONS AND FUTURE SCOPE

5.1 Conclusion

In this study a tool has been successfully developed to study the effect of hydrodynamics on floating wind turbines. The program FAST has been coupled with the program SIMDYN. Validation tests were done using the ITI Energy barge concept. Validation was done by comparing the results obtained by using FAST alone and those obtained by using SIMDYN alone. The coupling was successfully validated.

Before the validation and subsequent studies, a frequency domain analysis was conducted for the ITI Energy barge using the programs WAMIT v5, MDL HydroD and MDL MULTIDYN. It was shown that sloshing and pumping play a very important role in the hydrodynamics of ITI Energy barge. This can be a scope of future work. MDL MULTIDYN was chosen to carry out our studies.

The coupled program FAST-SIMDYN was then used to study the occurence of negative damping. It was used to show how negative damping occurred only above a particular wind speed, where the controllers changed. The effect of controllers on the platform surge motion was also demonstrated. It was noted that there was a high role played by the coupling between the platform pitch and surge motions.

The transition zone of controller algorithm played a greater role in the platform motions, than was expected by the author. It was found that the transition zone of controller algorithm was a main cause of the high amplitude oscillations of the platform. Wind speeds far away from the controller transition zone exhibited far less pitching motions.

It was also found out that wind speed history mattered. A bifurcation was observed in the system behavior. Cause of the bifurcation was the fluctuating relative wind speed at the rotor hub. The changing speed causes a switching between 2 controller algorithms. This

continuous switching back an forth triggered platform pitch excitation. This was a loop where the pitching motion triggers the controller switching and the controller switching triggers platform pitching motion. At certain wind speeds, if the system started at low amplitude oscillations, it would stay low. But if the amplitude of oscillations was high, it could stay high. Increasing or decreasing the wind speeds could trigger jumps in the orbital equilibrium states.

In the unsteady, large amplitude motion Orbital Equilibrium State (OES), waves do not play any significant role in the pitching motions. It is harder to study the effect, as it is more erratic. For wind speeds above 16 m/s, platform motions were more regular, due to a steady controller algorithm.

In the case of 17 m/s, the role of wave forces is more clear. Higher frequency waves trigger a larger relative wind velocity fluctuations. This resulted in larger platform pitch natural frequency excitation. Similarly irregular waves, such as those generated using a JONSWAP spectrum also show a higher excitation of the platform pitch motion.

In the last section, the role of non-linear Froude Krylov and non-linear hydrostatic restoring forces was studied. The platform heave and pitch motions are higher than those predicted by linear analysis. This was particularly evident in cases where the motions were dominated by waves. This difference in amplitude is important, as it would play an important role in determining the points of jump bifurcation more accurately. Non-linear forces will also play a significant role in other extreme phenomenon which have not been studied in the current work.

5.2 Future Scope of Work

While designing combined Wave-Wind Energy Converters such as the ITI Energy Barge concept, the role of sloshing and pumping modes needs to be studied. Hydrodynamics modules can possibly capture the sloshing effects. But in the case of an oscillating

water column, the air above is not the same as being in contact with the atmosphere. The air is pushed to generate power. Hence even this pumping action needs to be accounted for. In our study we have neglected all these effects by placing a lid in the moonpool near the water free surface. This is possibly something that can be studied later.

Controllers are very important when it comes to FOWTs. These need to be studied in more detail keeping in mind the platform behavior. Nonlinear analysis tool developed in this project can be used for doing this.

REFERENCES

[1] "Arkona offshore wind farm, https://www.equinor.com/en/what-we-do/new-energy-solutions/our-offshore-wind-projects.html, 2018-07-18."

[2] B. Skaare, T. David Hanson, F. Gunnar Nielsen, R. Yttervik, A. Melchior Hansen, K. Thomsen, and T. Juul Larsen, "Integrated Dynamic Analysis of Floating Offshore Wind Turbines," in *European Wind Energy Conference and Exhibition*, (Milan, Italy), 2007.

[3] J. M. Jonkman, *Dynamics Modeling and Loads Analysis of an Offshore Floating Wind Turbine*. Phd dissertation, University of Colorado, 2007.

[4] S. Shim and M. Kim, "Rotor-floater-tether coupled dynamic analysis of offshore floating wind turbines," in *Eighteenth International Offshore and Polar Engineering Conference*, (Vancouver, BC, Canada), pp. 455–460, 2008.

[5] Y. H. Bae, *Coupled Dynamic Analysis Of Multiple Unit Floating Offshore Wind Turbine*. PhD thesis, Texas A&M University, 2013.

[6] M. A. Lackner and M. A. Rotea, "Passive structural control of offshore wind turbines Matthew," *Wind Energy*, vol. 14, no. April 2013, pp. 373–388, 2010.

[7] K. Iijima, J. Kim, and M. Fujikubo, "Coupled Aerodynamic And Hydroelastic Analysis Of An Offshore Floating Wind Turbine System Under Wind And Wave Loads," in *ASME 2010 29th International Conference on Ocean, Offshore and Arctic Engineering*, (Shanghai, China), pp. 1–8, 2010.

[8] M. Masciola, A. Robertson, J. M. Jonkman, and F. Driscoll, "Investigation of a FAST-OrcaFlex Coupling Module for Integrating Turbine and Mooring Dynamics

of Offshore Floating Wind Turbines," in *2011 International Conference on Offshore Wind Energy and Ocean Energy*, (Beijing, China), pp. 1–10, 2011.

[9] C. Peng, F. Yan, and J. Zhang, "Coupled Dynamic Response Of A Spar Type Floating Offshore Wind Turbine," in *ASME 2014 33rd International Conference on Ocean, Offshore and Arctic Engineering*, (San Francisco, California, USA), pp. 1–10, 2014.

[10] H. Ormberg and E. E. Bachynski, "Global Analysis of Floating Wind Turbines : Code Development , Model Sensitivity and Benchmark Study," in *Twenty-second (2012) International Offshore and Polar Engineering Conference*, (Rhodes, Greece), pp. 366–373, 2012.

[11] M. Karimirad and T. Moan, "A simplified method for coupled analysis of floating offshore wind turbines," *Marine Structures*, vol. 27, no. 1, pp. 45–63, 2012.

[12] C. Cermelli, D. Roddier, and A. Aubault, "Windfloat: A Floating Foundation For Offshore Wind Turbines Part II: Hydrodynamics Analysis," in *ASME 2009 28th International Conference on Ocean, Offshore and Arctic Engineering*, (Honolulu, Hawaii, USA), pp. 1–9, 2009.

[13] S. Gueydon, K. Lindenburg, and F. Savenije, "Coupling Of Two Tools For The Simulation Of Floating Wind Turbines," in *ASME 2013 32nd International Conference on Ocean, Offshore and Arctic Engineering*, (Nantes, France), pp. 1–12, 2013.

[14] M. Shen, Z. Hu, and G. Liu, "Dynamic response and viscous effect analysis of a TLP-type floating wind turbine using a coupled aero-hydro-mooring dynamic code," *Renewable Energy*, vol. 99, pp. 800–812, 2016.

[15] R. Antonutti, *Numerical Study of Floating Wind Turbines : Hydro- and Aero-mechanics*. PhD thesis, The University of Edinburgh, 2015.

[16] T. Zambrano, T. MacCready, T. Kiceniuk, D. G. Roddier, and C. A. Cermelli, "Dynamic Modeling of Deepwater Offshore Wind Turbine Structures in Gulf of Mexico Storm Conditions," in *25th International Conference on Offshore Mechanics and Arctic Engineering*, (Hamburg, Germany), 2006.

[17] T. Utsunomiya, S. Yoshida, H. Ookubo, I. Sato, and S. Ishida, "Dynamic Analysis Of A Floating Offshore Wind Turbine Under Extreme Environmental Conditions," in *ASME 2012 31st International Conference on Ocean, Offshore and Arctic Engineering*, (Rio de Janeiro, Brazil), pp. 1–10, 2012.

[18] K. Kokubun, S. Ishida, T. Nimura, T. Chujo, S. Yoshida, and T. Utsunomiya, "Model Experiment Of A Spar Type Offshore Wind Turbine In Storm Condition," in *ASME 2012 31st International Conference on Ocean, Offshore and Arctic Engineering*, (Rio de Janeiro, Brazil), pp. 1–7, 2012.

[19] J. M. Jonkman and M. L. Buhl Jr, "Loads analysis of a floating offshore wind turbine using fully coupled simulation," in *Wind Power Conference and Exhibition*, (Los Angeles, CA), 2007.

[20] Y. Mizukami, Y. Nihei, K. Iijima, and N. Hara, "A study on motion characteristics of wind turbine on a floating platform In blade pitch control malfunction," in *ASME 2016 35th International Conference on Ocean, Offshore and Arctic Engineering*, (Busan, South Korea), pp. 1–5, 2016.

[21] E. E. Bachynski, M. Etemaddar, M. I. Kvittem, C. Luan, and T. Moan, "Dynamic analysis of floating wind turbines during pitch actuator fault, grid loss, and shutdown," *Energy Procedia*, vol. 35, no. 1876, pp. 210–222, 2013.

[22] X. Shen, J. Chen, P. Hu, X. Zhu, and Z. Du, "Study of the unsteady aerodynamics of floating wind turbines," *Energy*, vol. 145, pp. 793–809, 2018.

[23] M. I. Kvittem, T. Moan, Z. Gao, and C. Luan, "Short-Term Fatigue Analysis Of Semi-Submersible Wind Turbine Tower," in *ASME 2011 30th International Conference on Ocean, Offshore and Arctic Engineering*, (Rotterdam, The Netherlands), 2011.

[24] M. Karimirad and T. Moan, "Extreme Dynamic Structural Response Analysis of Catenary Moored Spar Wind Turbine in Harsh Environmental Conditions," *Journal of Offshore Mechanics and Arctic Engineering*, vol. 133, no. 4, p. 041103, 2011.

[25] A. Sultania and L. Manuel, "Extreme loads on a spar buoy-supported floating offshore wind turbine," *51st AIAA/ASME/ASCE/AHS/ASC Structures, Structural Dynamics, and Materials Conference*, no. April, pp. 1–13, 2010.

[26] K. P. Thiagarajan, R. Urbina, and W. Hsu, "Nonlinear Pitch Decay Motion of a Floating Offshore Wind Turbine Structure," *Journal of Offshore Mechanics and Arctic Engineering*, vol. 137, no. February, p. 011902, 2014.

[27] L. Wang and B. Sweetman, "Simulation of large-amplitude motion of floating wind turbines using conservation of momentum," *Ocean Engineering*, vol. 42, pp. 155–164, 2012.

[28] B. Sweetman and L. Wang, "Floating Offshore Wind Turbine Dynamics: Large-Angle Motions in Euler-Space," *Journal of Offshore Mechanics and Arctic Engineering*, vol. 134, no. 3, p. 031903, 2012.

[29] A. Somayajula and J. Falzarano, "Validation of Volterra Series Approach for Modelling Parametric," in *OMAE 2015*, 2015.

[30] F. G. Nielsen, T. D. Hanson, and B. Skaare, "Integrated Dynamic Analysis Of Floating Offshore Wind Turbines," in *25th International Conference on Offshore Mechanics and Arctic Engineering*, (Hamburg, Germany), pp. 1–9, 2006.

[31] J. M. Jonkman, "Influence of Control on the Pitch Damping of a Floating Wind Turbine," in *ASME Wind Energy Symposium*, pp. 1–15, 2008.

[32] G. Bir and J. Jonkman, "Aeroelastic Instabilities of Large Offshore and Onshore Wind Turbines," *Journal of Physics: Conference Series*, vol. 75, p. 012069, 2007.

[33] T. J. Larsen and T. D. Hanson, "A method to avoid negative damped low frequent tower vibrations for a floating, pitch controlled wind turbine," *Journal of Physics: Conference Series*, vol. 75, no. 1, p. 012073, 2007.

[34] M. Karimirad and T. Moan, "Ameliorating the Negative Damping in the Dynamic Responses of a Downwind Tension Leg Spar Type Offshore Wind Turbine," in *European Wind Energy Conference (EWEC2011)*, (Brussels, Belgium), 2011.

[35] M. A. Lackner, "Controlling Platform Motions and Reducing Blade Loads for Floating Wind Turbines," *Wind Engineering*, vol. 33, no. 6, pp. 541–554, 2009.

[36] H. Namik and K. A. Stol, "Control Methods for Reducing Platform Pitching Motion of Floating Wind Turbines," *European offshore wind*, 2009.

[37] H. Namik and K. A. Stol, "Disturbance Accommodating Control of Floating Offshore Wind Turbines," in *47th AIAA Aerospace Sciences Meeting Including The New Horizons Forum and Aerospace Exposition*, (Orlando, Florida), 2009.

[38] R. Chaaban and C.-p. Fritzen, "Reducing Blade Fatigue and Damping Platform Motions of Floating Wind Turbines Using Model Predictive Control," in *9th International Conference on Structural Dynamics, EURODYN 2014*, (Porto, Portugal), pp. 3581–3588, 2014.

[39] T. C. Fu, E. E. Hackett, A. M. Fullerton, and C. Merrill, "Shipboard Measurement Of Ocean Waves," in *ASME 2011 30th International Conference on Ocean, Offshore and Arctic Engineering*, (Rotterdam, The Netherlands), pp. 1–8, 2011.

[40] W. M. Milewski, B. S. H. Connell, V. J. Vinciullo, and I. N. Kirschner, "Reduced Order Model For Motion Forecasts Of One Or More Vessels," in *Proceedings of the ASME 2015 34th International Conference on Ocean, Offshore and Arctic Engineering*, (St. John's, Newfoundland, Canada), pp. 1–10, 2015.

[41] A. Somayajula and J. Falzarano, "Application of advanced system identification technique to extract roll damping from model tests in order to accurately predict roll motions," *Applied Ocean Research*, vol. 67, pp. 125–135, 2017.

[42] M. A. Rotea, M. A. Lackner, and R. Saheba, "Active Structural Control of Offshore Wind turbines," in *48th AIAA Aerospace Sciences Meeting Including the New Horizons Forum and Aerospace Exposition*, (Orlando, Florida), pp. 1–22, 2010.

[43] A. Guha and J. Falzarano, "Development of a Computer Program for Three Dimensional Analysis of Zero Speed First Order Wave Body Interaction in frequency domain," in *ASME 2013 32nd International Conference on Ocean, Offshore and Arctic Engineering*, (Nantes, France), pp. 1–9, 2013.

[44] A. Somayajula, A. Guha, J. Falzarano, H.-h. Chun, and K. H. Jung, "Added resistance and parametric roll prediction as a design criteria for energy efficient ships," *Ocean Systems Engineering*, vol. 4, no. 2, pp. 117–136, 2014.

[45] A. Guha and J. Falzarano, "The effect of hull emergence angle on the near field formulation of added resistance," *Ocean Engineering*, vol. 105, pp. 10–24, 2015.

[46] A. Guha and J. Falzarano, "The effect of small forward speed on prediction of wave loads in restricted water depth," *Ocean Systems Engineering*, vol. 6, no. 4, pp. 1–8, 2016.

[47] A. GUHA, *Development And Application Of A Potential Flow Computer Program: Determining First And Second Order Wave Forces At Zero And Forward Speed In*

Deep And Intermediate Water Depth. PhD thesis, Texas A&M University, 2016.

[48] A. Somayajula and J. Falzarano, "Large-amplitude time-domain simulation tool for marine and offshore motion prediction," *Marine Systems & Ocean Technology*, vol. 10, no. 1, pp. 1–17, 2015.

[49] J. Falzarano, A. Somayajula, and R. Seah, "An overview of the prediction methods for roll damping of ships," *Ocean Systems Engineering*, vol. 5, no. 2, pp. 55–76, 2015.

[50] A. Somayajula and J. Falzarano, "Critical assessment of reverse-MISO techniques for system identification of coupled roll motion of ships," *Journal of Marine Science and Technology (Japan)*, pp. 1–14, 2016.

[51] Y. Liu and J. M. Falzarano, "A method to remove irregular frequencies and log singularity evaluation in wave-body interaction problems," *Journal of Ocean Engineering and Marine Energy*, vol. 3, no. 2, pp. 161–189, 2017.

[52] Y. Liu and Jeffrey M. Falzarano, "Irregular frequency removal methods: theory and applications in hydrodynamics," *Marine Systems & Ocean Technology*, vol. 12, no. 2, pp. 49–64, 2017.

[53] Y. Liu and J. M. Falzarano, "Suppression of Irregular Frequency Effect in Hydrodynamic Problems and Free-Surface Singularity Treatment," *Journal of Offshore Mechanics and Arctic Engineering*, vol. 139, no. October, pp. 1–16, 2017.

[54] Y. Liu and J. M. Falzarano, "Frequency Domain Analysis Of The Interactions Between Multiple Ships With Nonzero Speed Inwaves Or Current-Wave Interactions," in *ASME 2017 36th International Conference on Ocean, Offshore and Arctic Engineering*, (Trondheim, Norway), pp. 1–17, 2017.

[55] A. Jose, J. Falzarano, and H. Wang, "A Study Of Negative Damping In Floating Wind Turbines Using Coupled Program FAST-SIMDYN," in *1st International Offshore Wind Technical Conference*, (San Francisco, California, USA), pp. 1–6, 2018.

[56] J. Jonkman, "The New Modularization Framework for the FAST Wind Turbine CAE Tool," in *51st AIAA Aerospace Sciences Meeting*, (Dallas, Texas), 2013.

[57] T. R. Kane, *Dynamics*. Holt, Rinehart and Winston; F First Edition edition (December 1968), 1968.

[58] J. Jonkman, A. Robertson, and G. Hayman, "HydroDyn user's guide and theory manual," tech. rep., National Renewable Energy Laboratory, Golden, Colorado, 2014.

[59] A. Somayajula, *Reliability Assessment of Hull Forms Susceptible to Parametric Roll in Irregular Seas*. Phd dissertation, Texas A&M University, 2017.

[60] J. M. Jonkman, S. Butterfield, W. Musial, and G. Scott, "Definition of a 5-MW Reference Wind Turbine for Offshore System Development," tech. rep., National Renewable Energy Laboratory, Golden, Colorado, 2009.

[61] J. C. Bandas and Jeffrey M Falzarano, "A Numerical Investigation into the Linear Seakeeping Ability of the T-Craft," in *11th International Conference on Fast Sea Transportation*, (Honolulu, Hawaii, USA), 2011.

[62] Y. Liu and J. M. Falzarano, "Suppression of irregular frequency in multi-body problem and Free-surface singularity treatment," in *ASME 2016 35th International Conference on Ocean, Offshore and Arctic Engineering*, (Busan, South Korea), 2016.

[63] J. Jonkman, "Definition of the Floating System for Phase IV of OC3," Tech. Rep. May, National Renewable Energy Laboratory, 2010.

[64] W. T. Thomson and M. D. Dahleh, *Theory of Vibrations with Applications*. Santa Barbara: Pearson, 5 ed., 1998.

[65] J. M. Falzarano, I. Esparza, and M. T. U. Mulk, “A combined steady-state and transient approach to study large-amplitude ship rolling motion and capsizing,” *Journal of Ship Research*, vol. 39, no. 3, pp. 213–224, 1995.

APPENDIX A - FREQUENCY DOMAIN ANALYSIS PLOTS

A.1 Plots for ITI Energy Barge Radiation Added Mass and Damping for Cases Without Moonpool Lid

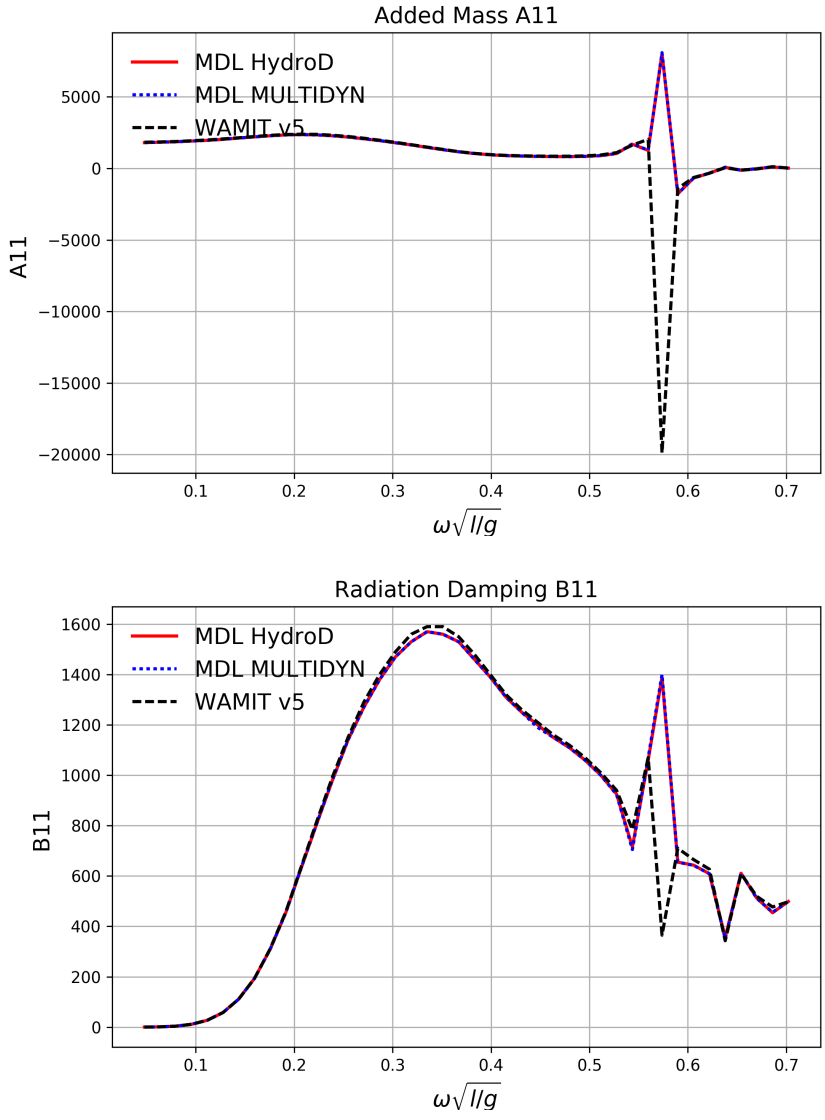

Figure A.1: Case without moonpool lid Added Mass A11 and Radiation damping B11

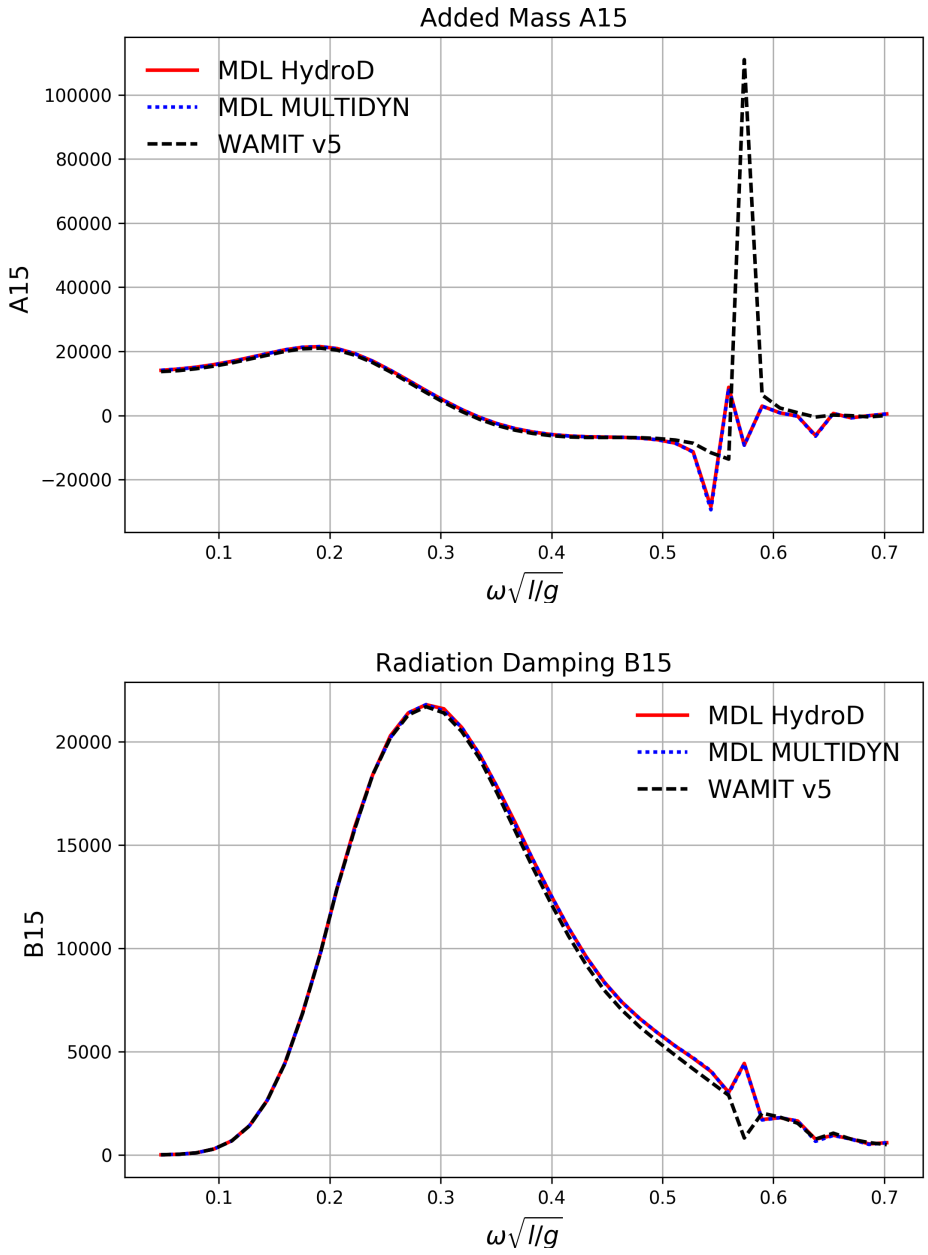

Figure A.2: Case without moonpool lid Added Mass A15 and Radiation damping B15

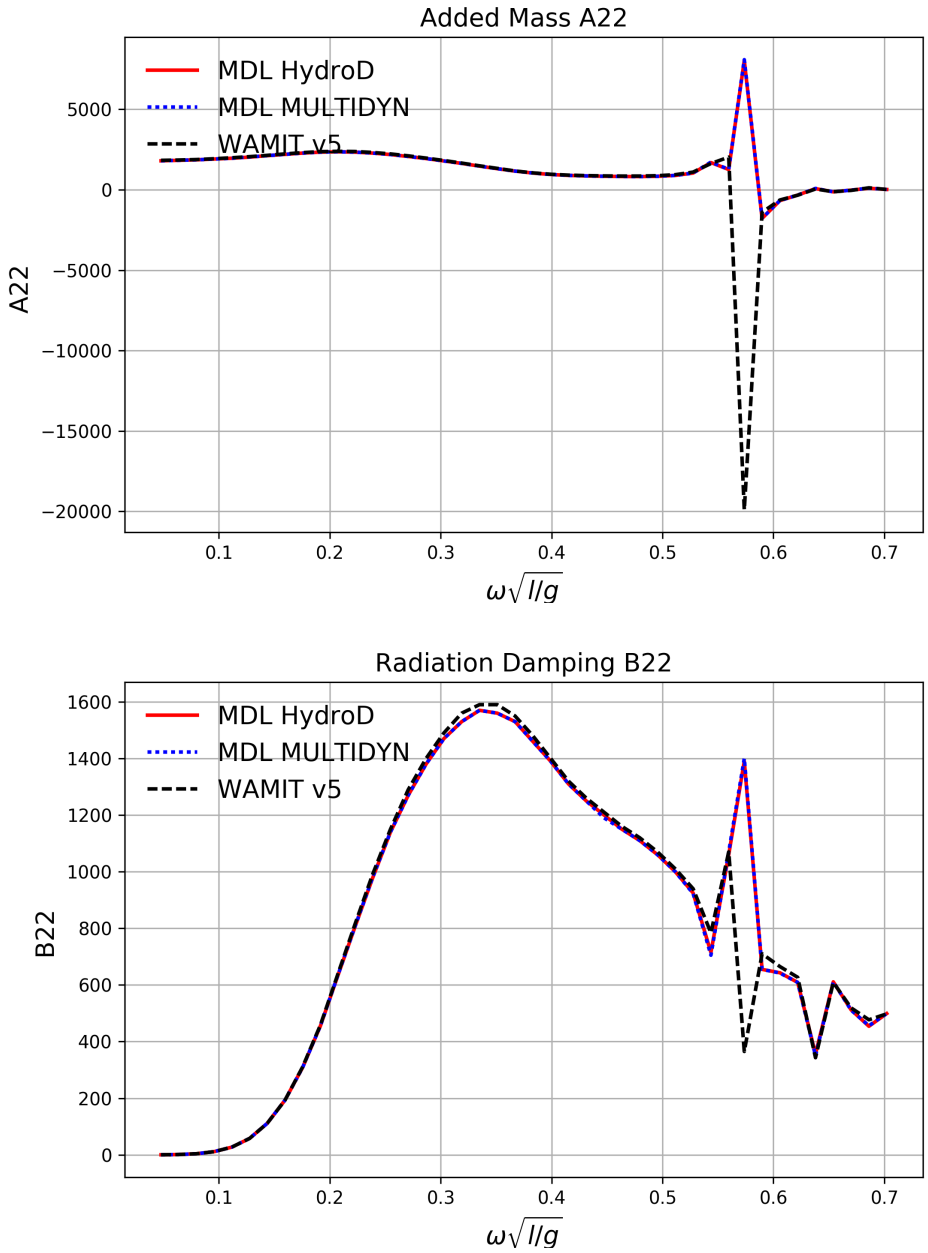

Figure A.3: Case without moonpool lid Added Mass A22 and Radiation damping B22

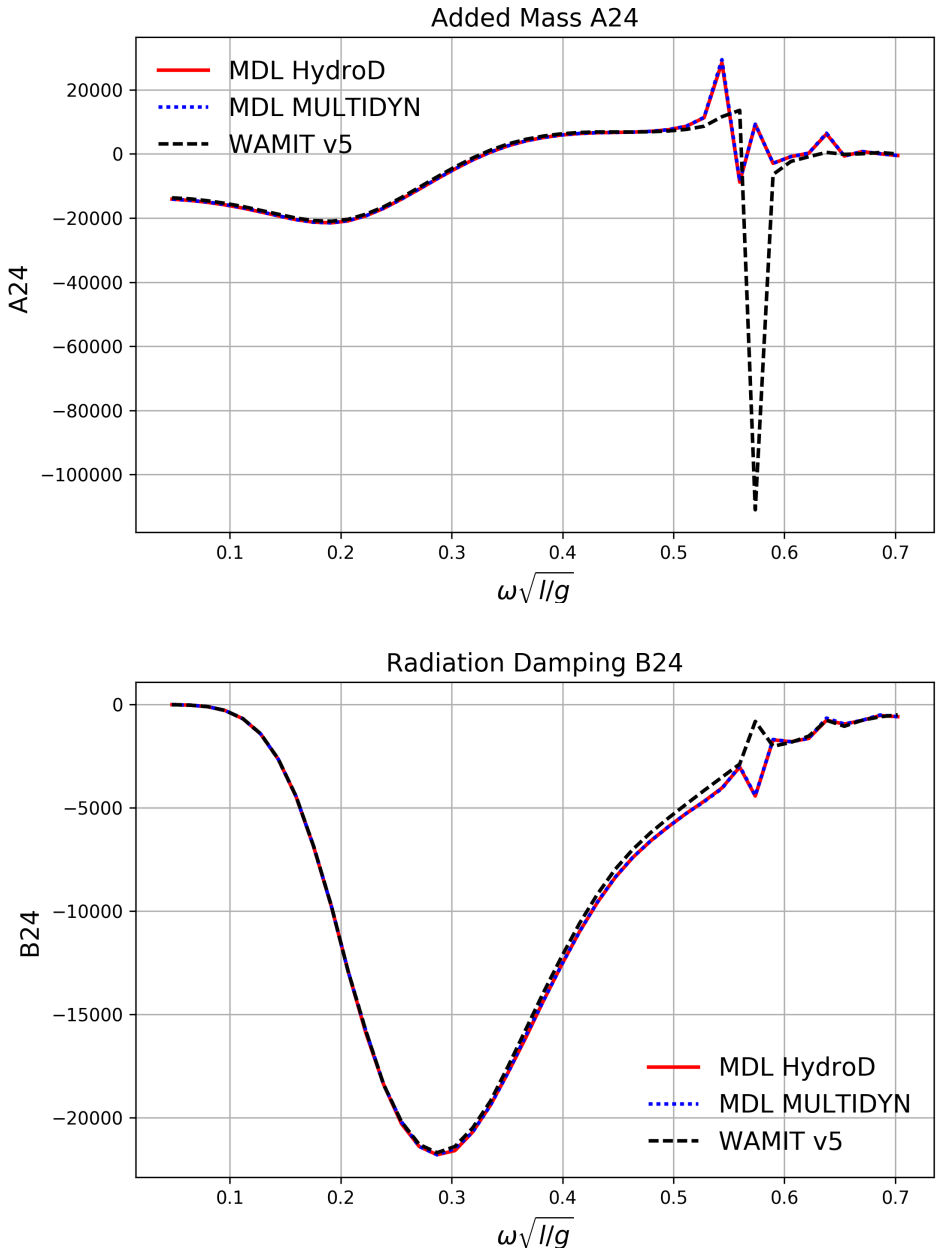

Figure A.4: Case without moonpool lid Added Mass A24 and Radiation damping B24

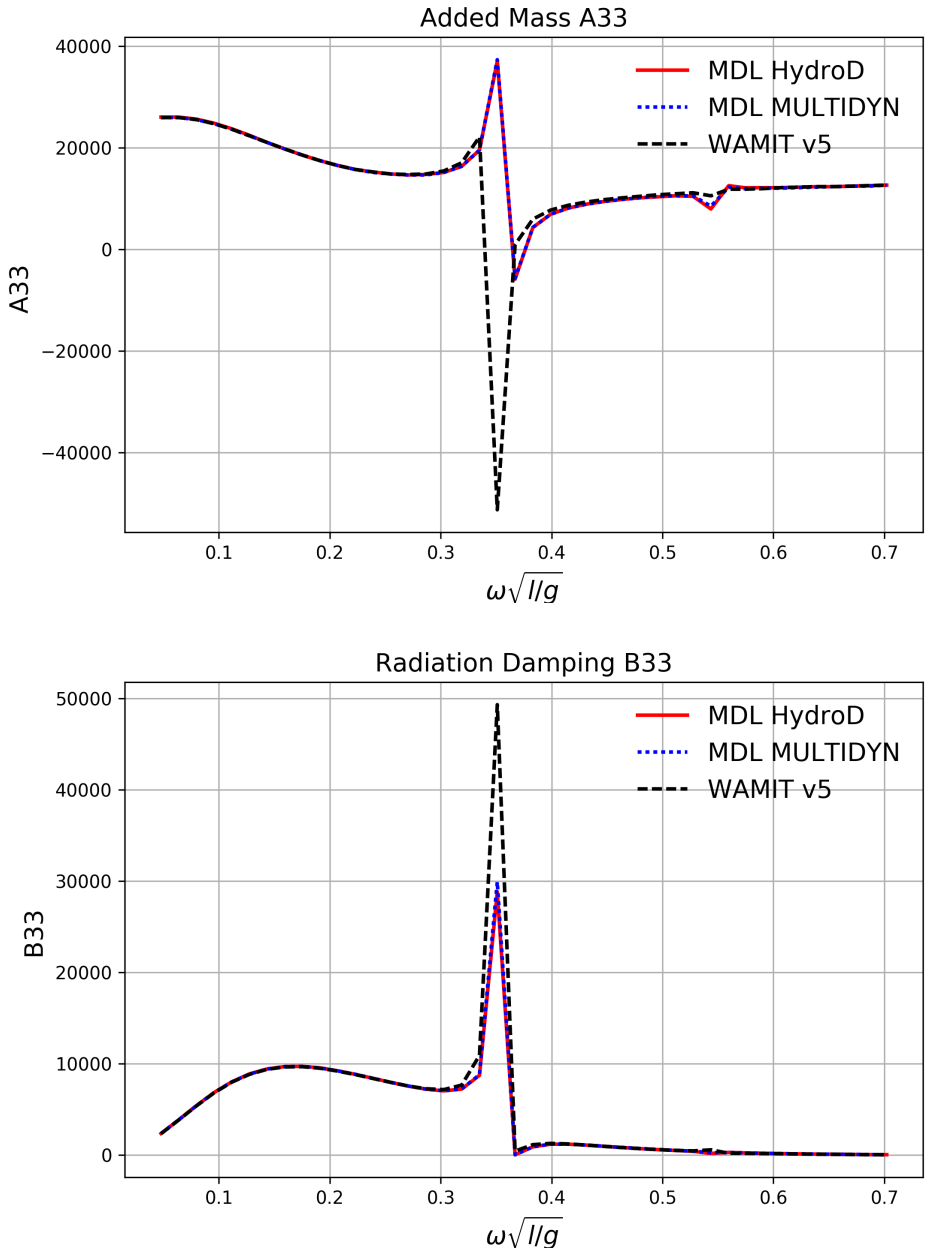

Figure A.5: Case without moonpool Added Mass A33 and Radiation damping B33

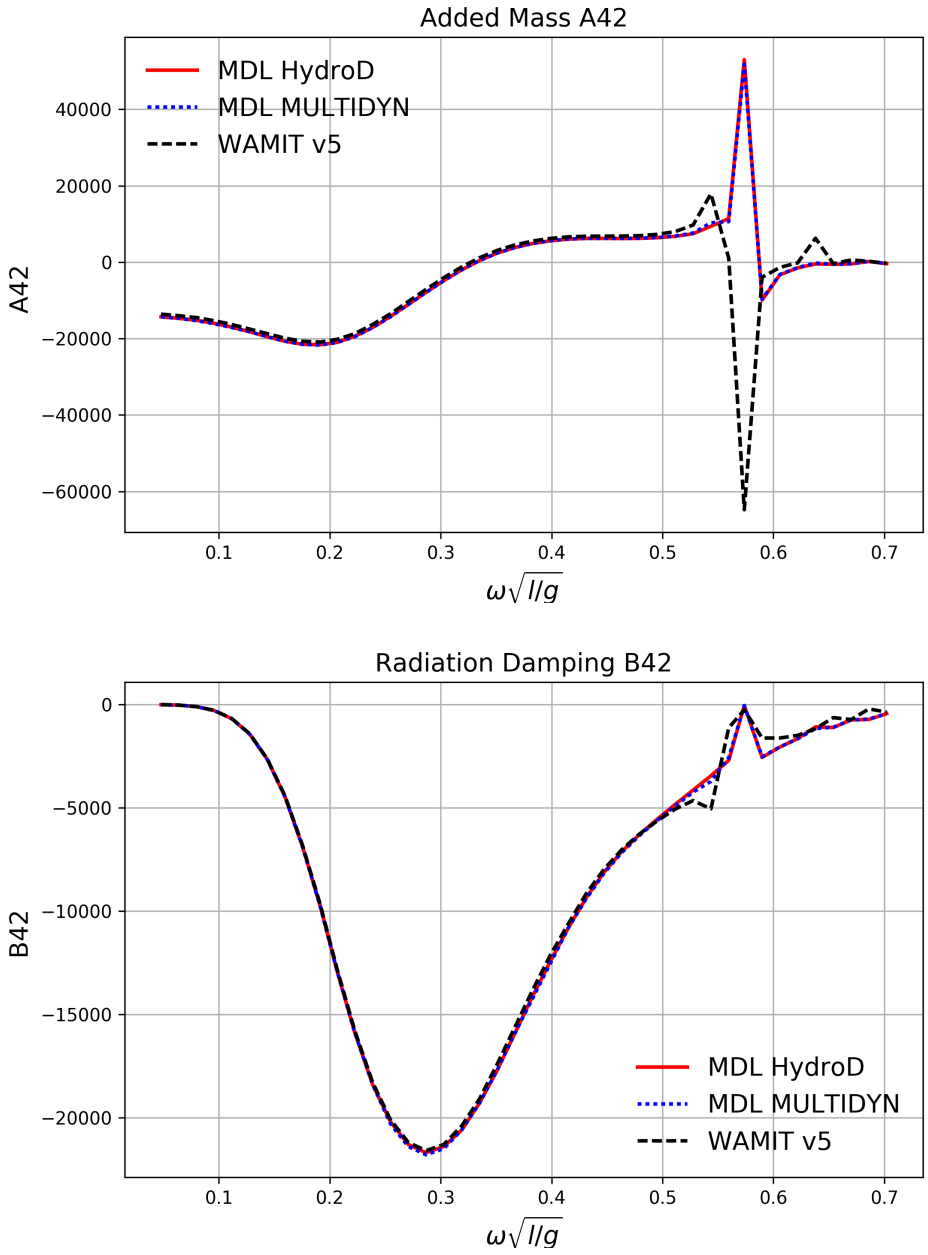

Figure A.6: Case without moonpool lid Added Mass A42 and Radiation damping B42

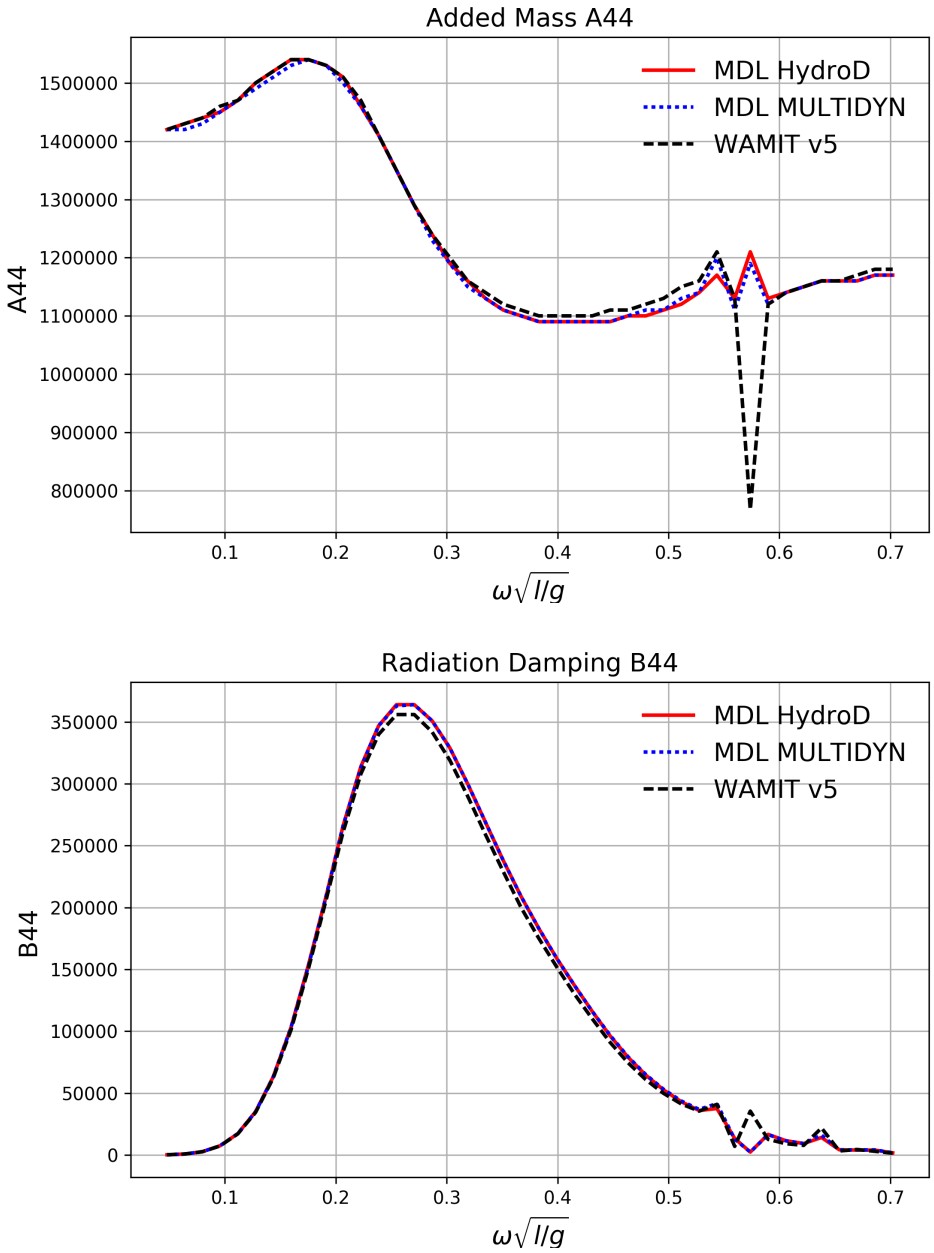

Figure A.7: Case without moonpool lid Added Mass A44 and Radiation damping B44

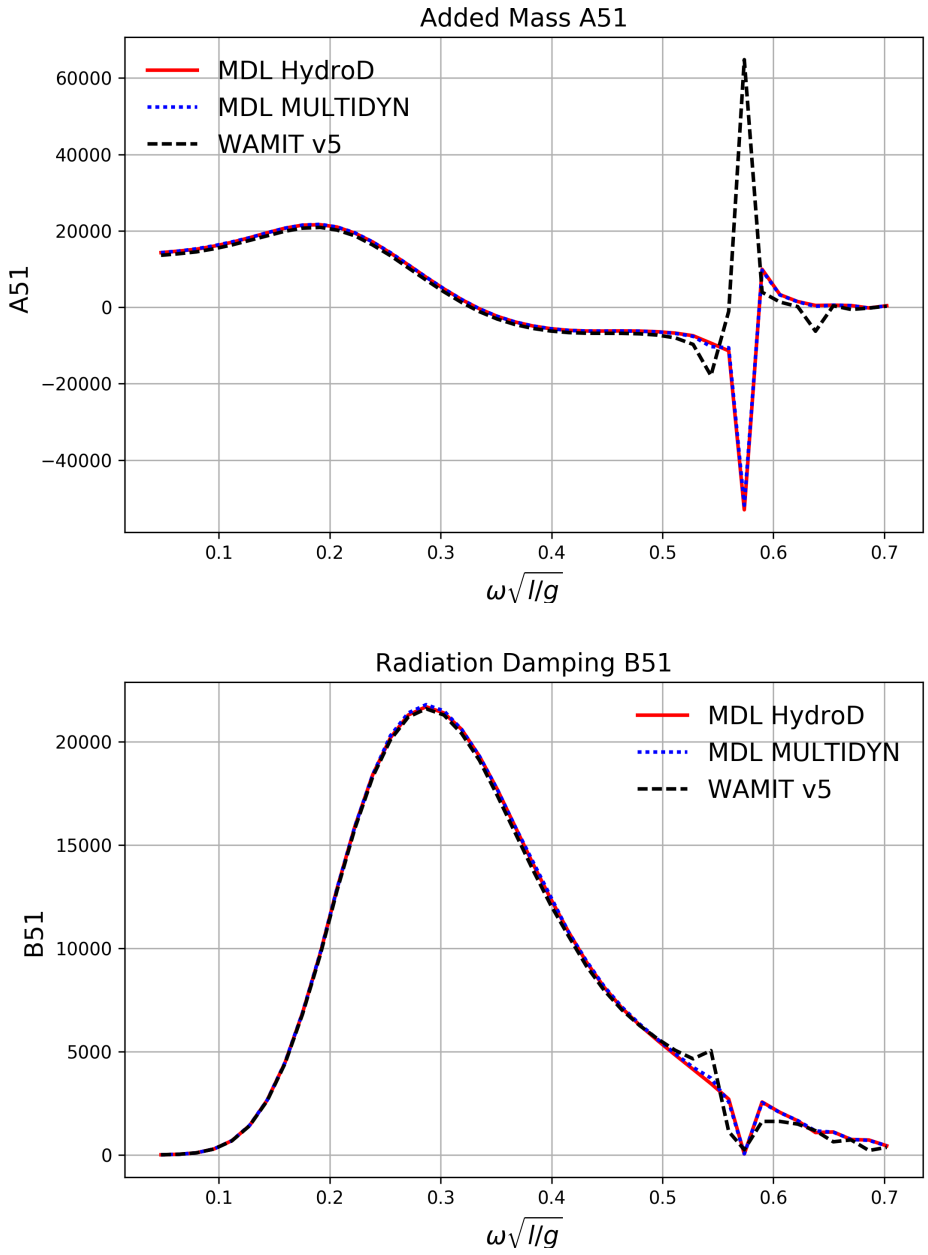

Figure A.8: Case without moonpool lid Added Mass A51 and Radiation damping B51

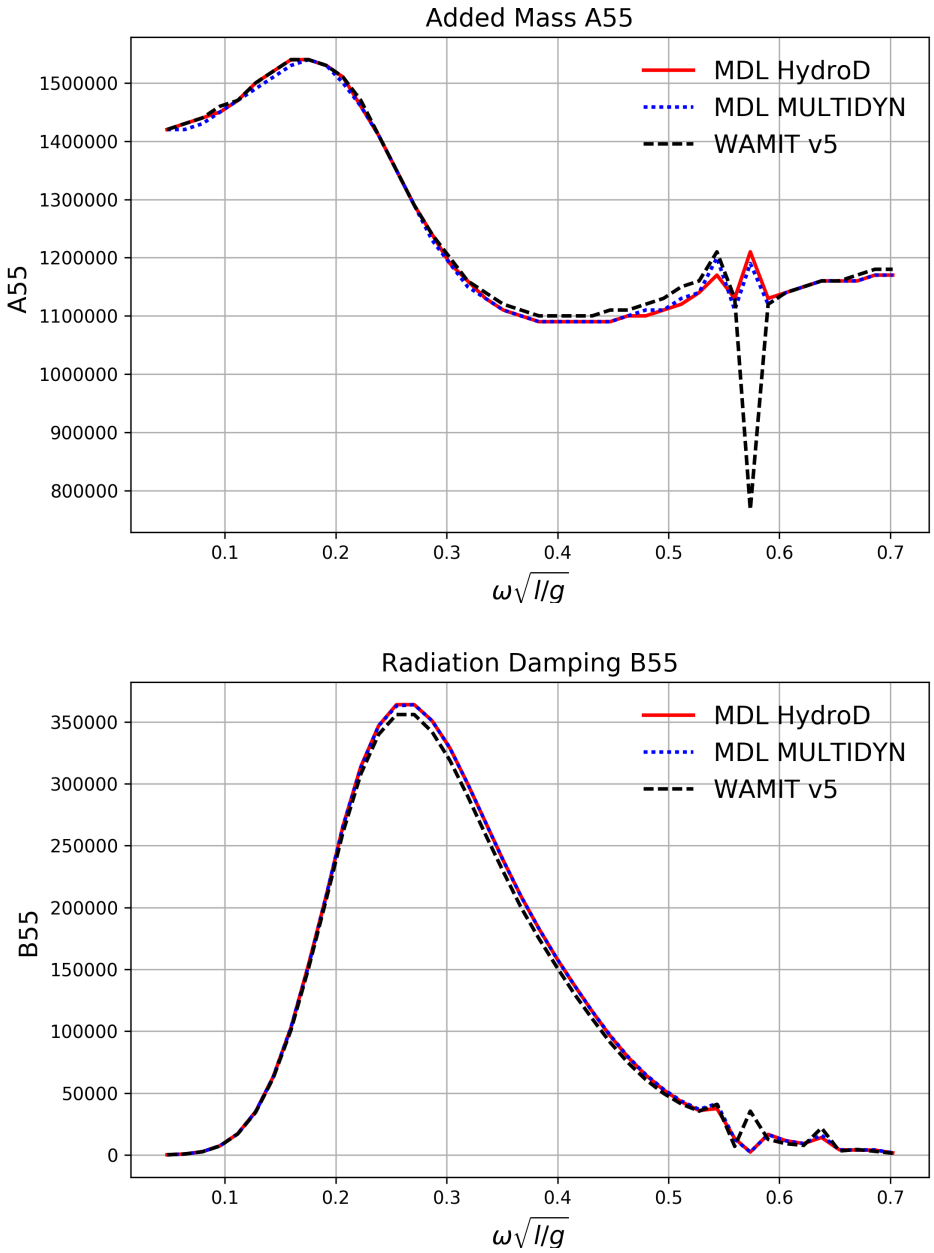

Figure A.9: Case without moonpool lid Added Mass A55 and Radiation damping B55

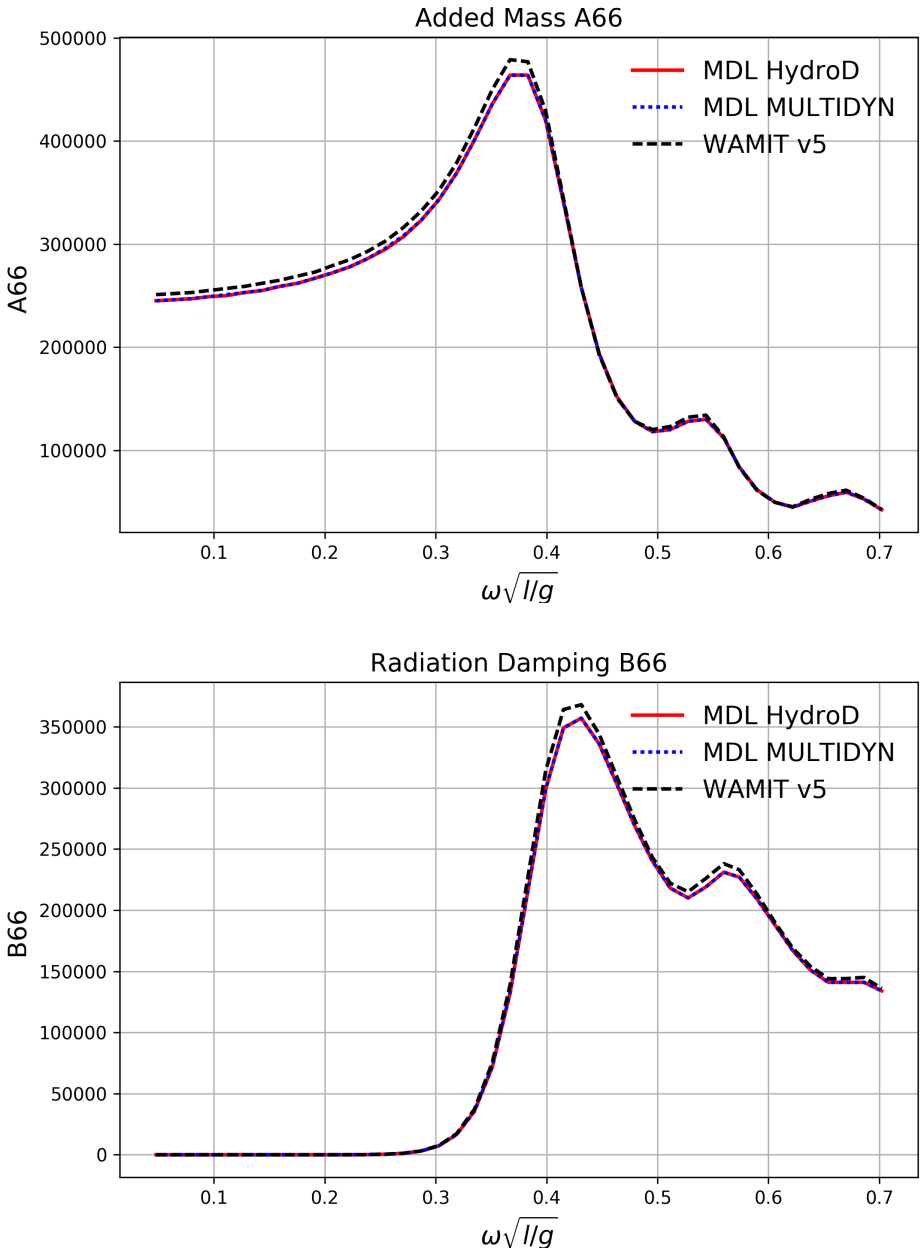

Figure A.10: Case without moonpool lid Added Mass A66 and Radiation damping B66

A.2 Plots for ITI Energy Barge Radiation Added Mass and Damping for Cases With Moonpool Lid

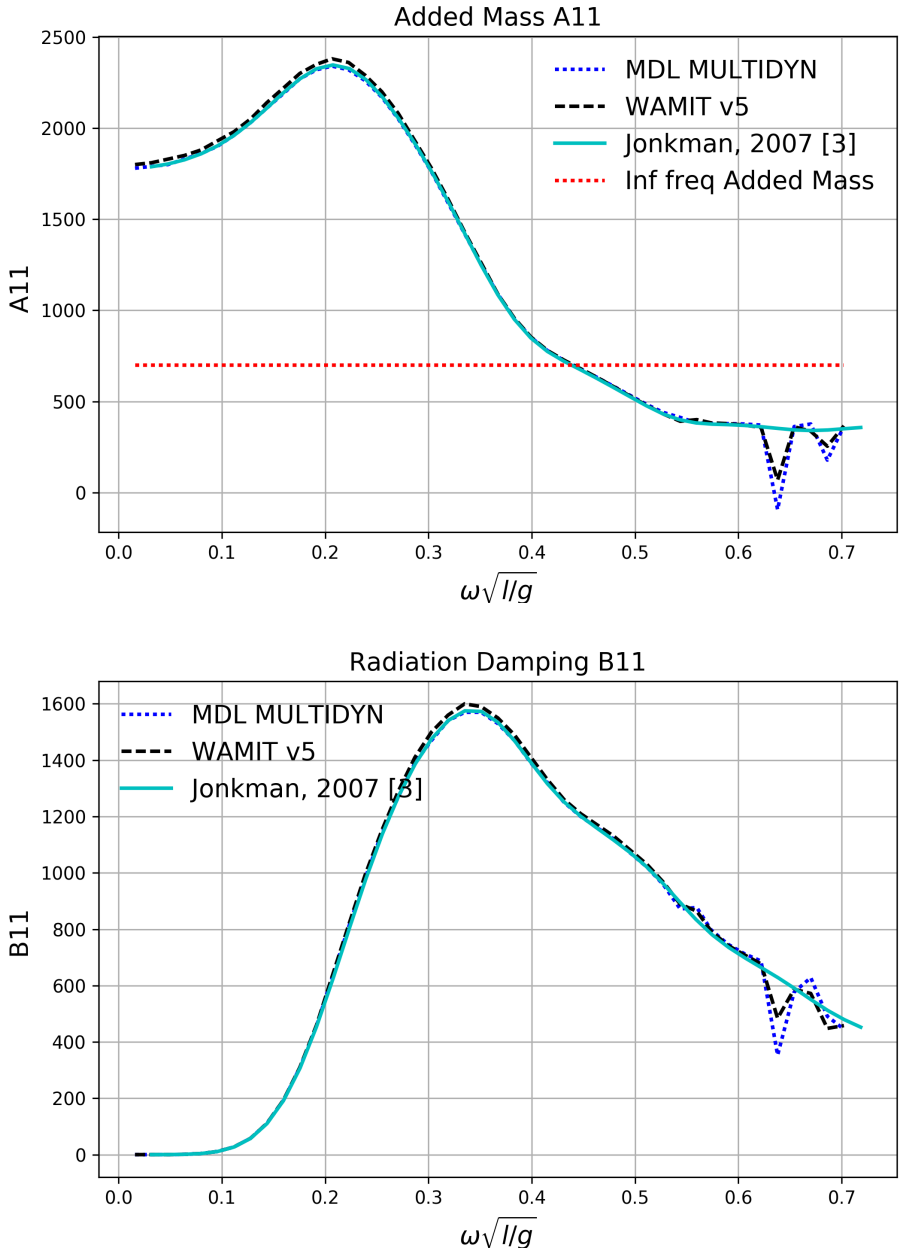

Figure A.11: Case with moonpool lid Added Mass A11 and Radiation damping B11

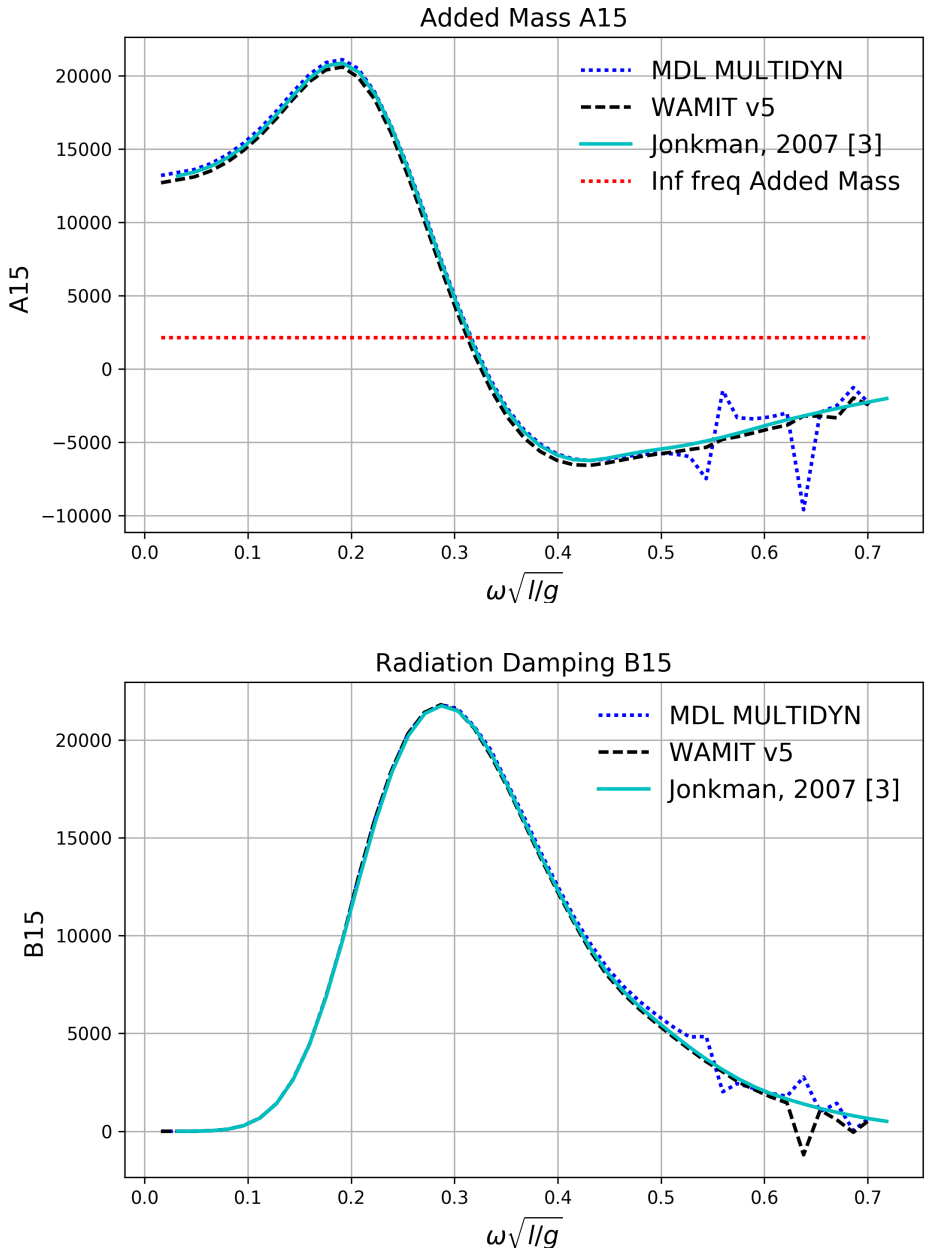

Figure A.12: Case with moonpool lid Added Mass A15 and Radiation damping B15

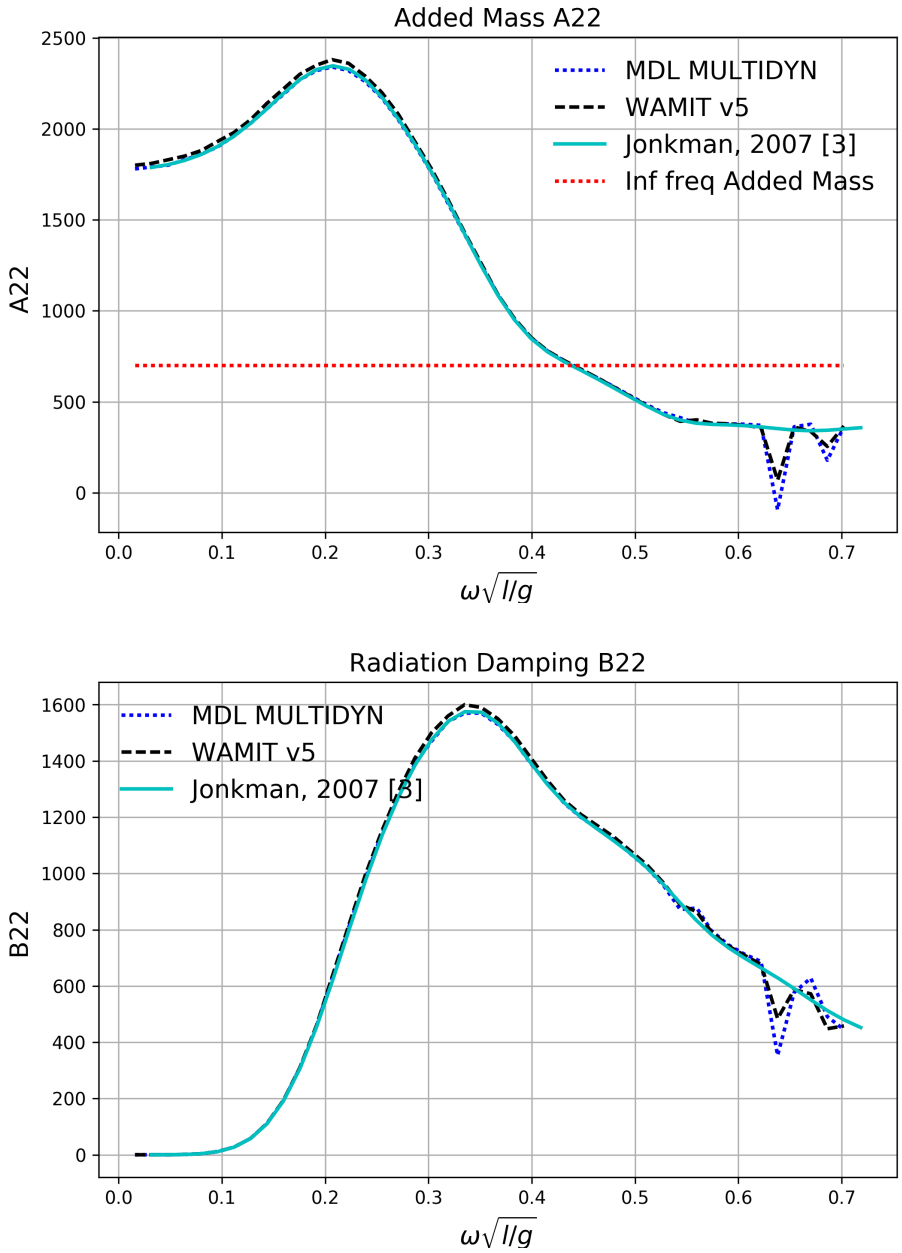

Figure A.13: Case with moonpool lid Added Mass A22 and Radiation damping B22

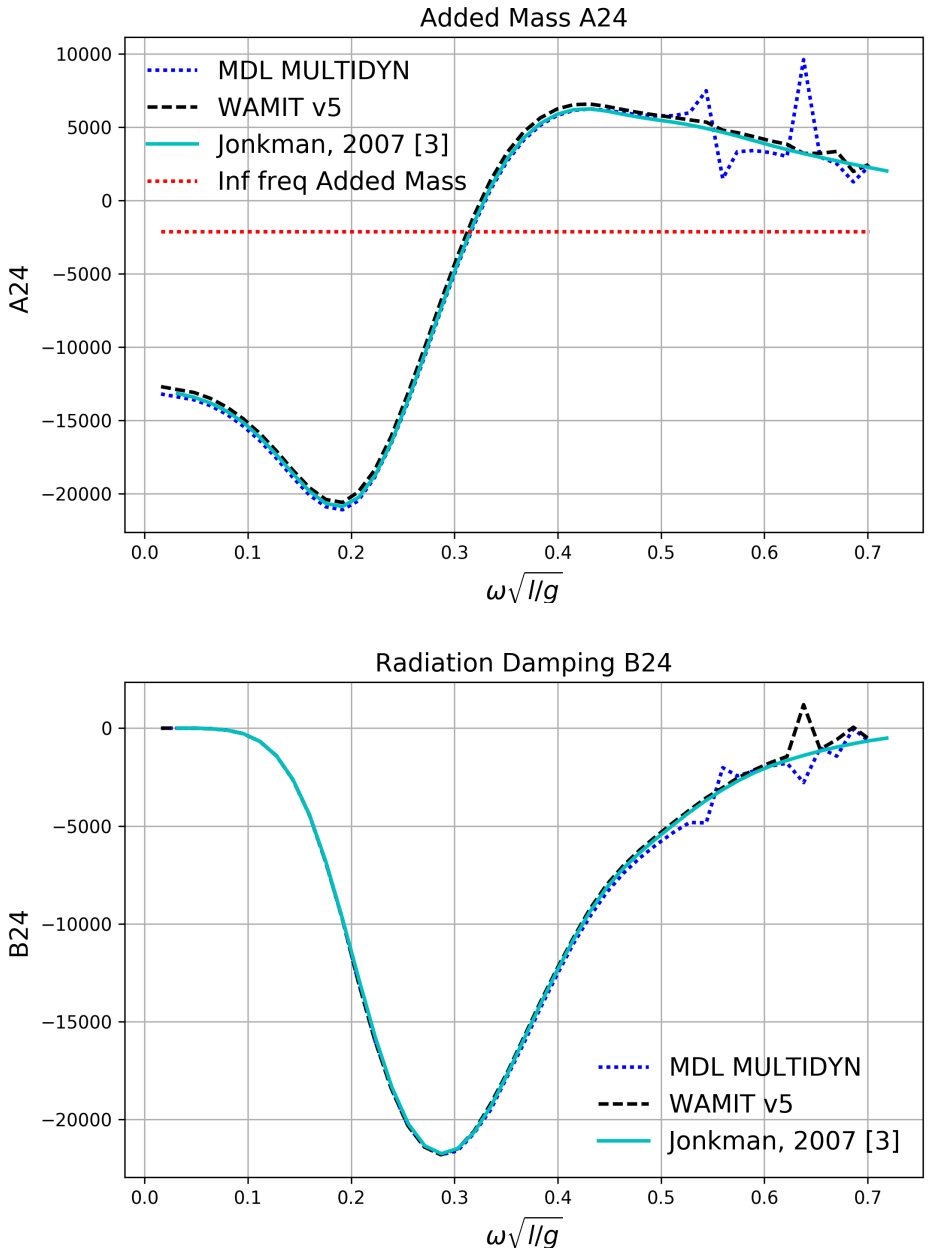

Figure A.14: Case with moonpool lid Added Mass A24 and Radiation damping B24

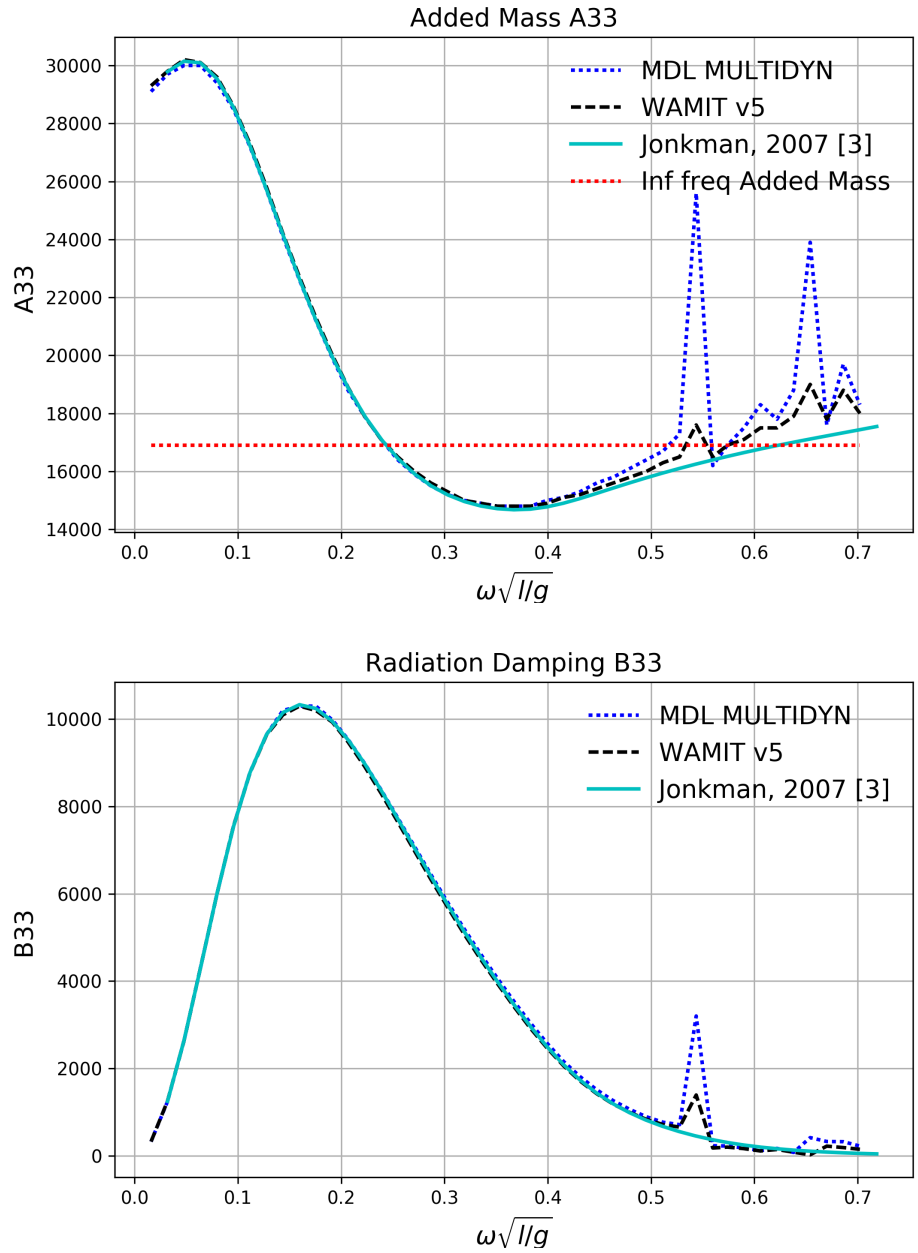

Figure A.15: Case with moonpool lid Added Mass A33 and Radiation damping B33

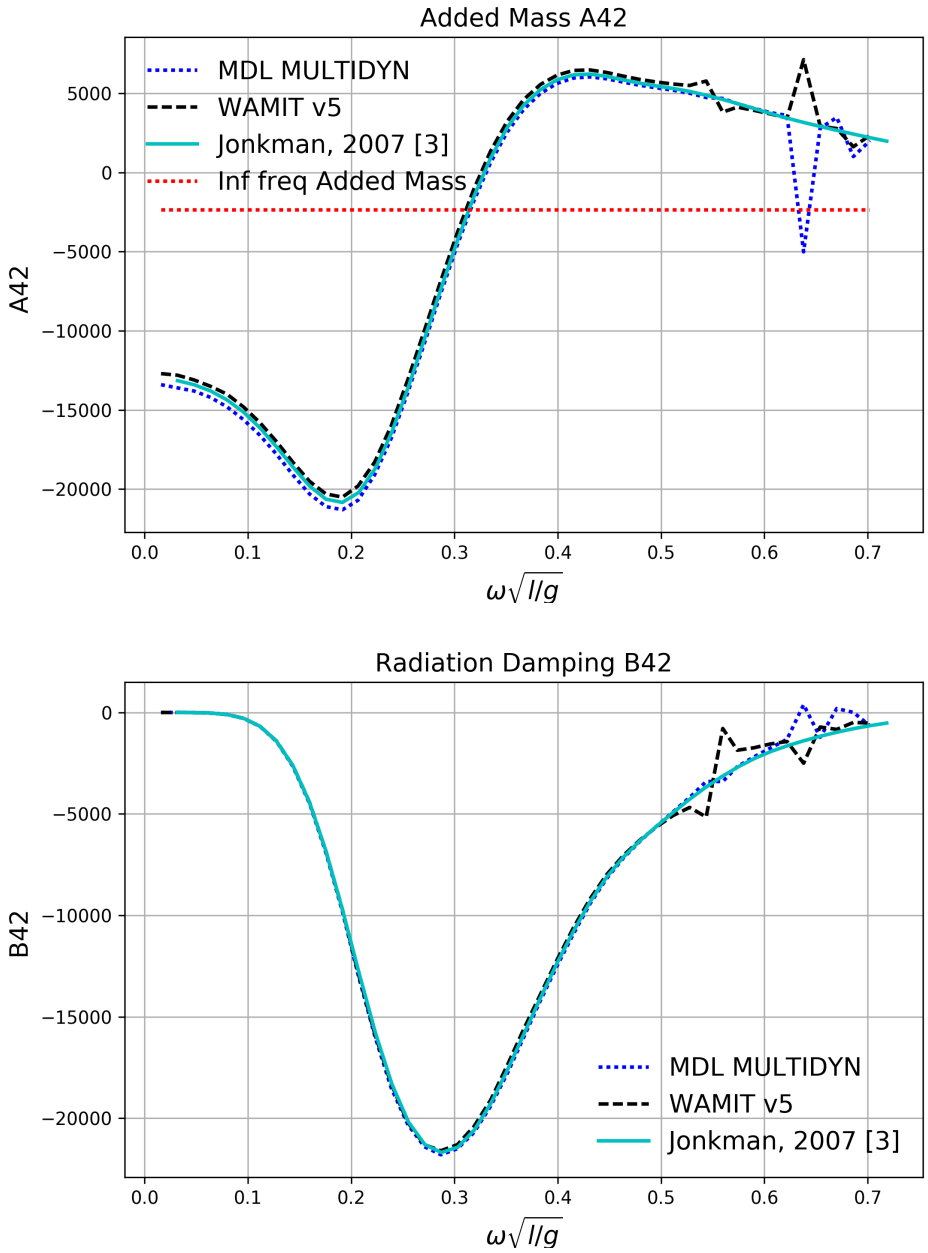

Figure A.16: Case with moonpool lid Added Mass A42 and Radiation damping B42

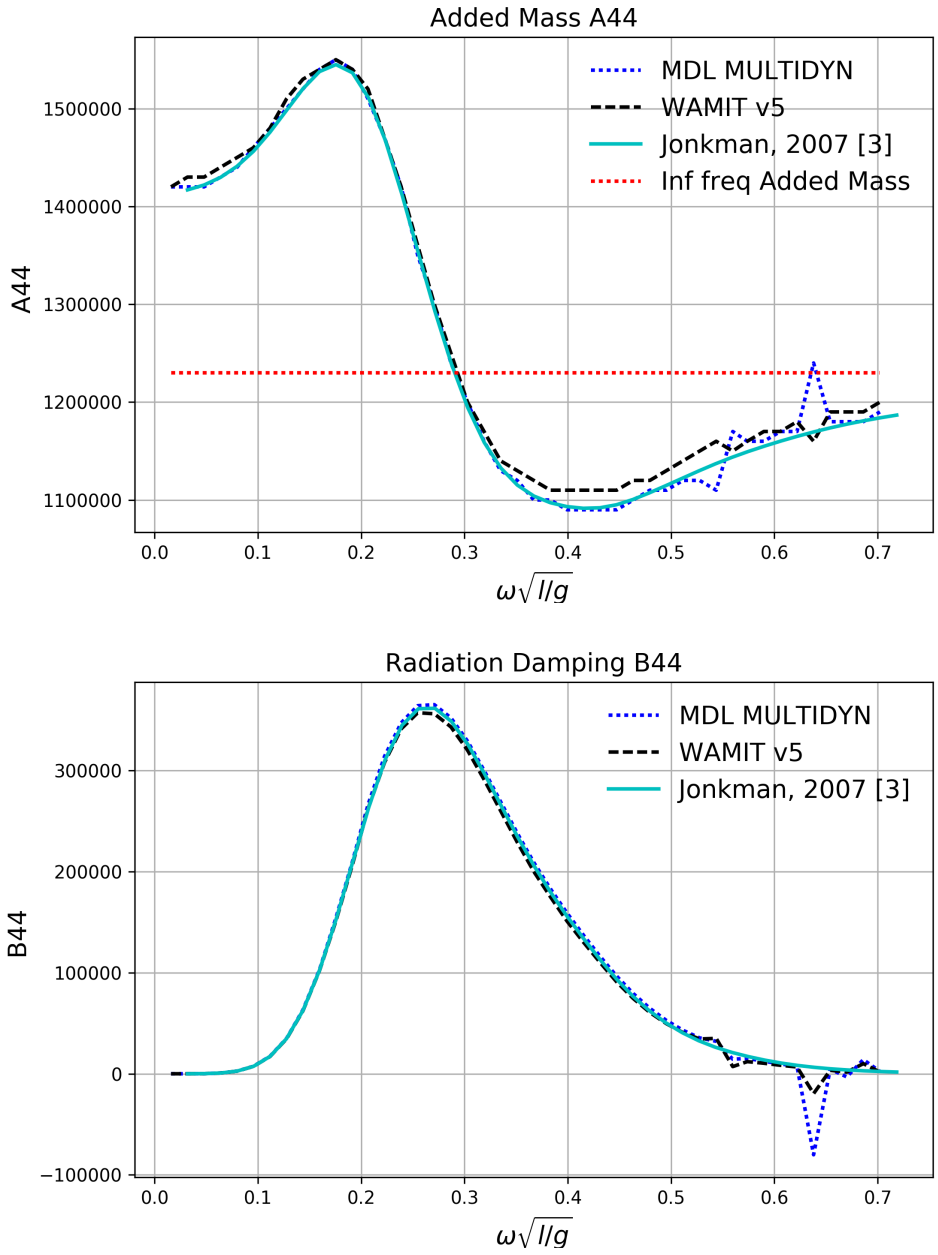

Figure A.17: Case with moonpool lid Added Mass A44 and Radiation damping B44

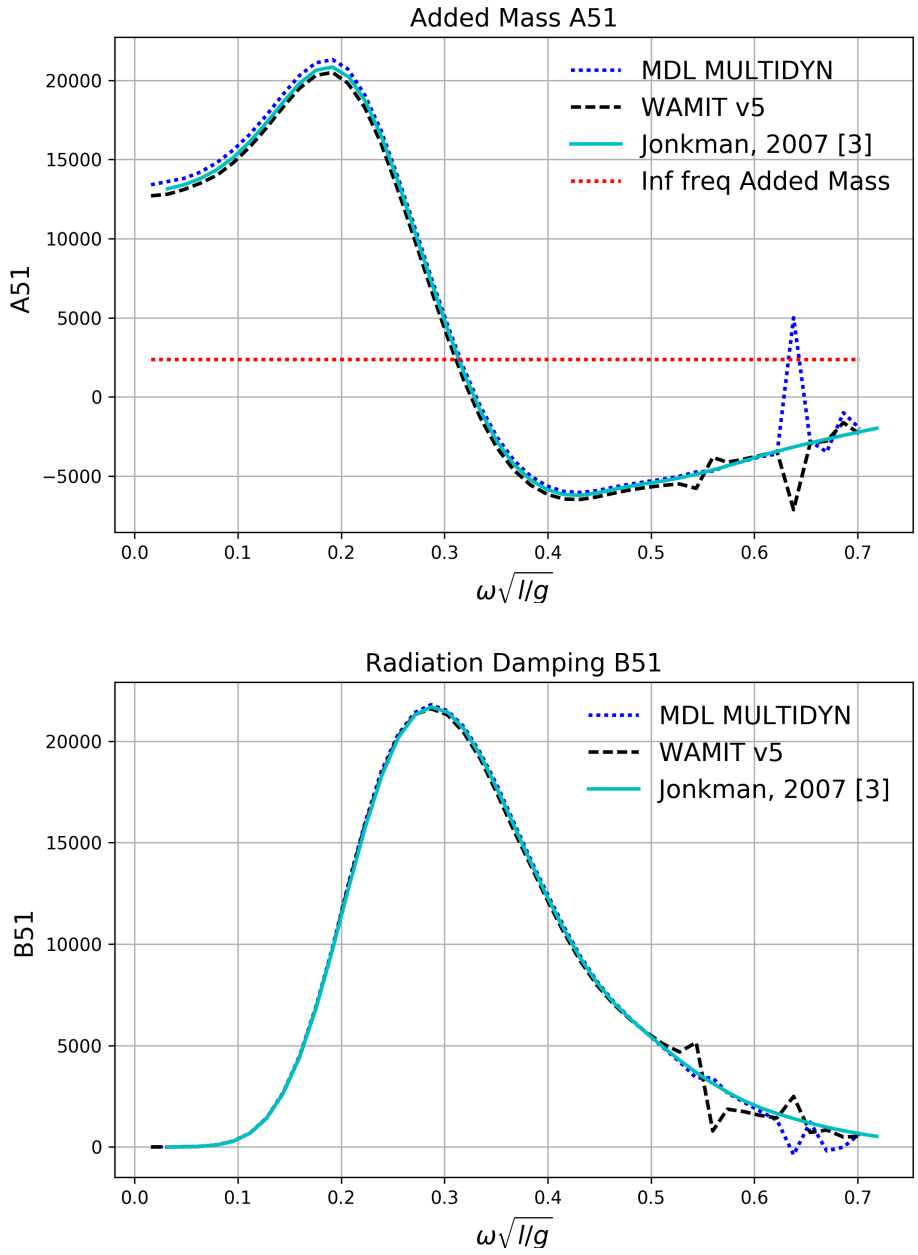

Figure A.18: Case with moonpool lid Added Mass A51 and Radiation damping B51

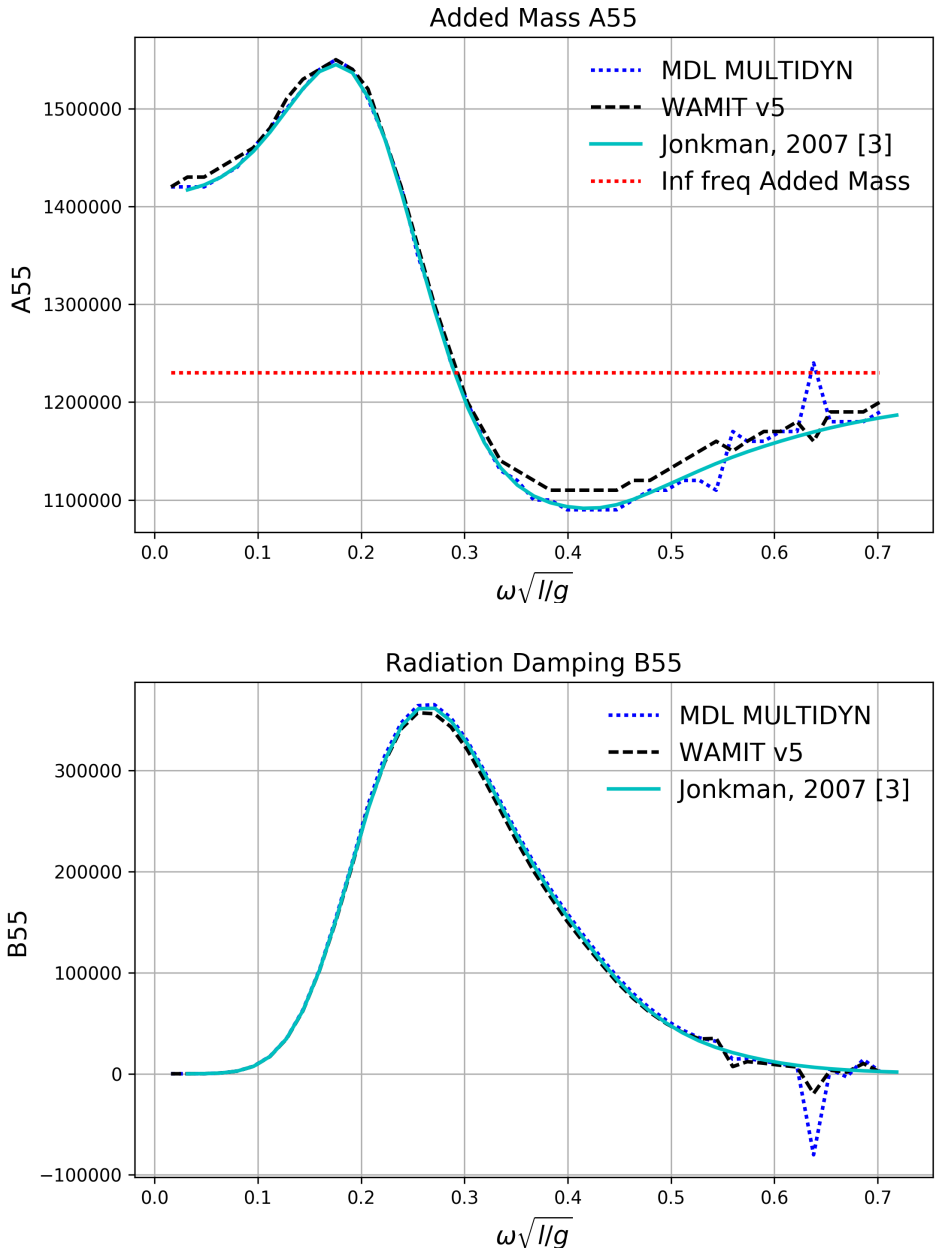

Figure A.19: Case with moonpool lid Added Mass A55 and Radiation damping B55

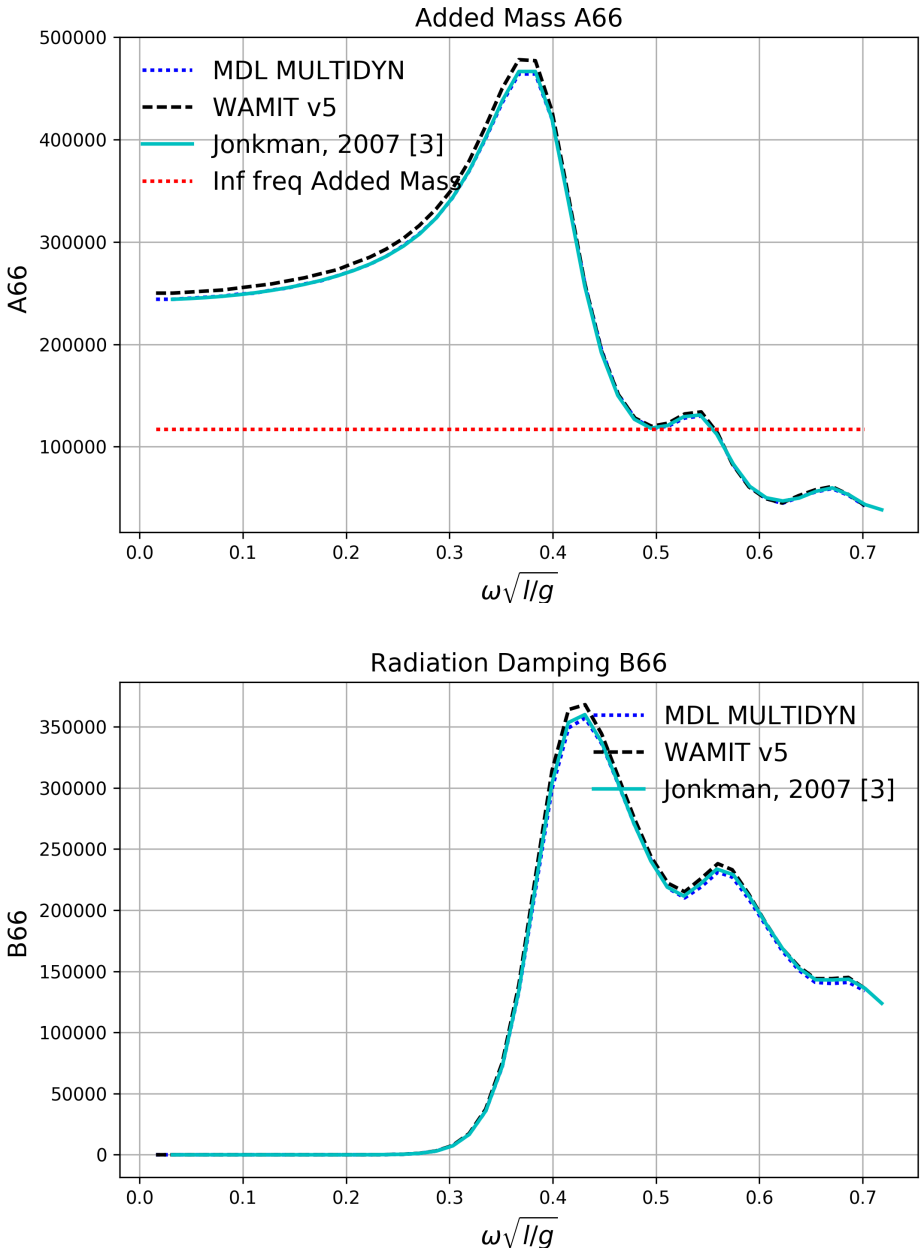

Figure A.20: Added Mass A66 and Radiation damping B66

APPENDIX B - VALIDATION PLOTS OF TIME DOMAIN COUPLED PROGRAM FAST-SIMDYN

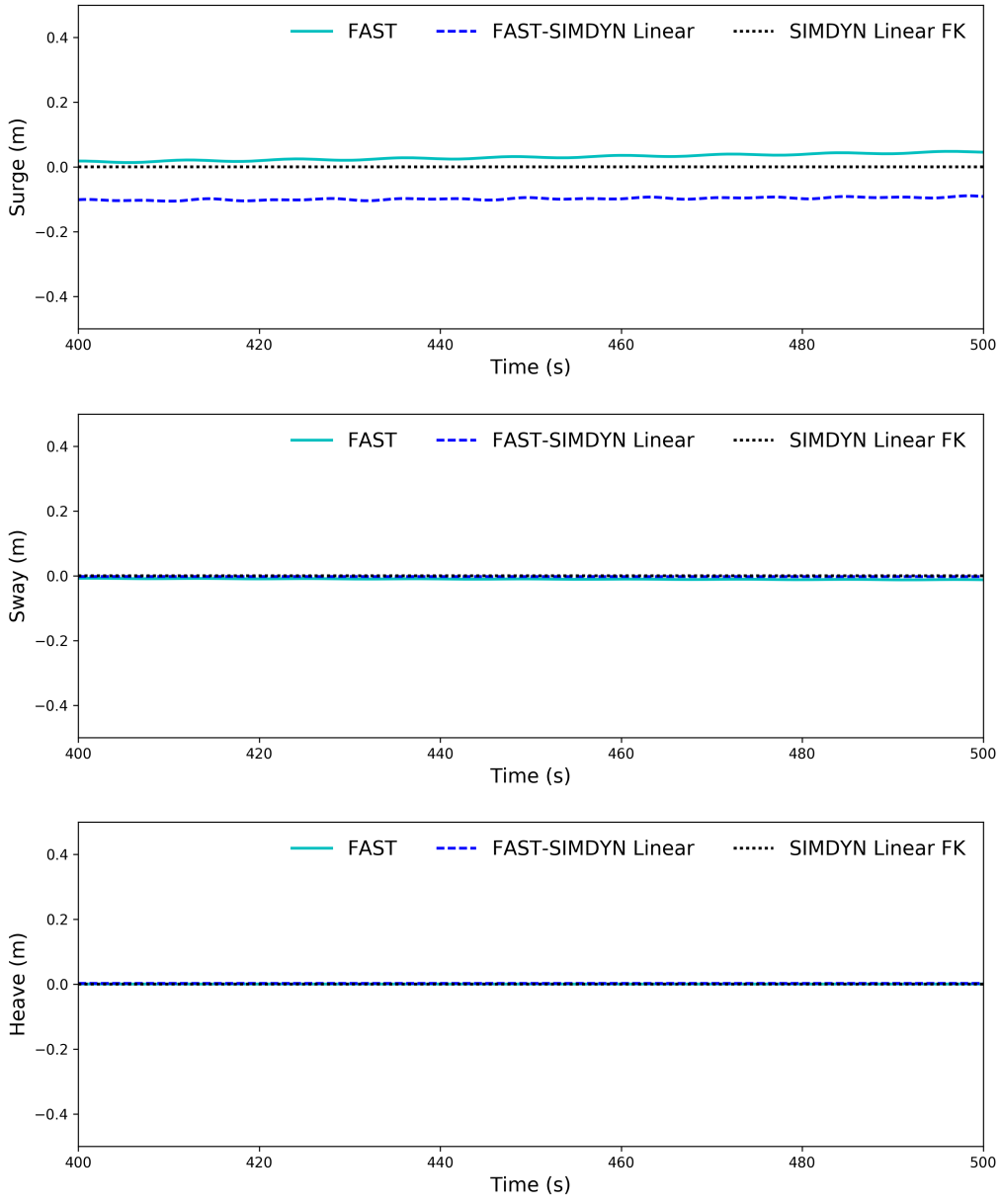

Figure B.1: Translation motion response in zero wind zero wave without mooring

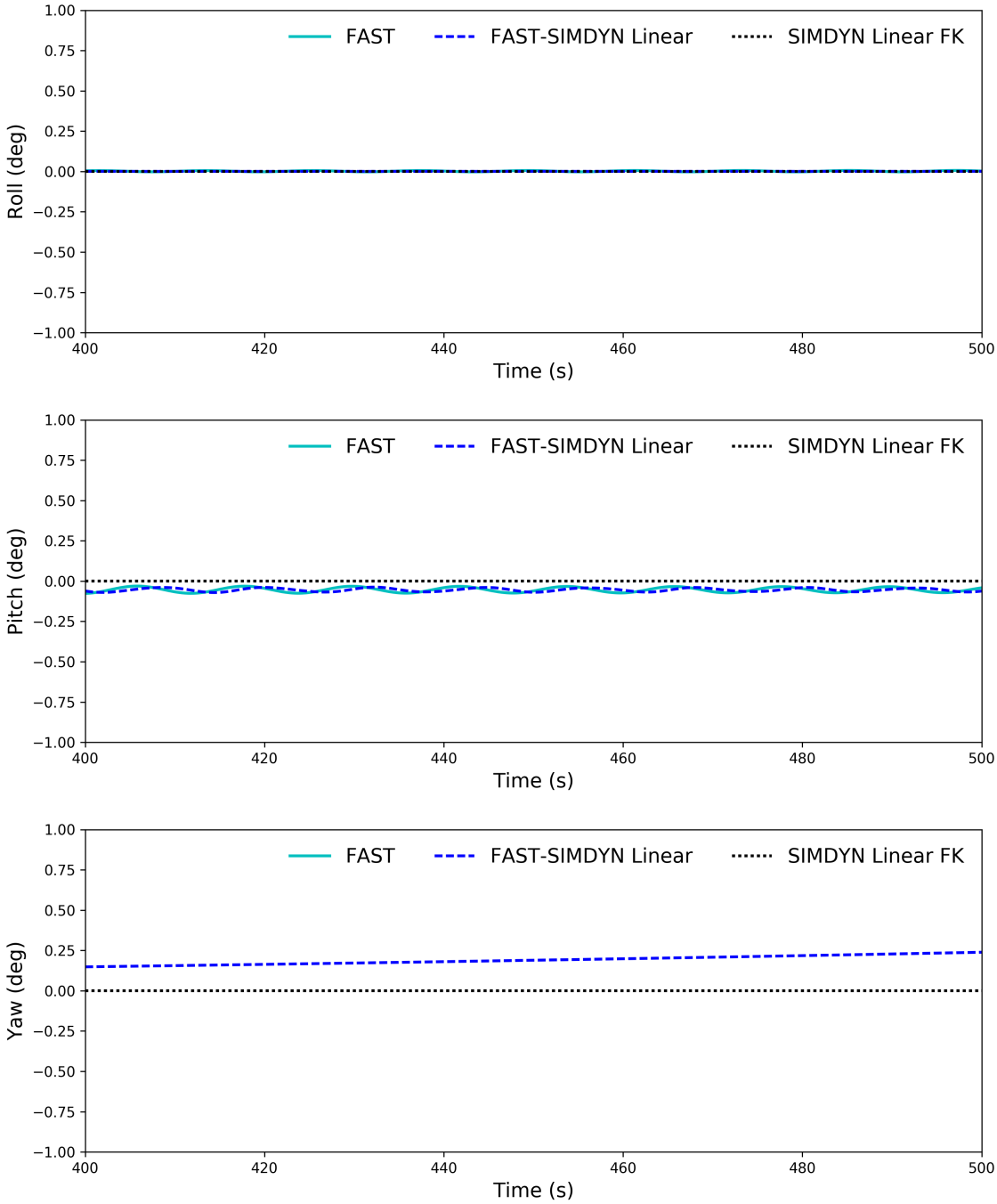

Figure B.2: Rotation motion response in zero wind zero wave without mooring

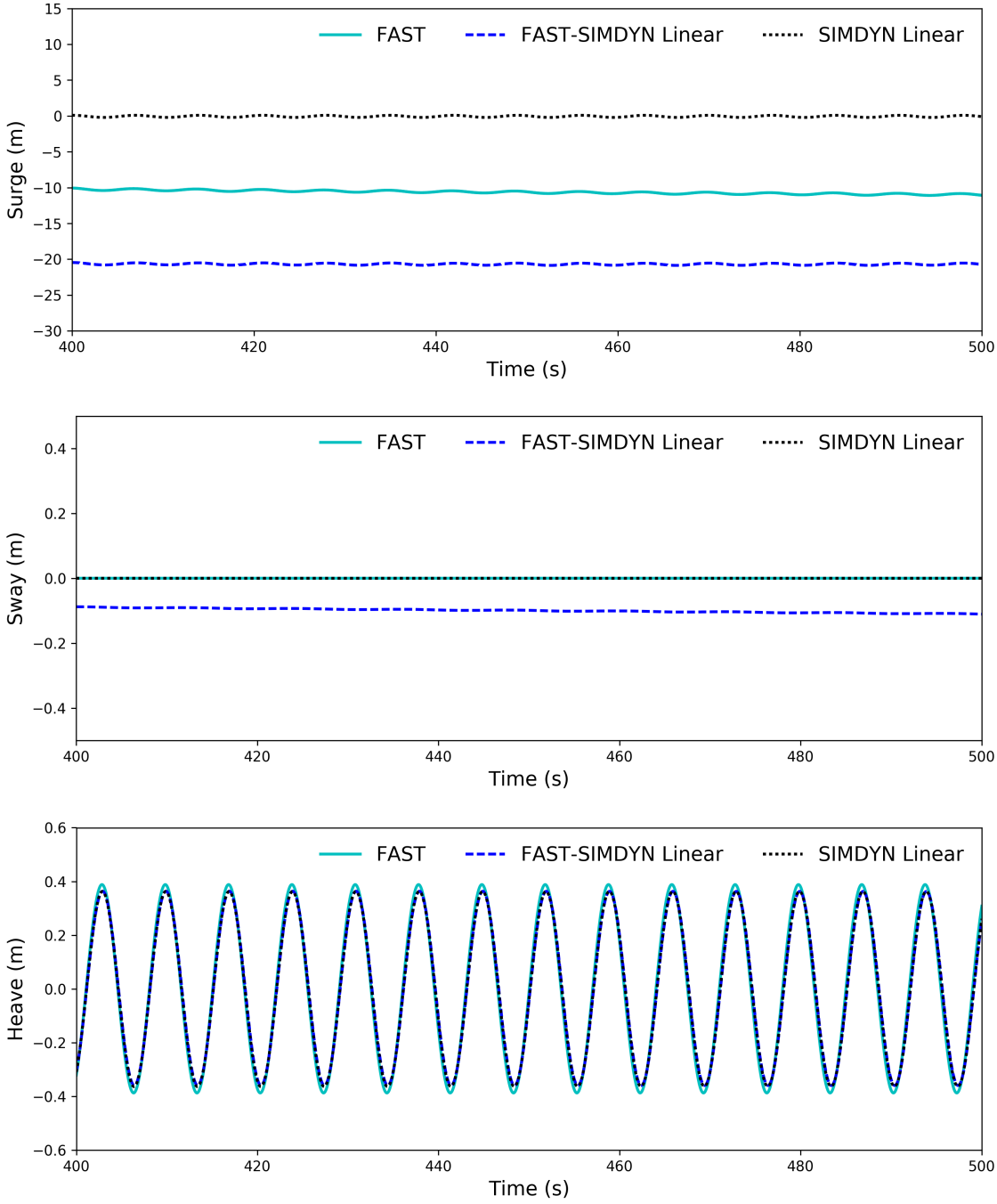

Figure B.3: Translation motion response in zero wind 1m 7s regular wave without mooring

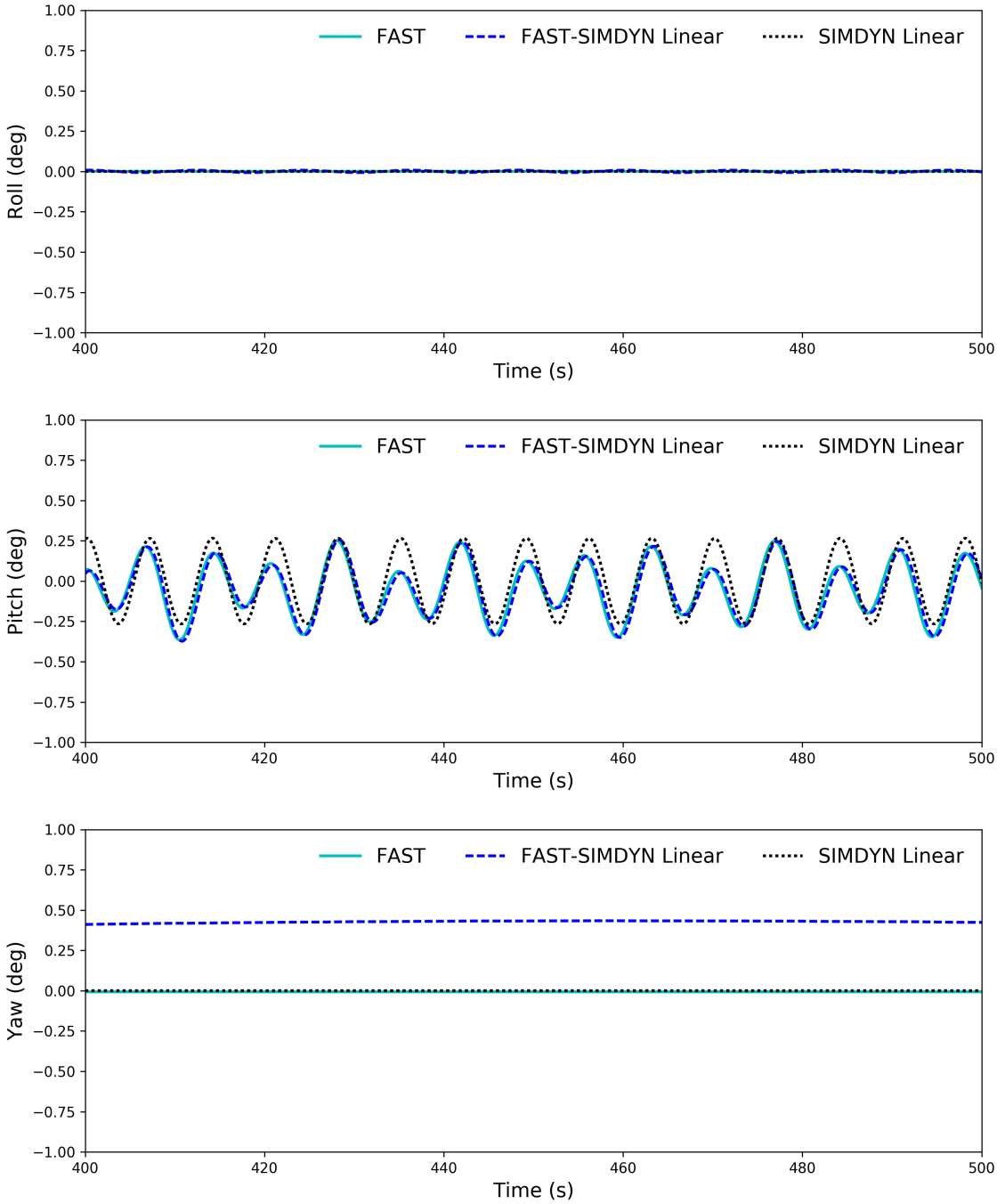

Figure B.4: Rotation motion response in zero wind 1m 7s regular wave without mooring

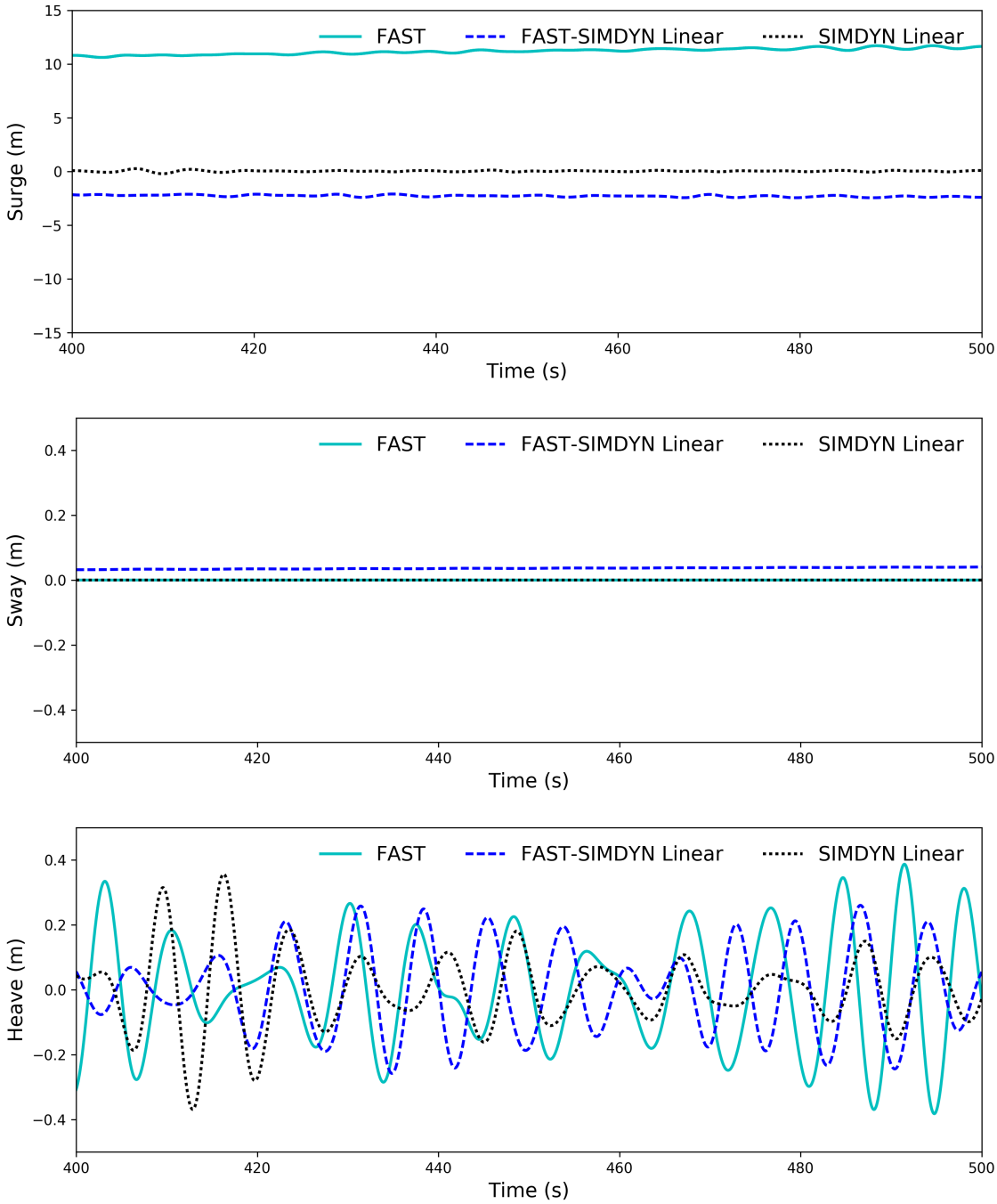

Figure B.5: Translation motion response in zero wind 1m 7s JONSWAP wave without mooring

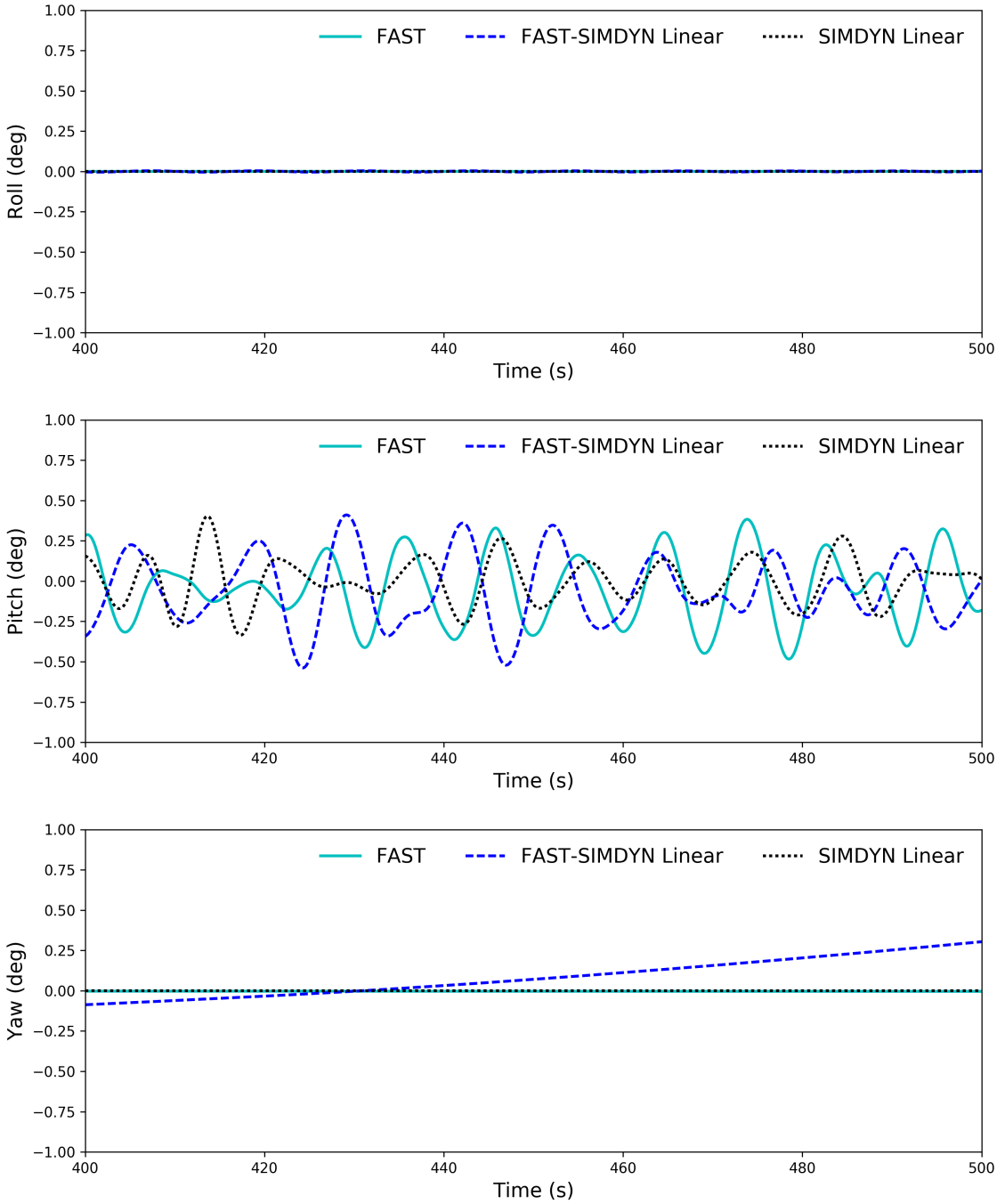

Figure B.6: Rotation motion response in zero wind 1m 7s JONSWAP wave without mooring

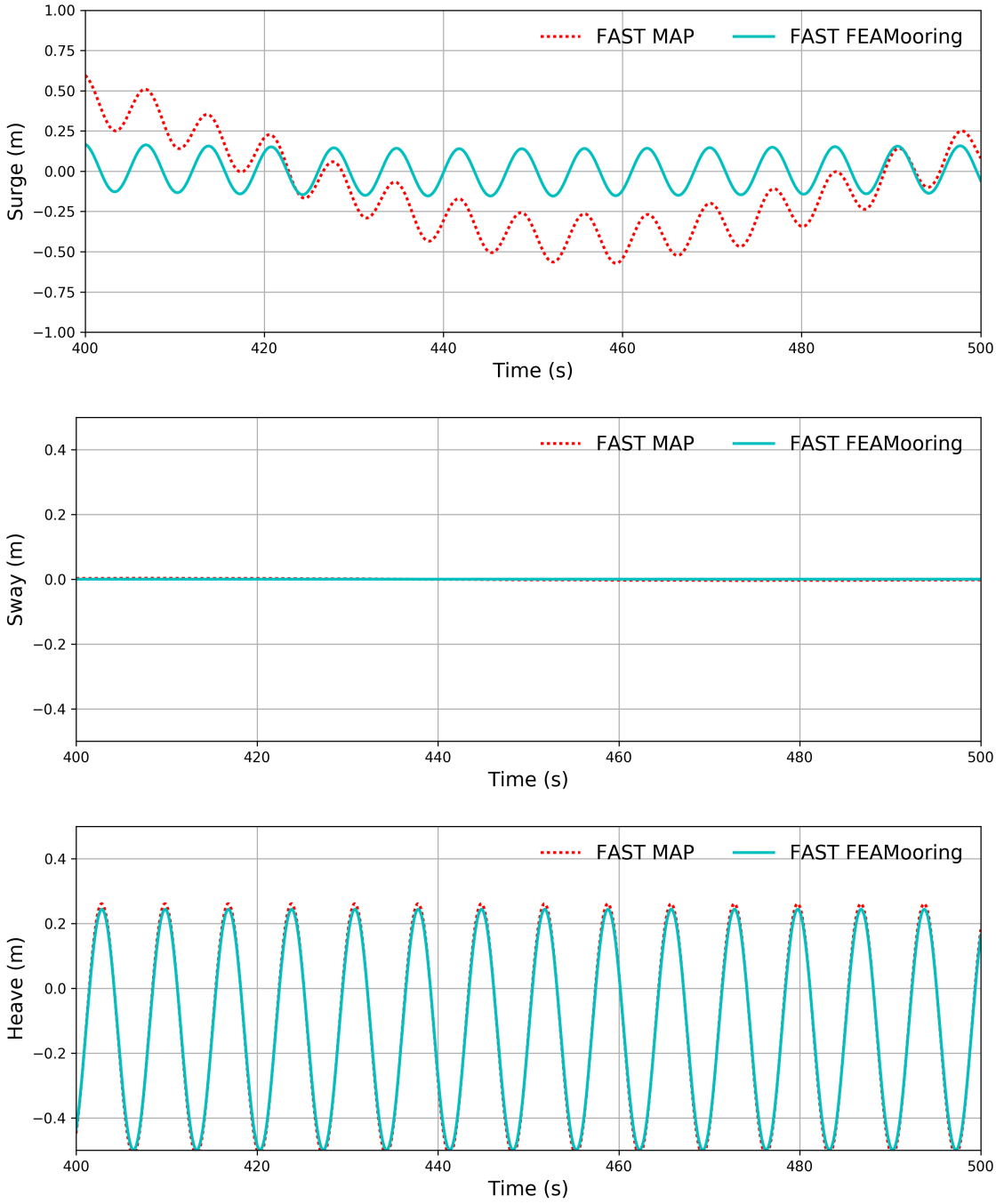

Figure B.7: Translation motion response in zero wind 1m 7s regular wave MAP vs FEAMooring

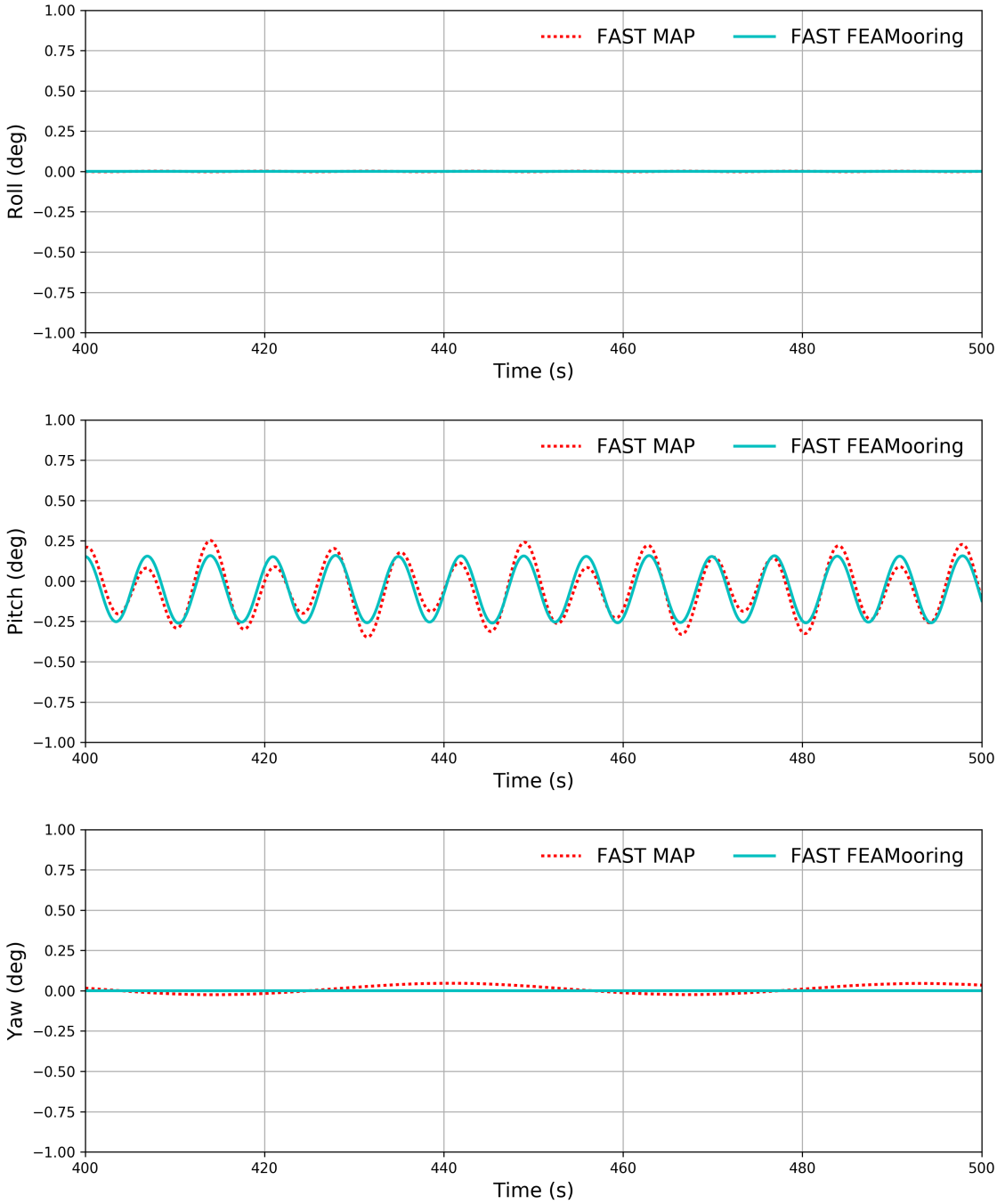

Figure B.8: Rotation motion response in zero wind 1m 7s regular wave MAP vs FEAMooring

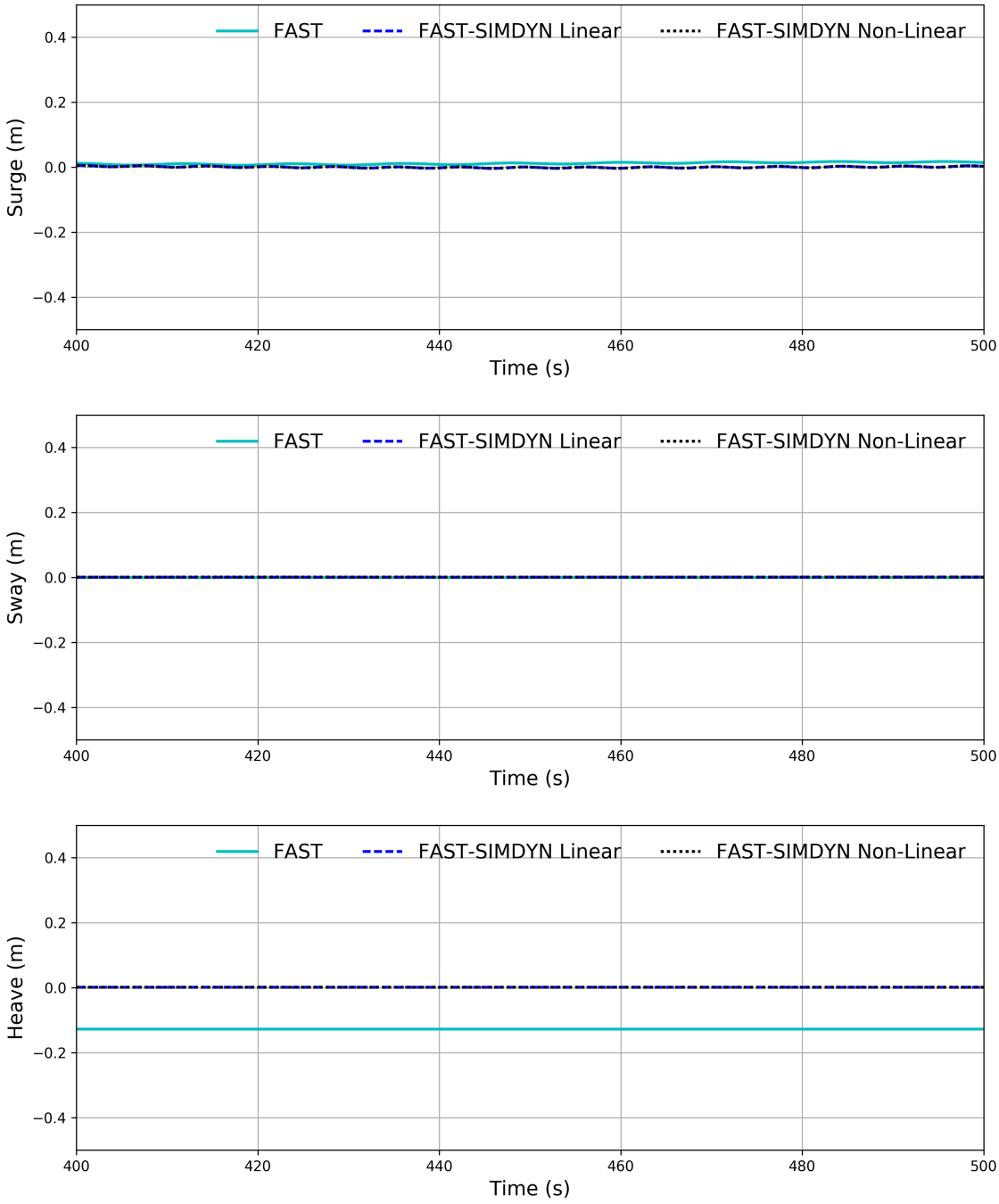

Figure B.9: Translation motion response in zero wind zero wave with FEAMooring

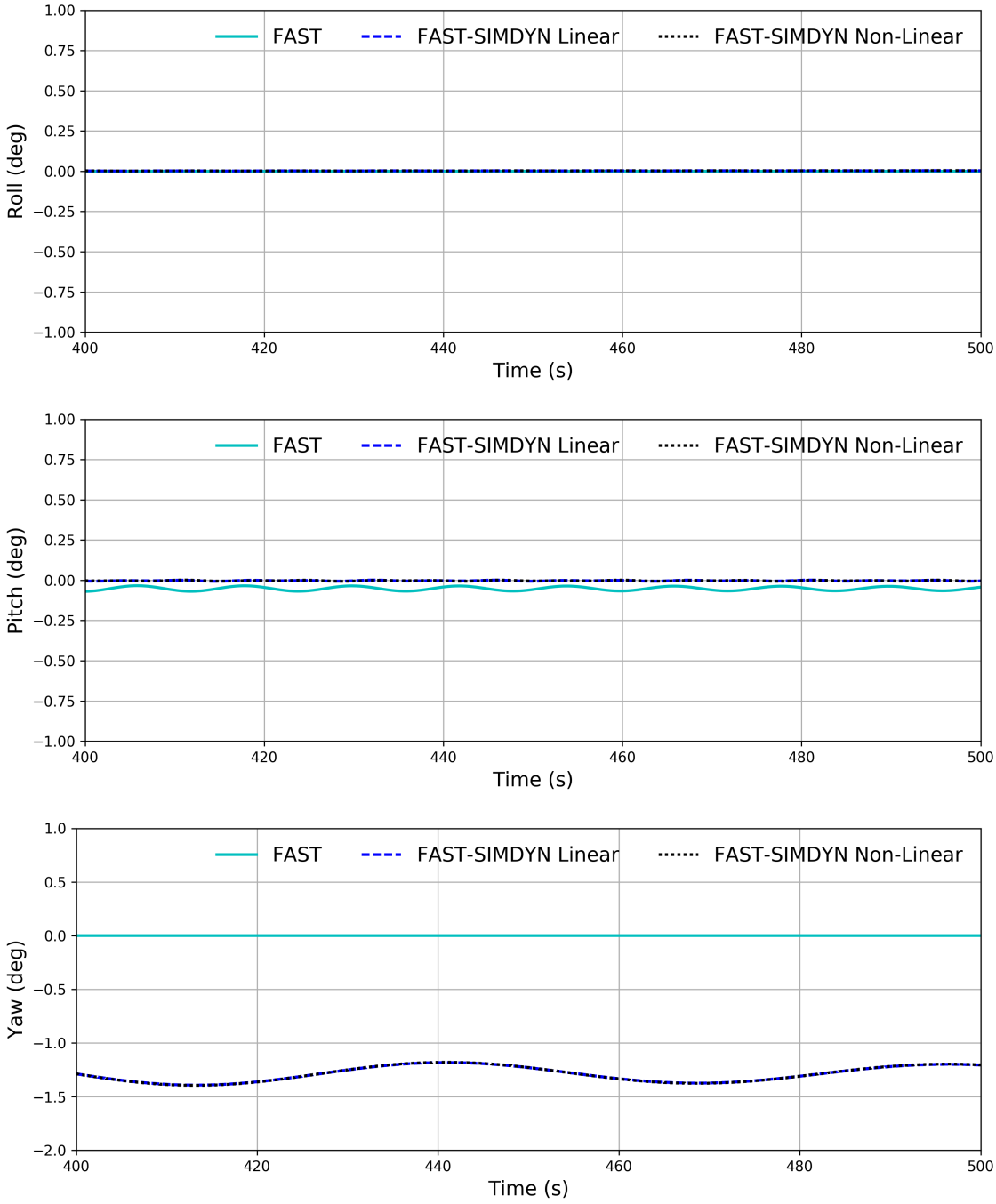

Figure B.10: Rotation motion response in zero wind zero wave with FEAMooring

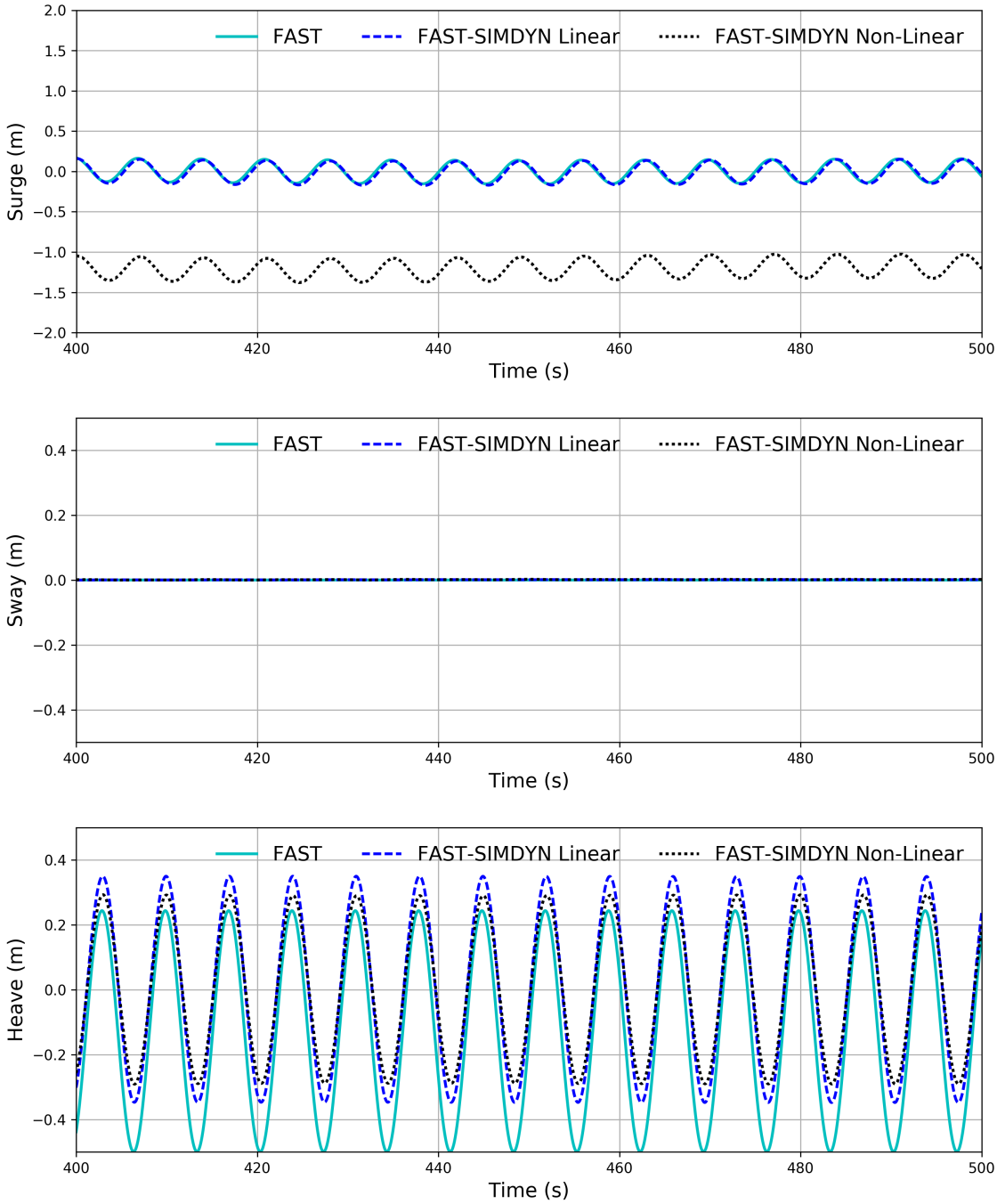

Figure B.11: Translation motion response in zero wind 1m 7s regular wave with FEAMooring

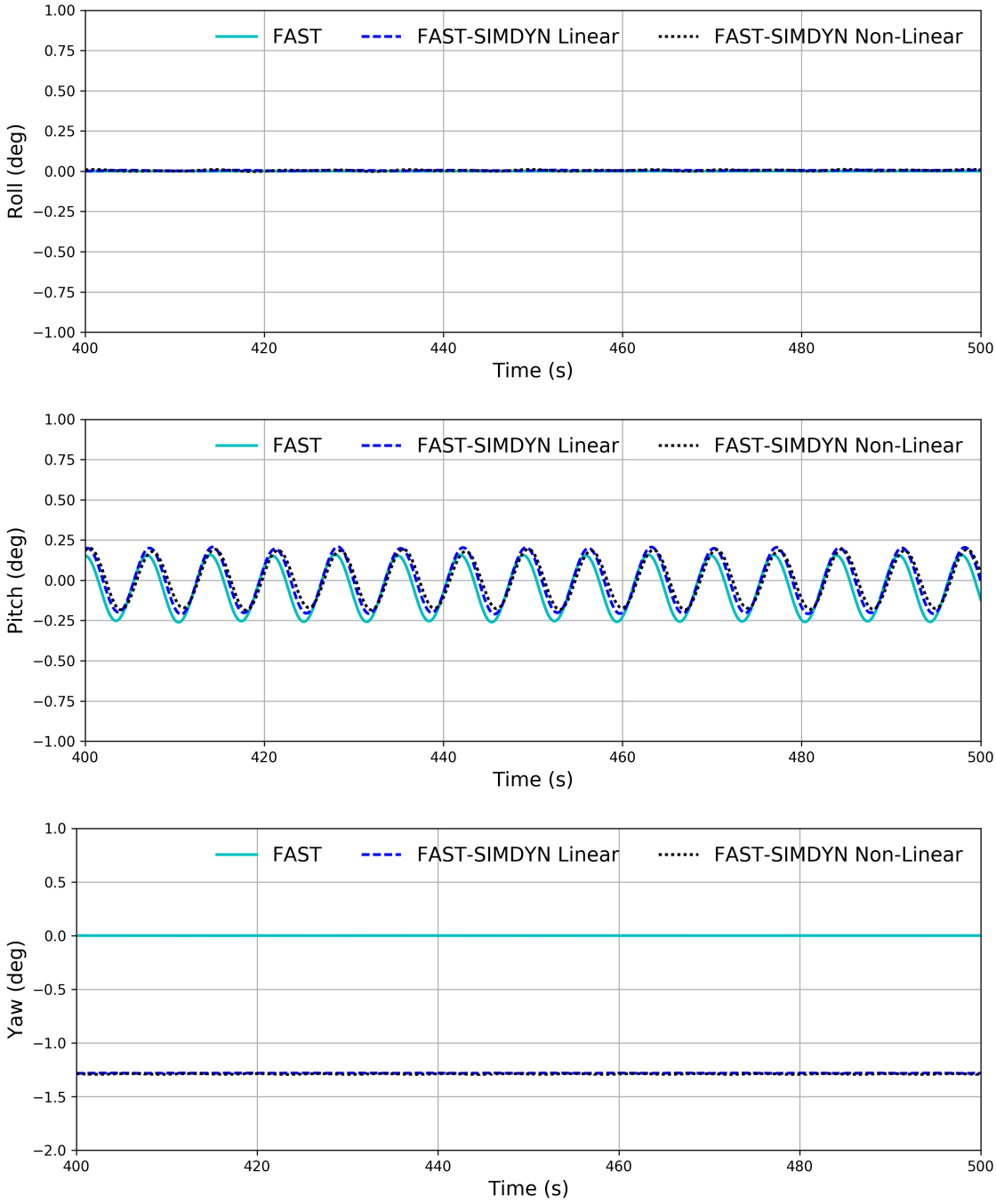

Figure B.12: Rotation motion response in zero wind 1m 7s regular wave with FEAMooring

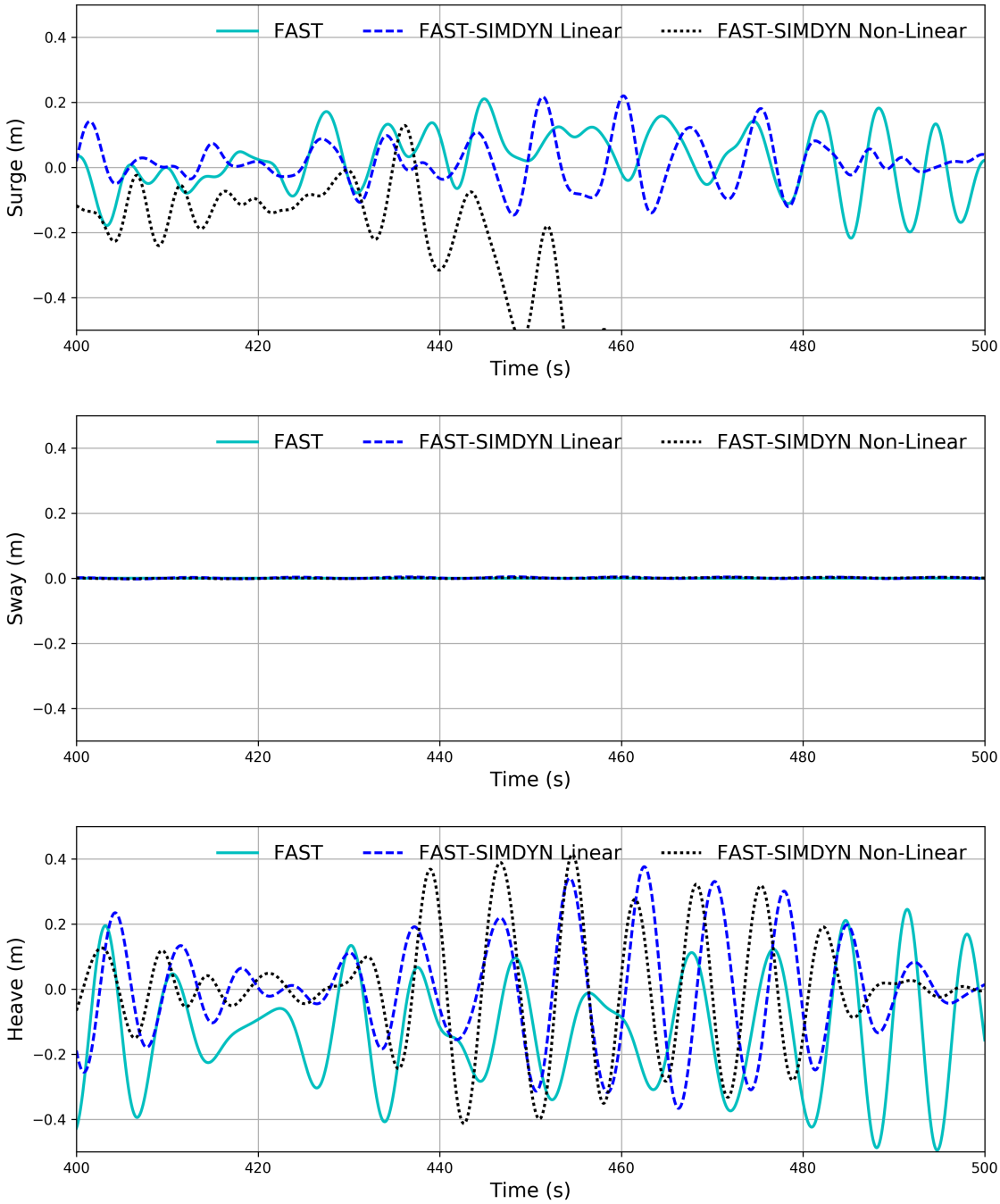

Figure B.13: Translation motion response in zero wind 1m 7s JONSWAP with FEAMooring

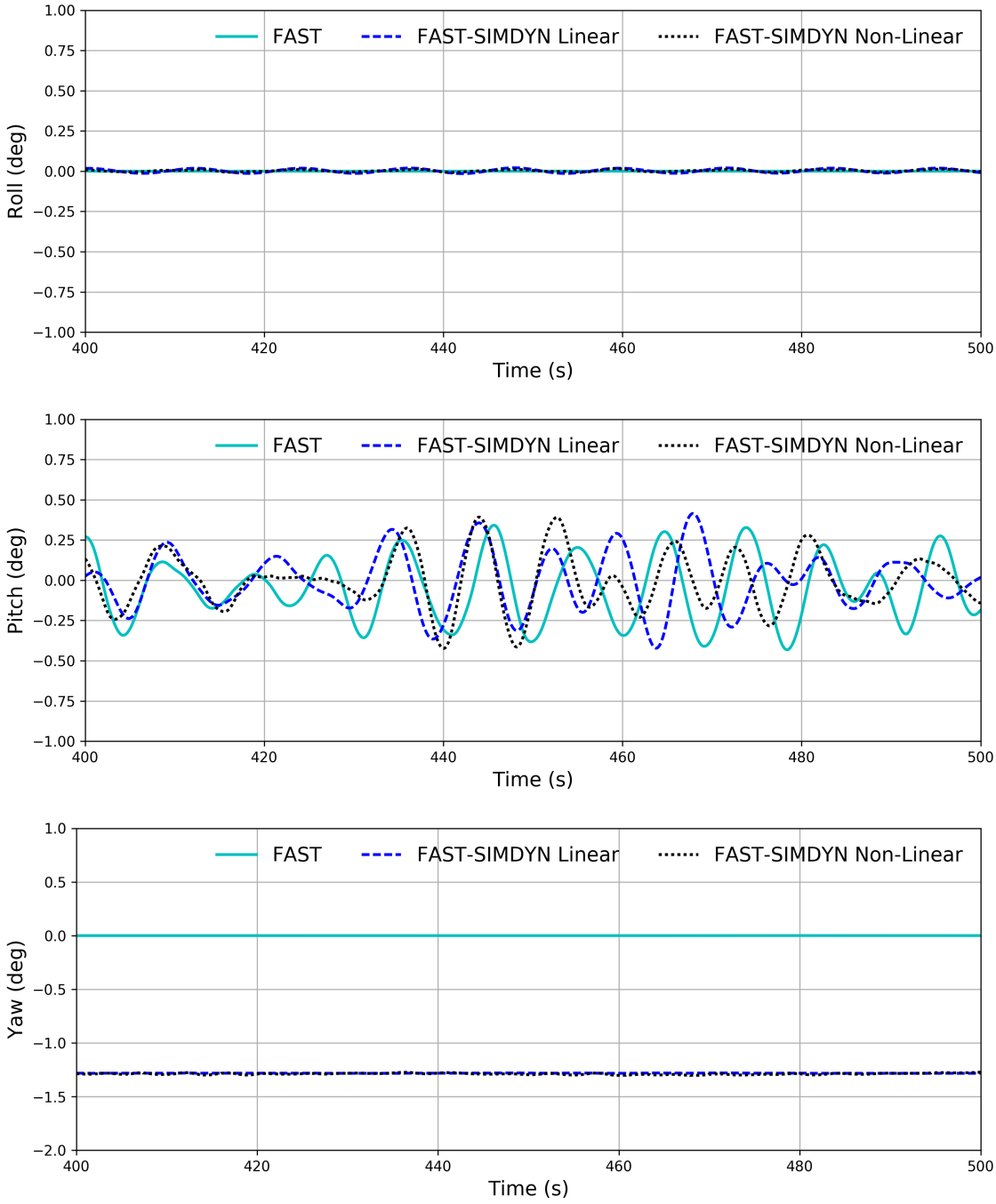

Figure B.14: Rotation motion response in zero wind 1m 7s JONSWAP with FEAMooring

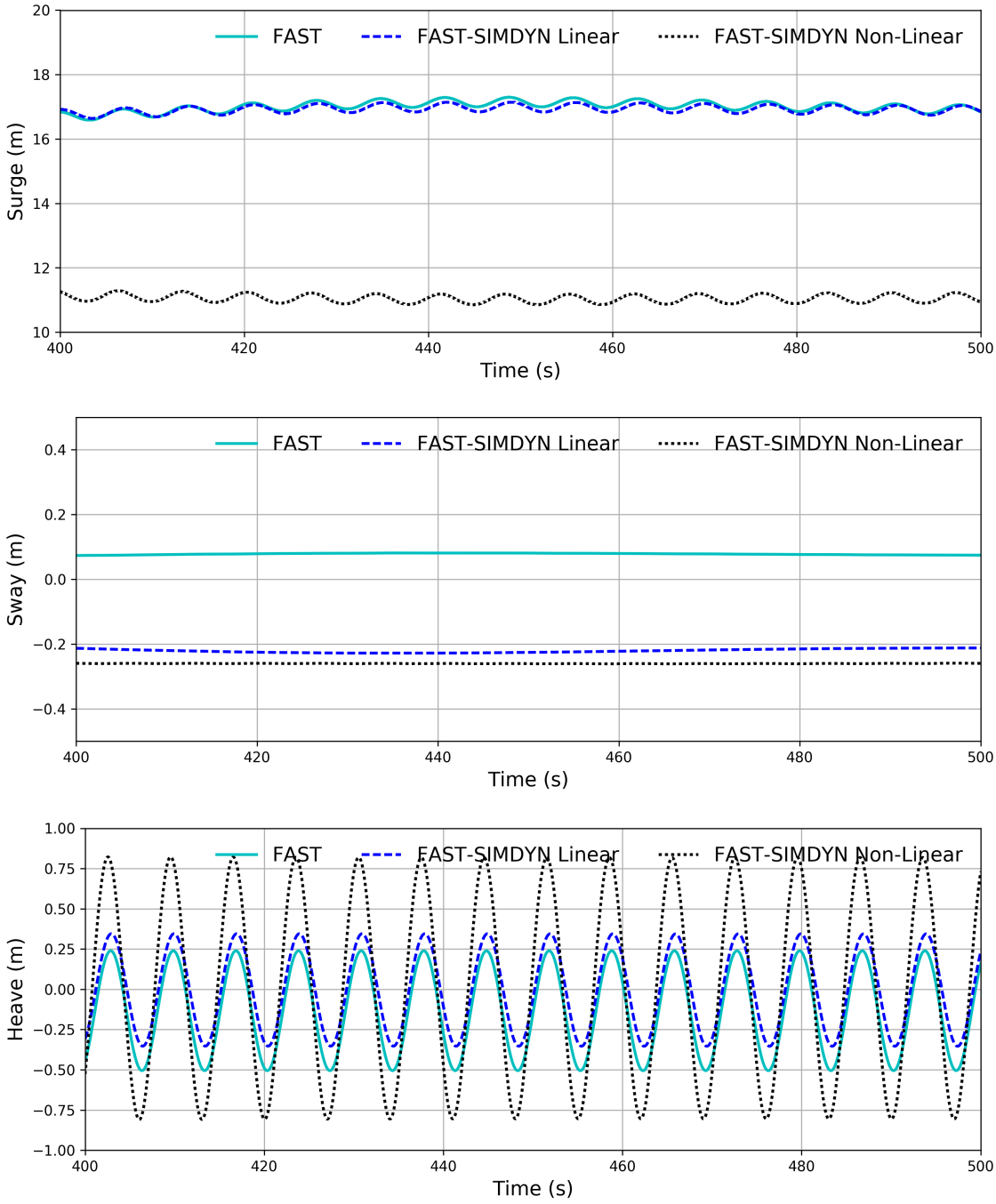

Figure B.15: Translation motion response in 7 m/s wind 1m 7s regular wave with FEAMooring

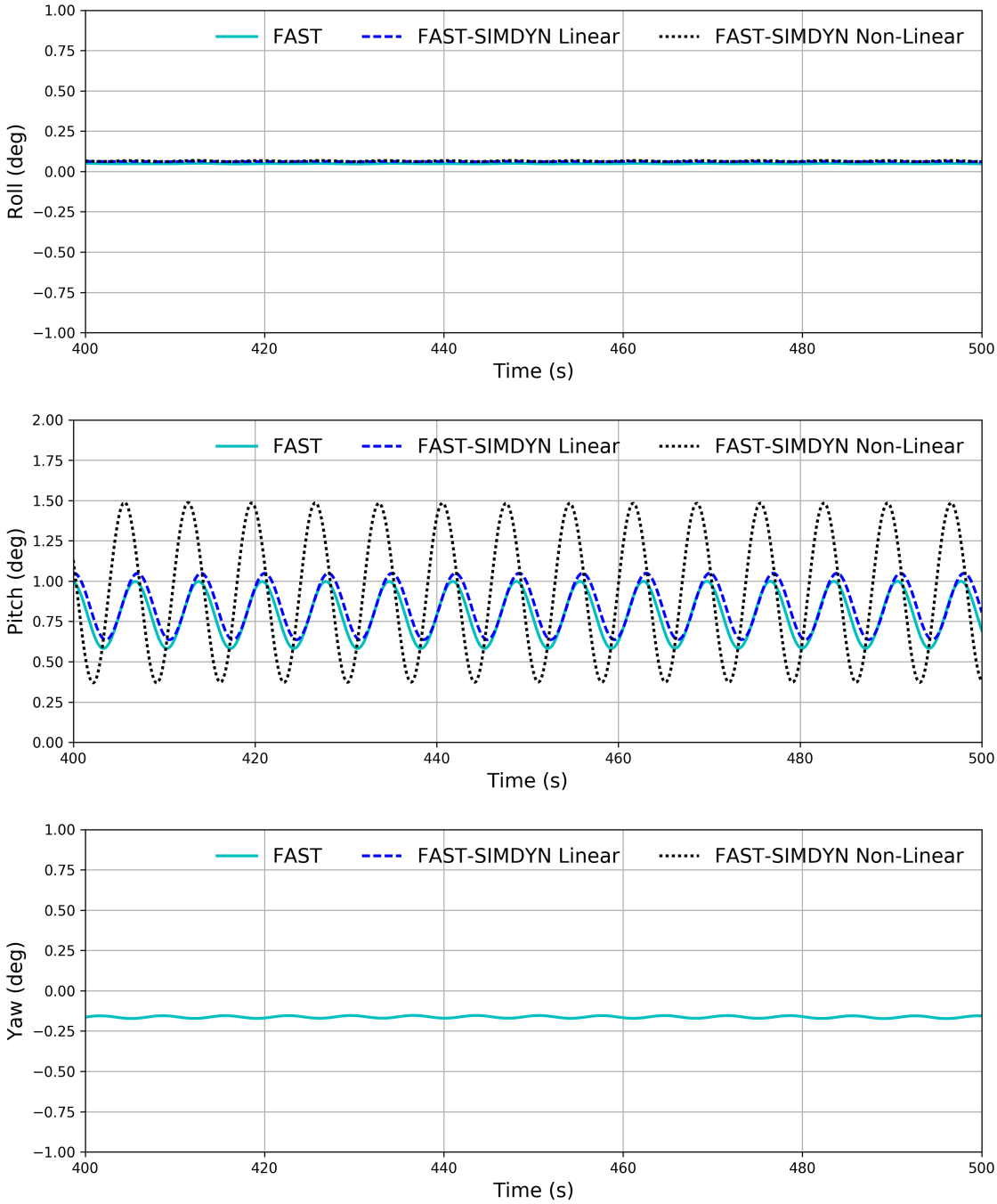

Figure B.16: Rotation motion response in 7 m/s wind 1m 7s regular wave with FEAMooring

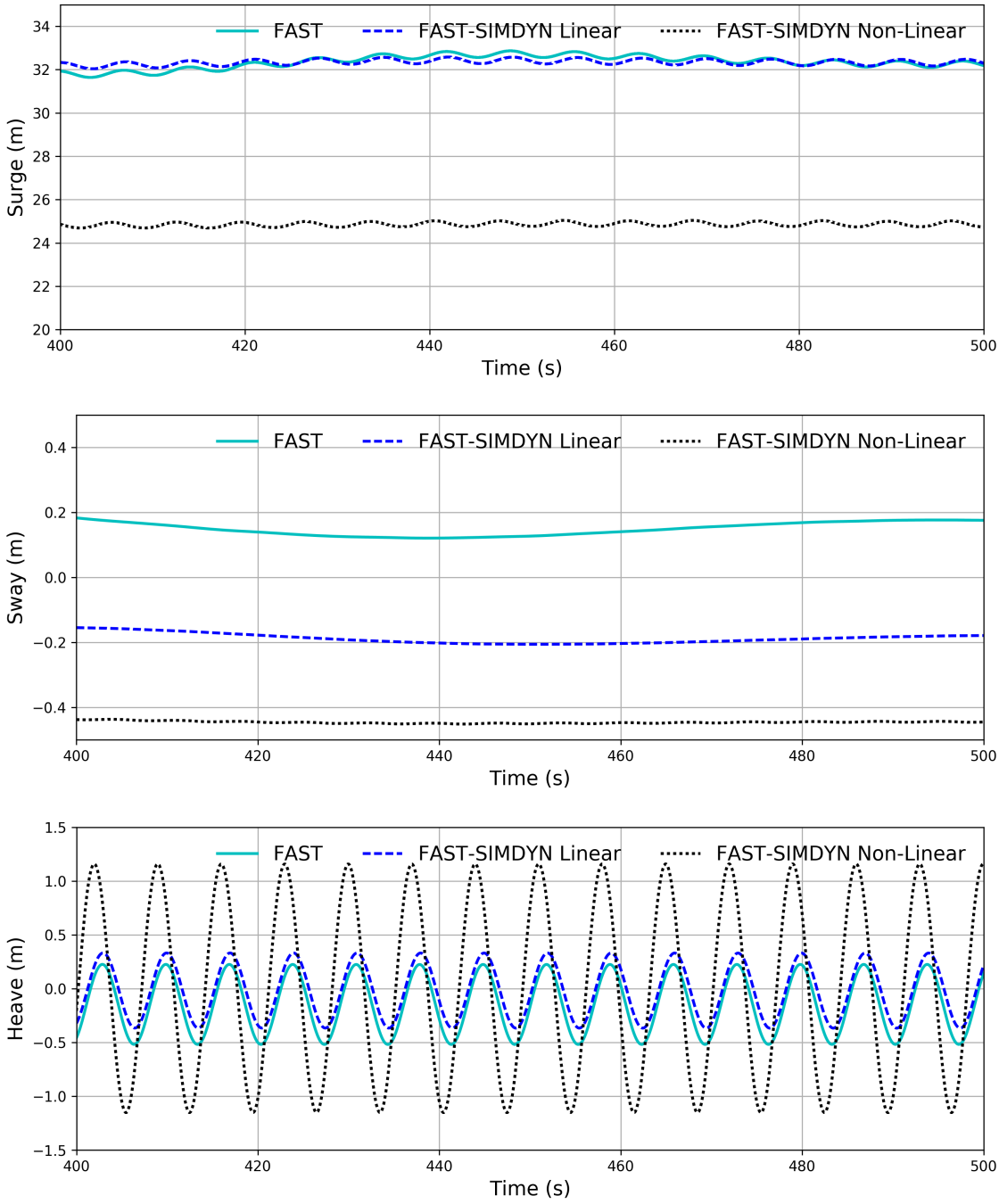

Figure B.17: Translation motion response in 11.4 m/s wind 1m 7s regular wave with FEAMooring

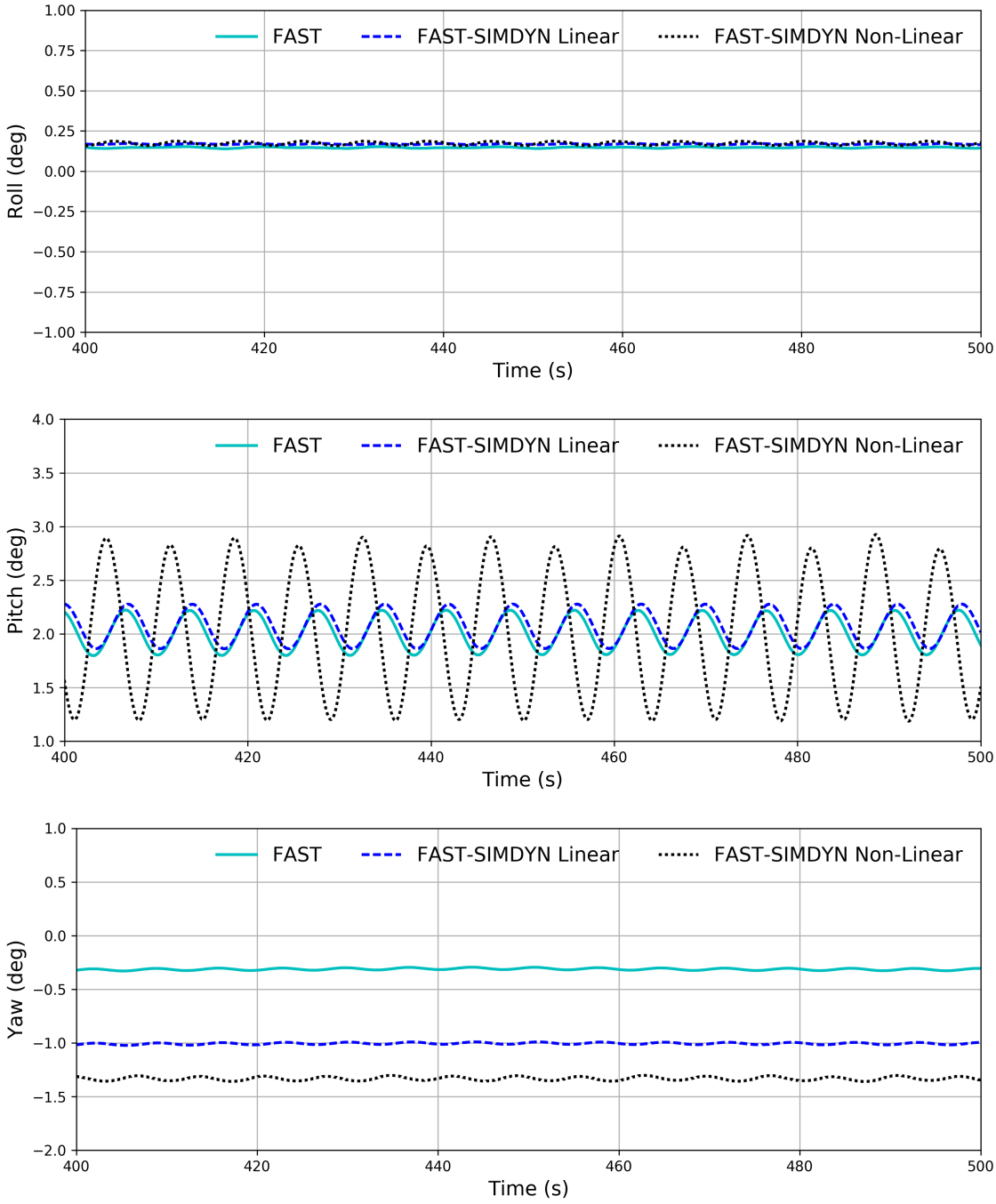

Figure B.18: Rotation motion response in 11.4 m/s wind 1m 7s regular wave with FEAMooring

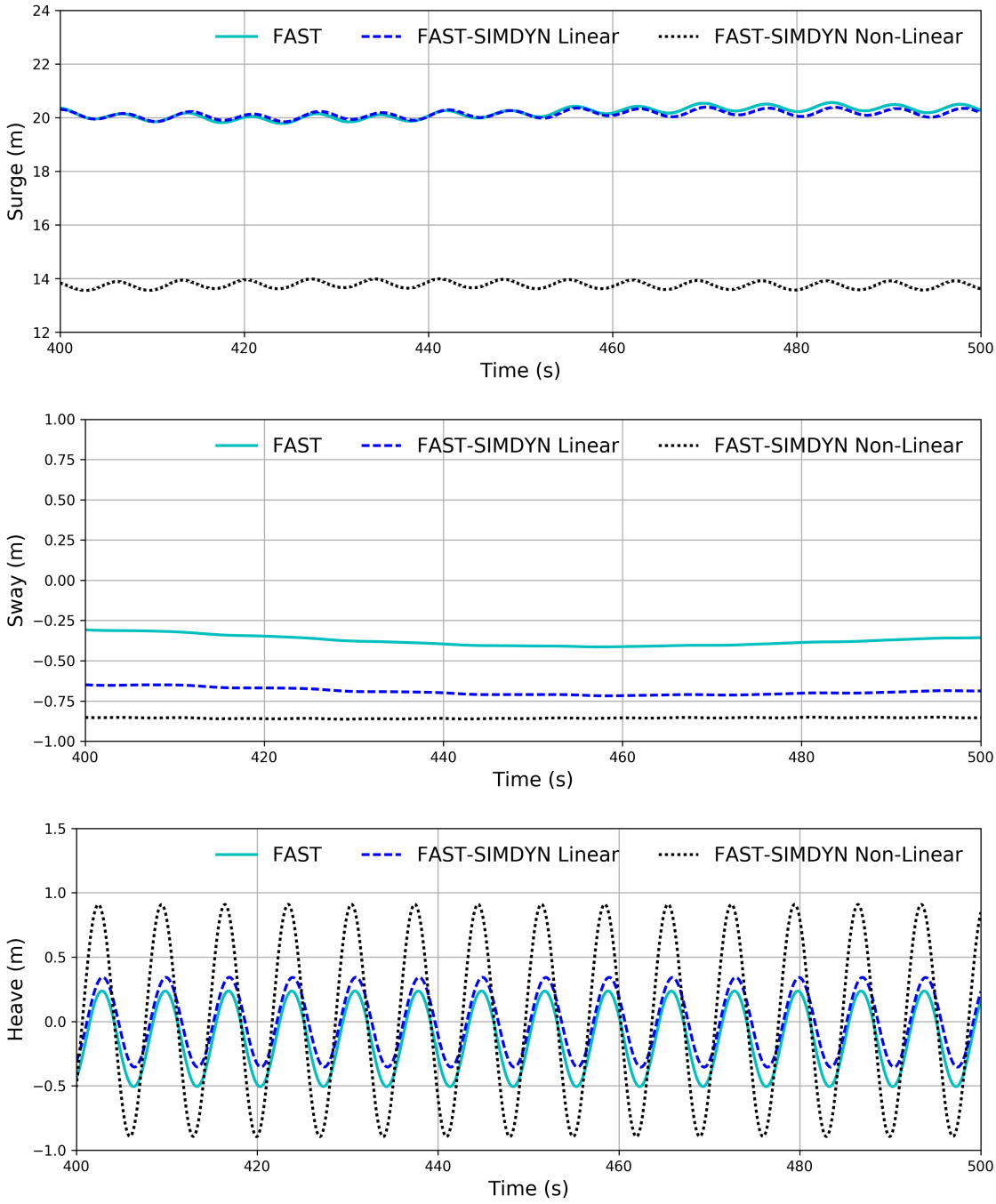

Figure B.19: Translation motion response in 17 m/s wind 1m 7s regular wave with FEAMooring

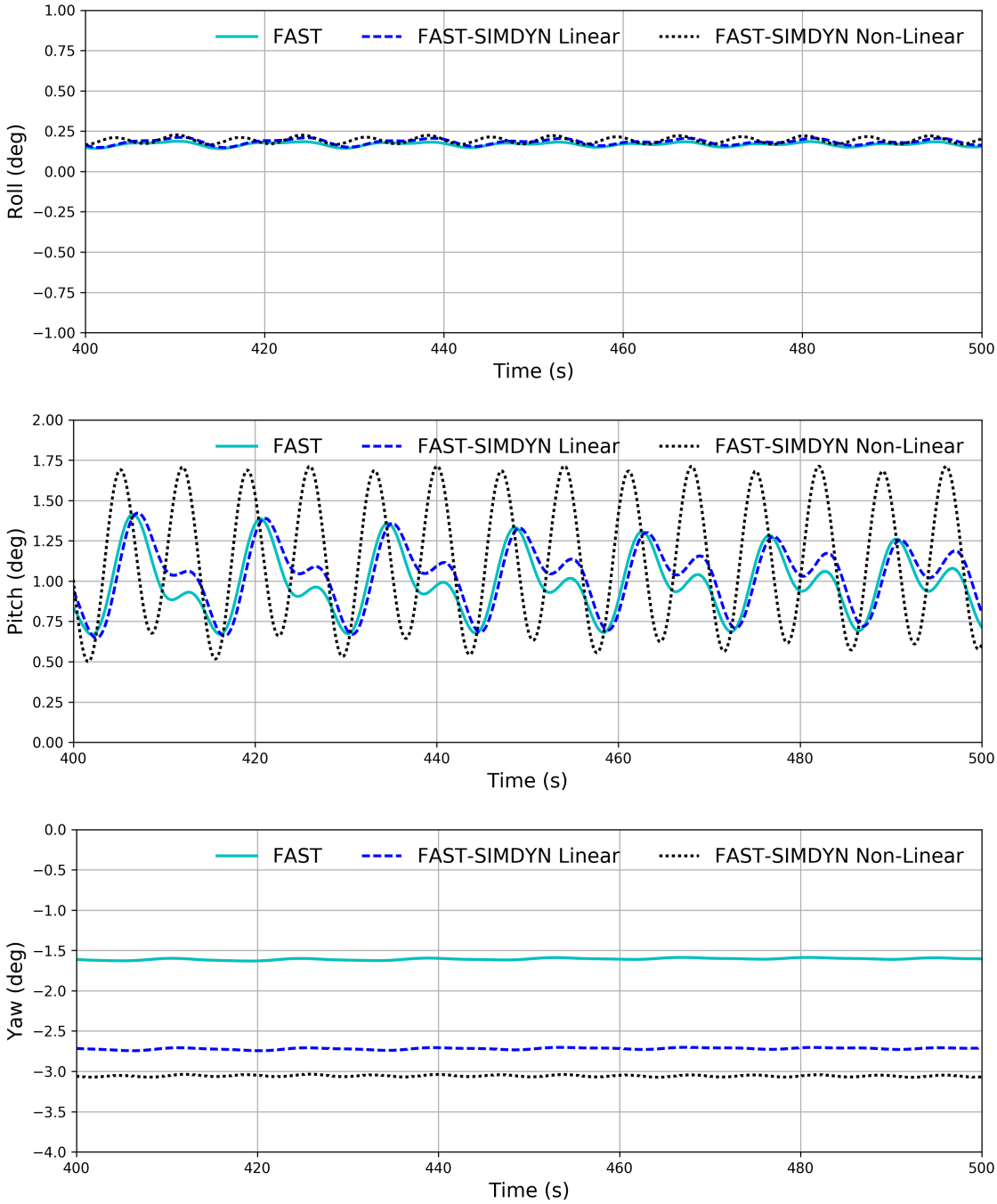

Figure B.20: Rotation motion response in 17 m/s wind 1m 7s regular wave with FEAMooring

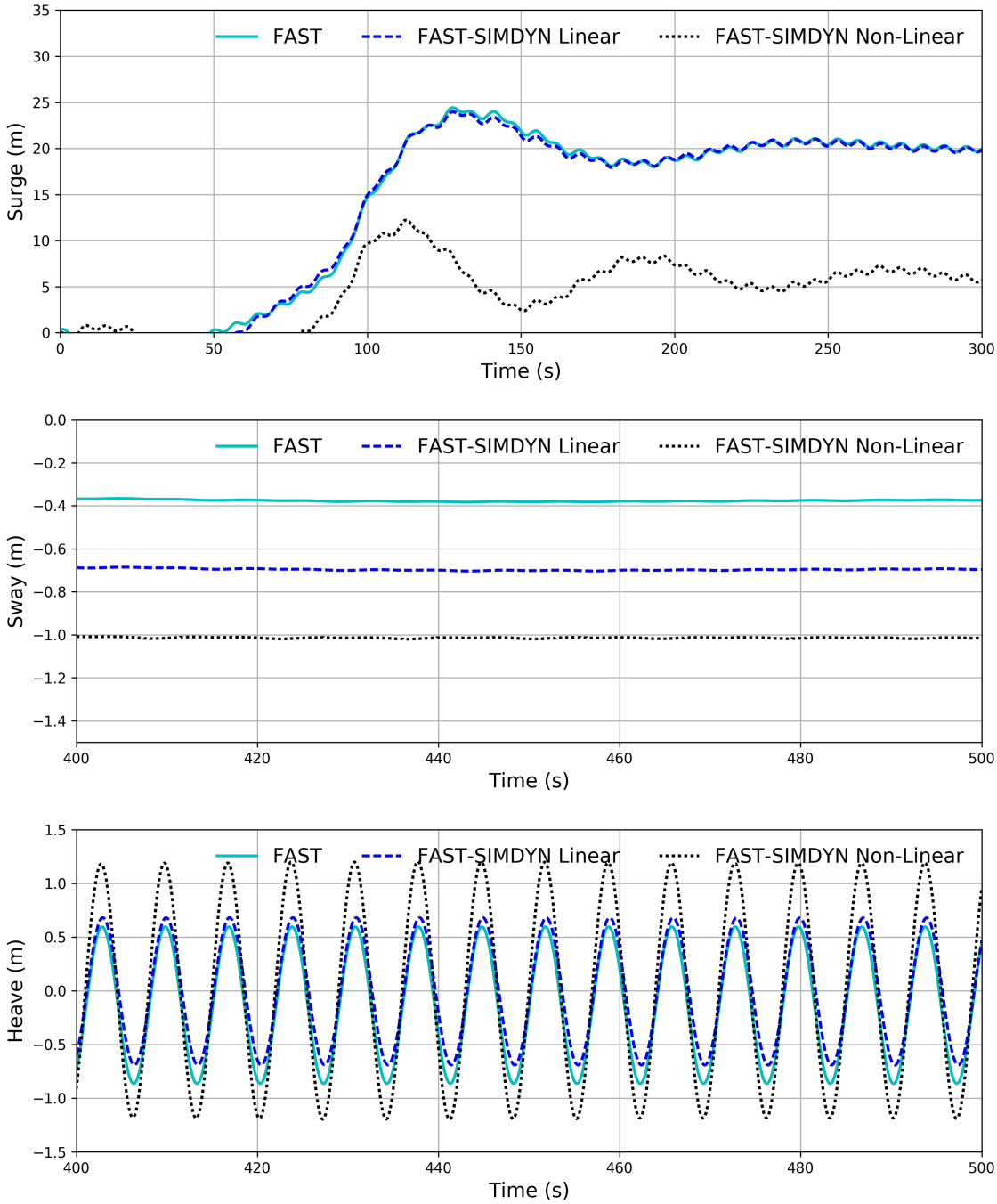

Figure B.21: Translation motion response in 17 m/s wind 2m 7s regular wave Linear vs Non-Linear Froude Krylov with FEAMooring

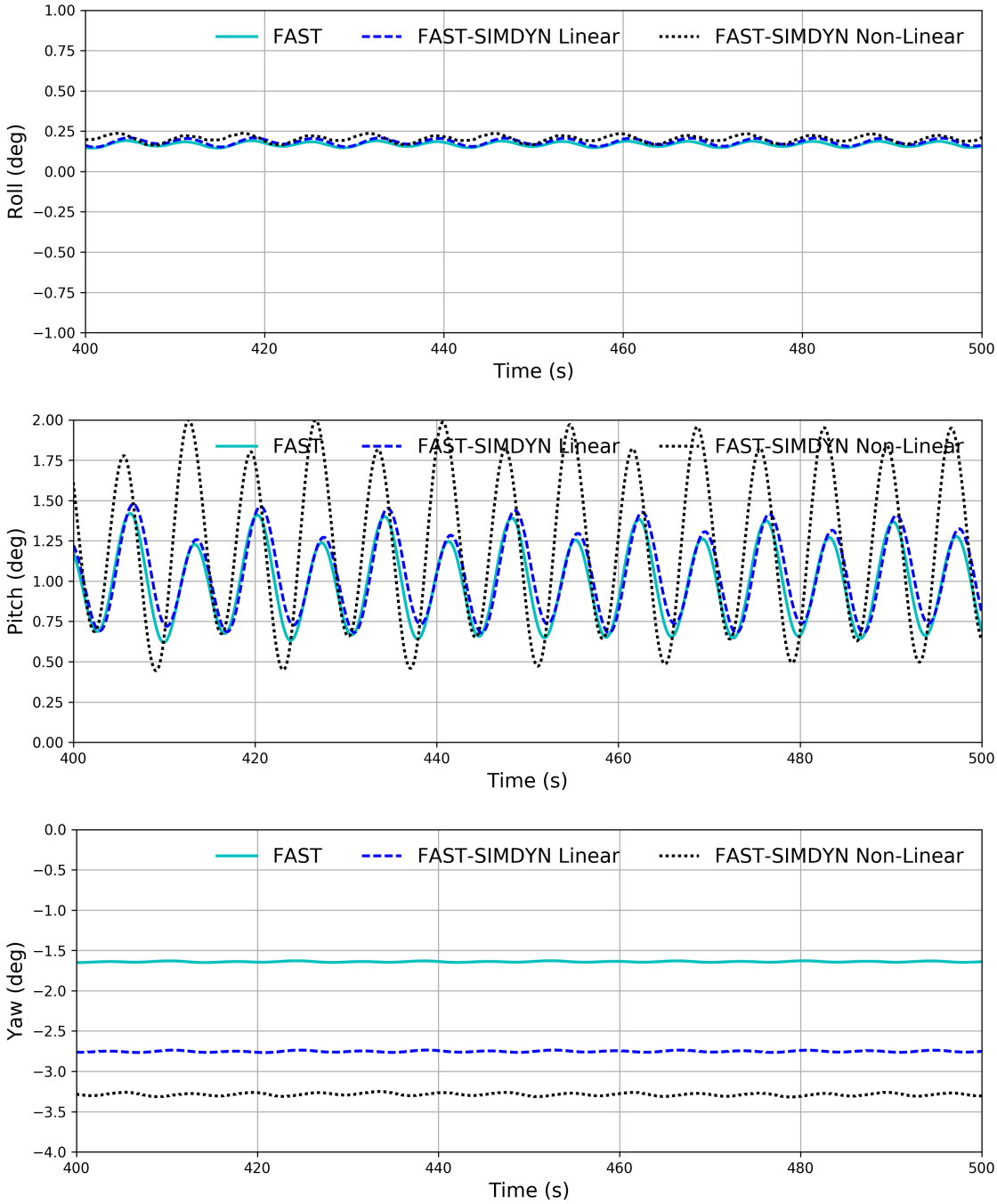

Figure B.22: Rotation motion response in 17 m/s wind 2m 7s regular wave Linear vs Non-Linear Froude Krylov with FEAMooring